國 立 交 通 大 學

電信工程研究所

博 士 論 文

多入/多出通訊系統之
新穎傳送與接收技術

New Transmit and Receive Techniques for

Multiple-Input-Multiple-Output (MIMO)

Communication Systems

研 究 生：郭志成

指導教授：沈文和　博士

王忠炫　博士

中 華 民 國 九 十 九 年 十 二 月

多入/多出通訊系統之

新穎傳送與接收技術

New Transmit and Receive Techniques for

Multiple-Input-Multiple-Output (MIMO)

Communication Systems

研 究 生：郭志成　　　　　　　Student：Chih-Cheng Kuo

指導教授：沈文和 博士　　　　　Advisor：Dr. Wern-Ho Sheen
　　　　　王忠炫 博士　　　　　　　　　　Dr. Chung-Hsuan Wang

國立交通大學

電信工程研究所

博 士 論 文

A Dissertation
Submitted to Institute of Communication Engineering
College of Electrical and Computer Engineering
National Chiao Tung University
in Partial Fulfillment of the Requirements
for the Degree of Doctor of Philosophy
in
Communication Engineering
Hsinchu, Taiwan

2010 年 12 月

多入/多出通訊系統之
新穎傳送與接收技術

研究生：郭志成　　　　　　　　指導教授：沈文和 博士
　　　　　　　　　　　　　　　　　　　　王忠炫 博士

國 立 交 通 大 學
電 信 工 程 學 系

摘要

多入/多出(multiple-input, multiple-output, MIMO)是適用於多種通訊系統之系統模型，含多傳送/接收天線系統(multiple transmit and receive antenna systems)、分碼多重存取(code-division multiple-access systems, CDMA)系統及符元間相互干擾系統(systems with inter-symbol interference channels)等。本論文針對 MIMO 系統提出新型傳送及接收處理技術。首先，本論文針對空間多工(spatial multiplexing)之多天線系統，提出兩種新型 MMSE(minimum mean-squared error)通道分解協助式偵測器(channel-factorization aided detector)；從硬體複雜度(hardware complexity)或位元錯誤率(bit-error-rate)上作比較，新型的偵測器具優於現存方法之效能。接著，本論文針對多天線 MIMO-OFDM (orthogonal frequency-division multiplexing)系統在 I-Q 失衡的干擾下，研究接收機架構並在運算複雜度及位元錯誤率的取捨下作最佳的設計。最後，本論文則針對二維 OFDM-CDMA 下行(forward link)系統提出新型傳輸端預處理技術(transmitter-based pre-processing)；數值模擬結果顯示： (i) 根據可達到之總資料速率，所提出的新方法之效能優於其他現存方法，(ii) 如果能夠依據通道選擇特性(channel selectivity)來適當的決定延展樣式(spreading pattern)，則二維延展(2-D spreading)之效能優於一維延展。

New Transmit and Receive Techniques for Multiple-Input-Multiple-Output (MIMO) Communication Systems

Student: Chih-Cheng Kuo

Advisor: Dr. Wern-Ho Sheen
Dr. Chung-Hsuan Wang

Department of Communication Engineering
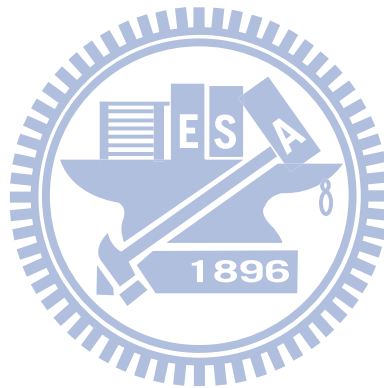National Chiao Tung University

Abstract

Multiple-input, multiple-output (MIMO) is a model for a variety of communication systems, including the multiple transmit and receive antenna systems, code-division multiple-access (CDMA) systems, systems with an inter-symbol interference channel, etc. In this dissertation, new transmit and receive techniques for the MIMO communication systems are proposed. Firstly, two new MMSE (minimum mean-squared error) channel-factorization aided detectors (CFAD) are proposed for the spatial multiplexing multiple antenna systems. The proposed detectors outperform the existing ones in terms of hardware complexity and/or bit error rate performance. Secondly, receiver designs with good trade-off between computational complexity and BER performance are investigated for the MIMO-OFDM (orthogonal frequency-division multiplexing) systems with the presence of I-Q imbalances. Lastly, new transmitter preprocessing techniques are proposed for the two-dimensional (2-D) OFDM-CDMA forward link systems. Numerical results show that (i) the new method outperforms the existing ones in terms of achievable sum data rate, and (ii) the 2-D spreading outperforms the 1-D one if spreading pattern is adapted according to channel selectivity.

Acknowledgement

Foremost, I would like to express my sincere gratitude to my advisors, Dr. Wern-Ho Sheen and Dr. Chung-Hsuan Wang, for providing me insights into important research problems, encouragement and support throughout my Ph.D. studies. This work could not have been done without their advice, guidance and comments. Special thanks go to my mates at BRAS Lab. in NCTU for their kindly help in many aspects.

Finally, I am deeply indebted to my family whose love and understanding have accompanied me through this long journey.

Contents

List of Figures

List of Tables

Notations

- m : number of transmit antennas

- n : number of receive antennas

- j : $\sqrt{-1}$

- $\otimes$: linear convolution operator

- $\delta(t)$: Dirac delta function

- $\delta(n)$: Kronecker delta function

- $(\cdot)^*$: complex conjugate operator

- $(\cdot)^T$: transpose of a matrix or vector

- $(\cdot)^H$: complex conjugate transpose of a matrix or vector

- $(\cdot)^{-1}$: inverse of a matrix

- $(\cdot)^\dagger$: pseudo-inverse of a matrix or vector

- $[\mathbf{A}]_{i,j}$: (i, j)-th entry of matrix $\mathbf{A}$

- $tr(\cdot)$: trace of a matrix
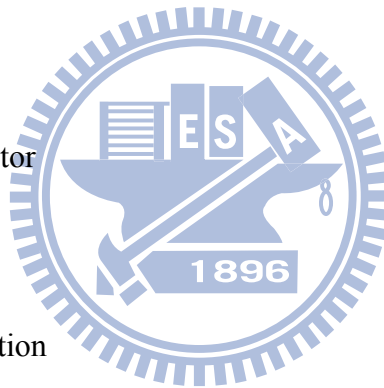
- $\det(\cdot)$: determinant of a matrix

- $\text{diag}\{\mathbf{x}\}$: diagonal matrix with vector $\mathbf{x}$ on the diagonal

- $\text{diag}\{\mathbf{X}_1,\ldots,\mathbf{X}_M\}$: block diagonal matrix with the submatrices $\mathbf{X}_1,\ldots,\mathbf{X}_M$ on the diagonal

- $\text{E}\{\cdot\}$: expectation operator

- $\text{Re}\{\cdot\}$: real parts

- $\text{Im}\{\cdot\}$: imaginary parts

- $\log_{10}(\cdot)$: base-10 logarithm

- $\mathbf{1}_N$: all 1 vector with dimension N

- $\mathbf{I}_N$: $N \times N$ identity matrix

- $\mathbf{0}_N$: $N \times 1$ all zero vector

- $\mathbf{O}_{M \times N}$: $M \times N$ all zero matrix

Chapter 1

Introduction

The next-generation mobile communication is envisioned to provide high spectrum-efficient, high data-rate multimedia services over a wide variety of operating environments: indoor, outdoor, high and low mobility, etc. To date, innovative techniques have been proposed in the mobile communication systems to achieve these goals, including the techniques of using multiple transmit and receive antennas [1], [2], code division multiple access (CDMA), orthogonal frequency division multiplexing (OFDM), and the combinations of them [3]-[5]. One general model for all these techniques is the multiple-input, multiple-output (MIMO) system model, as shown in Figure 1.1, where the system has m inputs and n outputs. In addition, the MIMO system can also be used to model the communication systems with an ISI (inter-symbol interference) channel [6]. In this dissertation, we focuses new transmit and receive techniques for the MIMO systems.
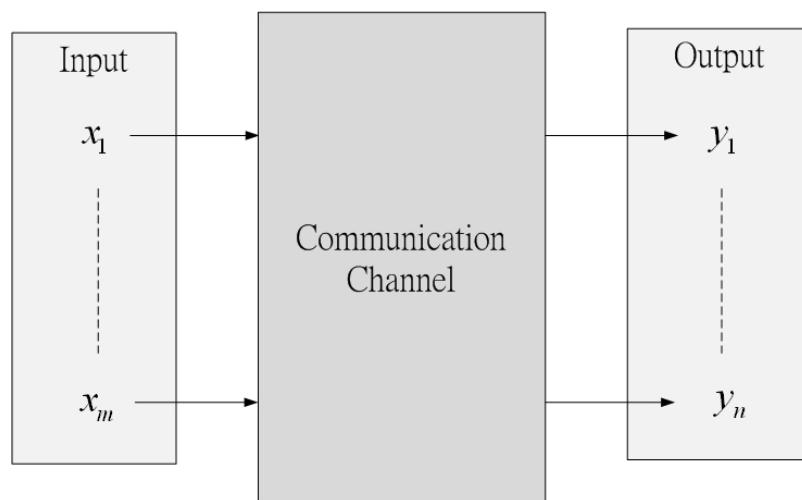
Figure 1.1: System model for MIMO communication systems

1.1 New Techniques for MIMO Systems with Multiple Transmit and Receive Antennas

A popular MIMO system is to use multiple transmit and receive antennas in a wireless communication system. The system is capable of providing diversity gain, array gain (power gain), and/or degree-of-freedom gain over single-input-single-output (SISO) systems, the single antenna systems [1], [2], [19]. Space-time coding, beam-forming and spatial multiplexing are the modes of operations to exploit the diversity gain, array gain, and degree-of-freedom gain, respectively. In particular, in spatial multiplexing, parallel data streams are transmitted over different transmit antennas to take advantage of the extra degree of freedom provided by a rich-scattered environment to increase spectral efficiency [19]-[23]. The spatial multiplexing MIMO systems have been one of the key technologies to enable high data-rate, high spectral-efficiency transmission in wireless environments.

1.1.1 Channel Factorization Aided MMSE Receiver for Multiple Transmit and Receive Antenna Systems

The first part of this dissertation focuses on the design of new receiver techniques for the spatial multiplexing MIMO systems. Specifically, two types of minimum mean-squared error (MMSE) channel-factorization aided detectors (CFAD) are proposed to improve the system performance.

For the spatial multiplexing MIMO systems, the optimal detector is the maximum-likelihood (ML) detector that minimizes the detection error probability, given the perfect channel estimation. Without imposing a special structure on the transmitted symbols, however, the complexity of the ML detector grows exponentially with the transmit antenna and/or the symbol constellation sizes,

because all the symbol vectors need to be searched exhaustively for the optimum detection. For the case of using QAM symbols, on the other hand, the complexity of the ML detector can be reduced by using the sphere decoding [24], [25], where the searching is limited to within a sphere around the received signal, although its complexity may still be too demanding for some applications. In viewing this, different reduced-complexity sub-optimal detectors have been proposed in real systems, including the linear and nonlinear detectors [20]-[23]. For an ill-conditioned channel, unfortunately, the performance of these detectors is significantly inferior to that of the ML detector.

Recently, CFADs have been proposed to narrow the performance gap between the ML and traditional reduced-complexity detectors [26]-[35], where channel factorization is mostly done with the lattice-reduction algorithms such as the Lenstra–Lenstra–Lovász (LLL) [36], [37] and Seysen's algorithms [38], [39]. Thus, the method is also called the lattice-reduction aided detector, LRAD. (Here, we prefer to use the term CFAD because the channel factorization is not necessarily done with a lattice-reduction algorithm.) In particular, in [26]-[29], the LLL-based LRAD was proposed to improve performance over the conventional ZF (zero forcing) MIMO detector. The authors of [30]-[32] proposed the MMSE-based LRAD to further improve its ZF counterpart. Later on, the LLL algorithm was proposed to operate on the dual lattice rather than the original lattice to reduce effective noise power [33], [34]. In addition, the Seysen's algorithm [39] which simultaneously reduces lattice basis and its dual was proposed to improve the performance of the LLL algorithm. Lastly, the authors of [35] conducted a comprehensive performance comparisons on the reduction algorithms mentioned above.

Traditionally, the design of the channel factorization algorithm in LRAD is somewhat intuitively; neither a specific detector nor a cost function is devised to search for good factorization algorithms. The LLL and Seysen's algorithms were employed to obtain a relatively short (orthogonal) basis with no consideration of the low-complexity detector used. In this part of

work, we propose a new approach: the factorization algorithm is designed specifically for the MMSE detector with the aim to minimize the cost function of sum mean-squared-error (MSE). Two new types of factorization algorithms are proposed. Type-I is LLL-based, where the best-performed factorization algorithm found in the literature, i.e., the LLL algorithm working on the dual matrix of the extended channel matrix (DLLL-extended algorithm), is a member of this type but has a higher complexity than the proposed one. In this regard, this work provides a theoretical foundation for the DLLL-extended algorithm. Type-II is greedy-search based, where its members are differentiated with different algorithm's parameters. Type-II algorithms can provide around 0.5-1.0 dB gain over Type-I algorithms and have a fixed computational complexity which is seen as an advantageous in hardware implementation.

1.1.2 Receiver Design for MIMO-OFDM Systems with I-Q Imbalances

Combining the techniques of multiple antennas and OFDM, i.e., the MIMO-OFDM technique, endows the communication systems with high data-rate, high spectral-efficiency transmissions. Using OFDM, ISI incurred in high data-rate transmission can be removed with a simple frequency-domain equalizer at the receiver. Currently, MIMO-OFDM has been adopted in the IEEE 802.11n, IEEE 802.16, and 3GPP Long Term Evolution (LTE) specifications.

From the viewpoint of low-cost transceiver designs, zero intermediate-frequency (IF) structure is very appealing thanks to its avoidance of using expensive IF components and the image rejection (IR) filter. It is more amenable to monolithic integration and, thus, facilitates a low cost, small form factor design. This architecture, however, is very sensitive to imperfections of the analog circuitry. In particular, mismatch between I and Q branch circuitry, called the in-phase-quadrature (I-Q) imbalance, induces mirror-frequency interference. These imbalances that may appear at both transmitter and receiver will significantly degrade communication

performance if not compensated properly. In this part of dissertation, we investigate the receiver design for the MIMO-OFDM systems with the presence of I-Q imbalance.

In the literature, the BER performance of the QPSK-modulated OFDM systems was evaluated to illustrate the impact of I-Q imbalance in [40]. In [41], the authors analyzed the impact of I-Q imbalance and phase noise in the MIMO-OFDM systems with different number of antennas. The authors of [42] evaluated the impact of carrier frequency offset (CFO), the sampling clock offset, and I-Q imbalance on the MC-CDMA downlink system, considering a receiver based on channel tracking designed to cope with high mobility. A new detection method was proposed for the OFDM systems with the presence of I-Q imbalance in [43] along with a new pilot design to estimate the channel. In [44], authors proposed a technique that jointly estimates the I-Q imbalance, dc offset, carrier frequency offset, and channel for receivers in frequency selective channels. In addition, new adaptive techniques were proposed to compensate I-Q imbalance [45]-[48]. The authors in [45] proposed an adaptive scheme to correct I-Q imbalances at the remote transmitter as well as at the receiver in the single carrier systems and OFDM systems [46]. With the presence of I-Q imbalance and dc offset, an adaptive compensation technique was proposed in [47]. The effect of both transmitter and receiver I-Q imbalance was studied under the effect of carrier frequency offset in the OFDM systems. Also, an algorithm was developed in [48] to adaptively compensate for such distortion in the digital domain.

Instead of using adaptation correction, I-Q imbalance correction methods were proposed for the quadrature receiver [49] and OFDM receiver [50]. In [51], an estimation technique that resorts to the iterative Expectation-Maximization (EM) algorithm to converge to the ML estimation was proposed for both channel and I-Q imbalance coefficients in presence of unknown transmitted data symbols. In addition, some jointly compensation schemes for front-end impairments were proposed in [52]-[60]. A digital signal processing techniques for compensating

both the I-Q imbalance and the DC offset in communication receivers were derived in [52]. The authors in [53] developed an estimation/compensation scheme to jointly combat the I-Q imbalance and phase noise at baseband. In [54], the authors proposed and analyzed a joint I-Q, CFO estimation/compensation method. In addition, a pilot-based scheme for both CFO and I-Q imbalance compensations at the baseband was developed in [55]. The authors studied the effect of both the transmitter and receiver I-Q imbalances in an OFDM system [56], [57] and MIMO-OFDM systems [58], and developed the algorithms to compensate for such distortions in the digital domain. Also, the authors proposed to compensate I-Q imbalances with a cascaded connection of MMSE and MLD [59] and ordered successive interference cancellation (OSIC) [60].

Different from previous works that regard I-Q imbalance as impairment and than compensates it, in this part of work, we model it as a part of whole system for MIMO-OFDM transceiver, and examine receiver structure designs based on the trade-off between BER performance and computational complexity.

1.1.3 Transmitter-Based Pre-Processing for Forward-Link 2-D OFDM-CDMA System

Transmitter pre-processing has been known as a technique to increasing the system capacity and/or performance and to shifting the signal processing complexity from a mobile unit to the base station in forward-link transmission of a multiple access environment [12]-[18]. A transmitter pre-coding was studied for the down-link of a synchronous direct sequence CDMA (DS-CDMA) system in [12]. Based on the minimum mean square error (MMSE) criterion with power scaling, both ISI and MAI (multiple access interference) can be removed in a multi-path channel if RAKE receiver is employed in the mobile unit. The authors in [16] proposed to apply the *filtering* directly to the transmitted waveform, rather than to the data symbols as in [12], in

order to achieve better performance and further reduce the complexity of a mobile unit. Furthermore, a similar structure as those in [12], [16] with multiple transmit antennas was investigated in [13], where a set of transmit filters was designed, based on the maximization of signal to interference-plus-noise ratio (SINR) at each receiver output. Without jointly considering all the users, the system performance is similar to that of pre-rake diversity combining in [14]. In [15], a combined transmitter frequency-time domain power adaptation with maximum ratio combining (MRC) receiver was explored for the forward-link of a MC-CDMA system. Performance gain is obtained by using a simple power adaptation strategy that drops bad sub-carriers and distributes the transmission power uniformly over other better ones. Transmitter-based pre-processing has also been applied to the MIMO systems. For example, in [17], the authors proposed a transmitter pre-processing technique for decomposing a multi-user MIMO downlink channel into multiple parallel independent single-user MIMO ones. As a result, any technique for single-user MIMO such as singular value decomposition (SVD) based techniques [18] can be applied for each user of the multi-user MIMO system.

OFDM-CDMA – a form of CDMA with multiple-carrier transmission – is a promising radio access technology for the next-generation mobile communication. By combining OFDM and CDMA, it is able to overcome the serious ISI in a high-data-rate environment with simple frequency-domain equalization, provide high spectral efficiency in the cellular environment with universal frequency reuse and gain reception diversity through spreading data over frequency and time domain. It can be shown later that the model of systems employing the technique of OFDM-CDMA is also a manner of multiple-input-multiple-output model.

Traditionally, OFDM and CDMA are combined in a one-dimensional (1-D) fashion; that is, a data symbol is either spread in frequency or time domain [3]-[5]. The former is called multi-carrier CDMA (MC-CDMA) and the latter multi-carrier direct-sequence CDMA (MC-DS-CDMA). In MC-CDMA, a data symbol is duplicated into several parallel copies with

each copy multiplied by a spreading chip before being modulated onto a sub-carrier in an OFDM format. In contrast, in MC-DS-CDMA, a data symbol is spread in the time domain first and then the chips are modulated onto the same sub-carrier. 1-D OFDM-CDMA has been investigated extensively in the literature including receiver design, performance evaluation and comparisons between different spreading methods, see [3]-[5] and references therein.

2-D OFDM-CDMA, where data symbols are spread over time and frequency domains, has been getting more and more attention recently because of its ability to exploit simultaneously the temporal and spectral characteristics of the fading channels. In [7], NTT DoCoMo proposed a 2-D orthogonal frequency and code division multiplexing (OFCDM) system with variable spreading factors for the forward link. The same principle was applied in [8], where the authors proposed a time-frequency localized CDMA (TFL-CDMA) system that utilizes the channel-correlation in both time and frequency in order to reduce multiple access interference (MAI). In contrast, a 2-D OFDM-CDMA system was studied with a spreading pattern designed to maximize the diversity order [9]. Application of a simplified multi-user detection (MUD) to the 2-D systems was explored in [10], and more recently, the adaptability of 2-D OFDM-CDMA systems was investigated in [11].

This part of work aims to investigate transmitter-based pre-processing techniques for the 2-D OFDM-CDMA forward-link systems over the time-variant multi-path Rayleigh fading channels, aiming to increase the system sum data rate and reduce the computational complexity of a mobile unit. For the non-selective channels, the optimum pre-processing that achieves the maximum sum data rate is obtained by applying the principle of multi-user water filling under the condition of zero MAI. For the selective channels, preprocessing methods based on the traditional criteria of ZF and MMSE are investigated first, and then a new method called zero forcing with multi-user water filling (ZF-MWF) is proposed to increase the system performance. The sum data rate of the system serves as the performance index for the design and comparison of different methods. The

merit of 2-D over 1-D spreading is highlighted and the design issues such as selection of spreading pattern and user scheduling are also discussed.

1.2   Dissertation Outline

This dissertation focuses on the investigations of transmit and receive techniques for the MIMO communication systems. In Chapter 2, two types channel factorization algorithms are proposed for channel factorization aided MMSE detector in multiple transmit and receive antenna systems. In Chapter 3, we explore the receiver structure designs based on the trade-off between BER performance and computational complexity for MIMO-OFDM systems with the transmitter and receiver I-Q imbalances. Chapter 4 investigates transmitter-based pre-processing techniques so as to increase the system sum data rate for the 2-D OFDM-CDMA forward-link systems over the time-variant multi-path Rayleigh fading channels. Finally, conclusions are given in Chapter 5.

Chapter 2

Channel Factorization Aided MMSE Receiver for MIMO Systems

Channel-factorization aided detector (CFAD) is one of the important low-complexity detectors used in the MIMO receivers. Through channel factorization, a CFAD transforms the original MIMO system into an equivalent system with a better-conditioned channel in which detection is performed with a low-complexity detector; the estimate is then transformed back to the original system to obtain the final decision. Traditionally, the channel factorization is done with the lattice reduction algorithms such as the Lenstra–Lenstra–Lovász (LLL) and Seysen's algorithms with no consideration of the low-complexity detector used. In this Chapter, we propose a different approach: the channel factorization is designed specifically for the minimum mean-square-error (MMSE) detector that is a popular low-complexity detector in CFADs. Two new types of factorization algorithms are proposed. Type-I is LLL based, where the LLL algorithm working on the dual matrix of the extended channel matrix (DLLL-extended) is a member of this type but with a higher complexity. DLLL-extended is the best-performed factorization algorithm found in the literature, Type-II is greedy-search based where its members are differentiated with different algorithm's parameters. Type-II algorithms can provide around 0.5-1.0 dB gain over Type-I algorithms and has a fixed computational complexity which is advantageous in hardware implementation. In addition, combining proposed MMSE channel factorization algorithm with the element-wise, candidate-list (EWCL) detector can approach to within a fractional dB of the ML performance.

2.1 System Model and Reduced-complexity Detectors

Figure 2.1 is the considered flat-faded MIMO channel with m transmit and $n \geq m$ receive antennas, where $h_{i,j}$ denotes the complex-valued gain from transmit antenna j to receive antenna i, $1 \leq j \leq m$ and $1 \leq i \leq n$. The corresponding signal model is given by

$$\mathbf{y} = \mathbf{Hx} + \mathbf{w} \tag{2.1}$$

where $\mathbf{y} = \begin{bmatrix} y_1 \cdots y_n \end{bmatrix}^T \in C^n$, $\mathbf{x} = \begin{bmatrix} x_1 \cdots x_m \end{bmatrix}^T \in C^m$, $\mathbf{w} = \begin{bmatrix} w_1 \cdots w_n \end{bmatrix}^T \in C^n$ are the received signal vector, transmitted signal vector, and noise vector, respectively, $\mathbf{H}$ is the composite channel matrix with m transmit antennas and n receive antennas, and C is the set of complex numbers. Using the notations in Figure 2.1 and Equation (2.1), the channel matrix is $\mathbf{H} = \begin{bmatrix} h_{i,j} \end{bmatrix}$. The popular correlated channel model for $\mathbf{H} = \mathbf{J}_R^{1/2} \mathbf{F} \mathbf{J}_T^{1/2}$ in [31] is adopted in this chapter, where $\mathbf{F}$ consists of zero-mean, uncorrelated complex Gaussian coefficients of unit variance, and $\mathbf{J}_T$ and $\mathbf{J}_R$ are the spatial correlation matrices at transmitter and receiver, respectively. Furthermore, as in [31], we adopt the commonly used correlation matrices

$$\mathbf{J}_T = \begin{bmatrix} 1 & \rho & \rho^4 & \cdots & \rho^{(m-1)^2} \\ \rho & 1 & \rho & \ddots & \vdots \\ \rho^4 & \rho & 1 & \ddots & \rho^4 \\ \vdots & \ddots & \ddots & \ddots & \rho \\ \rho^{(m-1)^2} & \cdots & \rho^4 & \rho & 1 \end{bmatrix}, \tag{2.2}$$

and

$$\mathbf{J}_R = \begin{bmatrix} 1 & \rho & \rho^4 & \cdots & \rho^{(n-1)^2} \\ \rho & 1 & \rho & \ddots & \vdots \\ \rho^4 & \rho & 1 & \ddots & \rho^4 \\ \vdots & \ddots & \ddots & \ddots & \rho \\ \rho^{(n-1)^2} & \cdots & \rho^4 & \rho & 1 \end{bmatrix}, \tag{2.3}$$

with $0 \le \rho \le 1$. Note that $\rho = 0.0$ gives the uncorrelated channel and $\rho = 1.0$ gives the fully correlated one.
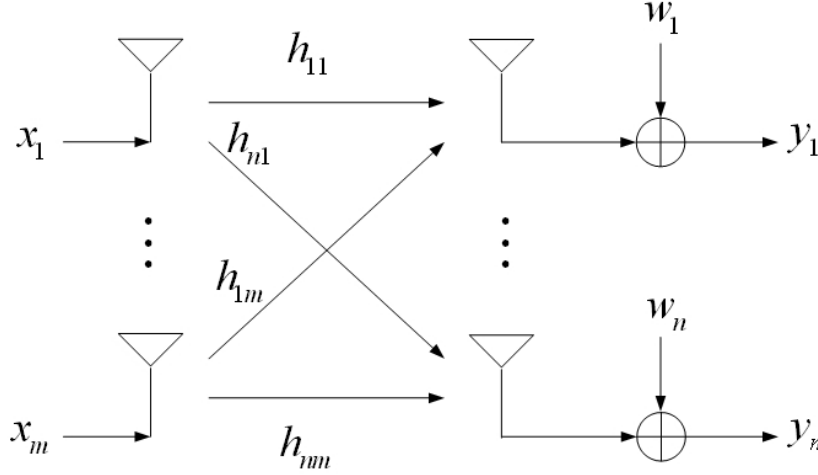
Figure 2.1: The considered MIMO channel with m transmit and n receive antennas.

For quadrature amplitude modulation (QAM) constellations, it is easy to see that, after proper shifting and scaling, $\mathbf{x} = [x_1 \cdots x_m]^T \in \Omega^m$, where $\Omega \subset Z$, and Z is the set of complex integers. Also, the signal vector $\mathbf{x} \in \Omega^m$ has independent and identical distributed (i.i.d.) entries with the power constraint $E\left[\|\mathbf{x}\|^2\right] = m\sigma_x^2$, where $\|\cdot\|^2$ denotes the squared Euclidean norm, and $\mathbf{w} = [w_1 \cdots w_n]^T$ is a circularly symmetric complex Gaussian vector with the correlation matrix $E\left[\mathbf{w}\mathbf{w}^H\right] = \sigma_w^2 \mathbf{I}_n$. $\mathbf{x}$ and $\mathbf{w}$ are independent of each other, and $\mathbf{I}_n$ denotes the $n \times n$ identity matrix.

Basically, a linear detector is to find an $\hat{\mathbf{x}} \in \Omega^m$ that is closest to the filtered vector $\mathbf{B}^H \mathbf{y}$, i.e.,

$$\hat{\mathbf{x}} = \arg\min_{\mathbf{x} \in \Omega^m} \left\| \mathbf{B}^H \mathbf{y} - \mathbf{x} \right\|^2 = Q\left[\mathbf{B}^H \mathbf{y} \right], \tag{2.4}$$

where $\mathbf{B}^H$ is the receive filter, and $Q[\cdot]$ is the operation of rounding its argument to the nearest

$\hat{\mathbf{x}} \in \Omega^m$. For the MMSE linear detector, $\mathbf{B} = \left[\left(\mathbf{H}^H \mathbf{H} + \dfrac{\sigma_w^2}{\sigma_x^2} \mathbf{I}_m \right)^{-1} \mathbf{H}^H \right]^H$ [20]-[23]. Without

considering the effect of noise, i.e., $\dfrac{\sigma_w^2}{\sigma_x^2} = 0$, the detector degenerates to ZF linear detector, where

inter-symbol interference in $\mathbf{y}$ is cancelled completely. It is well known that linear detectors

suffer from severe noise enhancement in an ill-conditioned channel and have diversity order of

$n - m + 1$ which is less than the full diversity order n [20]-[23].

Successive interference cancellation (SIC) is a popular low-complex non-linear detector.

Firstly, the channel matrix is QR decomposed, i.e., $\mathbf{H} = \mathbf{QR}$, where $\mathbf{Q}^H \mathbf{Q} = \mathbf{I}_m$, and $\mathbf{R}$ is an

upper triangular matrix given by

$$\mathbf{R} = \begin{bmatrix} r_{11} & r_{12} & \cdots & r_{1m} \\ 0 & r_{22} & \cdots & r_{2m} \\ \vdots & \ddots & \ddots & \vdots \\ 0 & 0 & \cdots & r_{mm} \end{bmatrix}. \tag{2.5}$$

The detection is then carried out as

$$\hat{x}_j = Q\left[\frac{1}{r_{jj}} \left(\tilde{y}_j - \sum_{i=j+1}^{m} r_{ji} \hat{x}_i \right) \right], \quad j = m, \cdots 1, \tag{2.6}$$

where $\tilde{\mathbf{y}} \doteq \left[\tilde{y}_1 \cdots \tilde{y}_m \right]^T = \mathbf{Q}^H \mathbf{y}$. SIC reduces the effect of noise enhancement but suffers from error

propagation which can be lessened if the sequence of detection of $x_i, i = 1 \cdots m$ is properly

ordered [22], [23]. With the perfect ordering, SIC is equivalent to the well-known V-BLAST

detector [20], [21]. Ideally, the diversity order of detecting x_j is equal to $n - j + 1$,

$j = m, m - 1, \cdots 1$.

2.2 Channel-Factorization Aided Detection

In the literature, LRAD has been proposed to improve the performance of the traditional reduced-complexity detectors while retains a low complexity [26]-[35]. It was shown in [33], [34] that LRAD achieves full diversity order. Recall that in this paper LRAD will be viewed as a special case of a more general class of detectors, CFAD, where channel factorization can be done with any algorithms including the LLL and Seysen's lattice-reduction algorithms.

Let $\mathbf{H} \doteq [\mathbf{h}_1 \mathbf{h}_2 \cdots \mathbf{h}_m]$, where $\{\mathbf{h}_1, \mathbf{h}_2, \cdots, \mathbf{h}_m\}$ is a set of linearly independent vectors in C^n. The set of points $\Lambda_{\mathbf{H}} = \left\{ \mathbf{v} \mid \mathbf{v} = \sum_{i=1}^{m} \mathbf{h}_i x_i, x_i \in Z \right\}$ is called a lattice of dimension m, generated by the basis $\{\mathbf{h}_1, \mathbf{h}_2, \cdots, \mathbf{h}_m\}$, and $\mathbf{H} \doteq [\mathbf{h}_1 \mathbf{h}_2 \cdots \mathbf{h}_m]$ is the generator matrix. It is clear that different bases can be used to generate the same lattice. In particular, $\mathbf{H}$ and $\widetilde{\mathbf{H}}$ generate the same lattice $\Lambda_{\mathbf{H}}$ if and only if $\mathbf{H} = \widetilde{\mathbf{H}}\mathbf{D}$, where $\mathbf{D}$ is a unimodular matrix [37]. A complex integer matrix $\mathbf{D}$ is called unimodular if $|\det(\mathbf{D})| = 1$. Clearly, $\mathbf{D}^{-1}$ is also a unimodular matrix. In Equation (2.1), the noiseless received signal vector is a lattice point in $\Lambda_{\mathbf{H}}$. Therefore, the detection problem is to find a lattice point in $\Lambda_{\mathbf{H}}$ that is as close as possible to the received signal vector $\mathbf{y}$.

A block diagram of the channel-factorization aided detector (CFAD) is shown in Figure 2.2; the original system in Equation (2.1) is transformed into an equivalent one by factorizing the channel matrix into $\mathbf{H} = \widetilde{\mathbf{H}}\mathbf{D}$, where $\mathbf{D}$ is a unimodular matrix. That is,

$$\mathbf{y} = \mathbf{H}\mathbf{x} + \mathbf{w} = \widetilde{\mathbf{H}}\mathbf{D}\mathbf{x} + \mathbf{w} = \widetilde{\mathbf{H}}\mathbf{z} + \mathbf{w}, \tag{2.7}$$

where $\mathbf{z} = \mathbf{D}\mathbf{x}$ is a symbol vector in the transform domain. If the channel factorization is done with a lattice-reduction algorithm, then it is the well-known LRAD. The key idea of CFAD is

firstly to find a factorization such that $\widetilde{\mathbf{H}}$ is
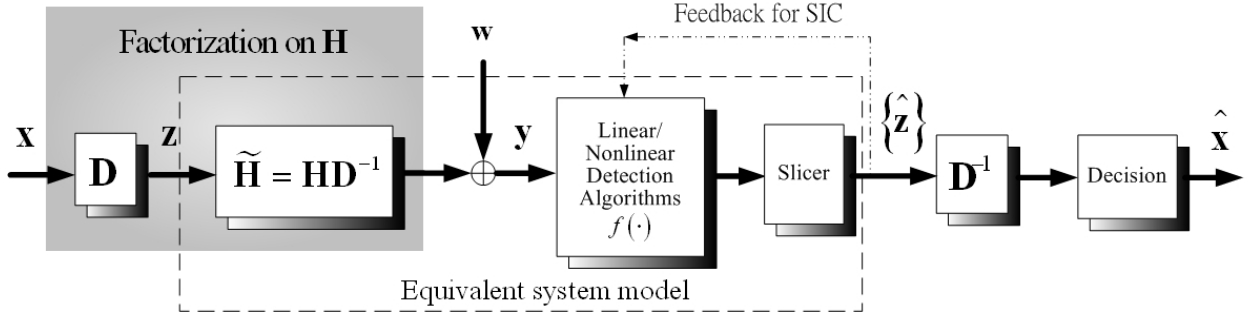
Figure 2.2: A simplified diagram for the channel-factorization aided detection.

better-conditioned than $\mathbf{H}$, then a reduced-complexity detection, i.e., "Slicer", is performed in the $\mathbf{z}$-domain to obtain an initial estimate $\hat{\mathbf{z}}$. The "Slicer" in Figure 2.2 performs the operation of element-wise rounding after a proper shifting and scaling as that given in [32]. Eventually, the estimate is transformed back to the original $\mathbf{x}$-domain to obtain the final estimate

$$\hat{\mathbf{x}} = \arg \min_{\mathbf{x}\in\Omega^m} \left\| \mathbf{D}^{-1}\hat{\mathbf{z}} - \mathbf{x} \right\|^2 . \tag{2.8}$$

Figure 2.3 shows the advantage of CFAD for 2×2 real system. As shown in figure, black points are the set of received noiseless signals. For non-factorized case, that is to detect symbol $\mathbf{x}$, the channel matrix encountered is $\mathbf{H}$ labeled with blue; by contrast, if channel is properly factorized, the channel matrix becomes $\widetilde{\mathbf{H}}$ labeled with red for the detection of transformed symbol $\mathbf{z}$. It is obviously that the performance of detecting symbol $\mathbf{z}$ is better than that of detecting symbol $\mathbf{x}$, because the decision region for the factorized case is square, which results from the fact that the columns of matrix $\widetilde{\mathbf{H}}$ are orthogonal. This illustrates why remarkable performance improvement can be obtained by CFAD.
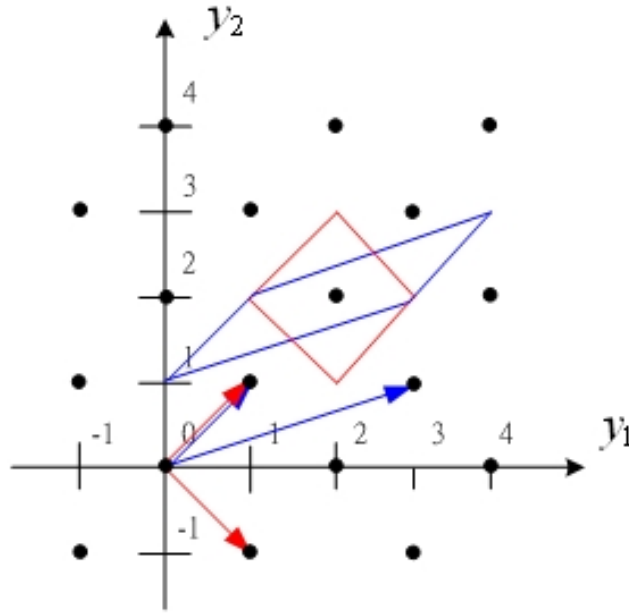
$$y = Hx = \widetilde{\mathbf{H}}\mathbf{D}x = \widetilde{\mathbf{H}}z$$

$$\begin{bmatrix} y_1 \\ y_2 \end{bmatrix} = \begin{bmatrix} 1 & 3 \\ 1 & 1 \end{bmatrix}\begin{bmatrix} x_1 \\ x_2 \end{bmatrix} = \begin{bmatrix} 1 & 1 \\ 1 & -1 \end{bmatrix}\begin{bmatrix} 1 & 2 \\ 0 & 1 \end{bmatrix}\begin{bmatrix} x_1 \\ x_2 \end{bmatrix} = \begin{bmatrix} 1 & 1 \\ 1 & -1 \end{bmatrix}\begin{bmatrix} z_1 \\ z_2 \end{bmatrix}$$

Figure 2.3: An example for the channel factorization

The LLL algorithm is well-known for searching a good factorization $\mathbf{H} = \widetilde{\mathbf{H}}\mathbf{D}$. Through size reduction and reordering of the sequence of basis vectors, a relatively short (orthogonal) basis can be found with a polynomial time complexity [36], [37]. The complex version of the LLL algorithm in [68] is summarized in Table 2.1. The LLL algorithm can be applied to the primal lattice [26]-[32] generated by the generator matrix $\mathbf{H}$, the dual lattice [33], [34] generated by the

generator matrix $\mathbf{H}^{\#} \doteq \left[\left(\mathbf{H}^{H}\mathbf{H}\right)^{-1}\mathbf{H}^{H}\right]^{H}$, and the extended lattice generated by $\underline{\mathbf{H}} \doteq \begin{bmatrix} \mathbf{H} \\ \dfrac{\sigma_w}{\sigma_x}\mathbf{I}_m \end{bmatrix}$

[30]. Seysen's algorithm (SA) is another popular lattice-reduction algorithm for the channel factorization [38], [39]. Since SA reduces the primal and dual lattices simultaneously, it

16

Table 2.1: Complex version of the LLL algorithm

Input: lattice matrix $\mathbf{H} = [\mathbf{h}_1 \mathbf{h}_2 \cdots \mathbf{h}_m] \overset{\text{GSO}}{=} \mathbf{Q}\mathbf{U}^T = [\mathbf{q}_1 \mathbf{q}_2 \cdots \mathbf{q}_m] \begin{bmatrix} 1 & & & & \\ \mu_{2,1} & 1 & & 0 & \\ \mu_{3,1} & \mu_{3,2} & 1 & & \\ \vdots & \vdots & \vdots & \ddots & \\ \mu_{m,1} & \mu_{m,2} & \mu_{m,3} & \cdots & 1 \end{bmatrix}^T$.

Output: $\widetilde{\mathbf{H}}$ and unimodular matrix $\mathbf{T}$ such that $\mathbf{H} = \widetilde{\mathbf{H}}\mathbf{T}$.

---

1. $i = 2$, and $\mathbf{T} = \mathbf{I}_m = \begin{bmatrix} \mathbf{t}_1 \\ \vdots \\ \mathbf{t}_m \end{bmatrix}$

2. while $(i \le m)$ do

3. $\quad \mathbf{h}_i = \mathbf{h}_i - [\![\mu_{i,i\text{-}1}]\!]\mathbf{h}_{i\text{-}1}, \ \mathbf{t}_{i\text{-}1} = \mathbf{t}_{i\text{-}1} + [\![\mu_{i,i\text{-}1}]\!]\mathbf{t}_i$

4. $\quad$ update GSO of $\mathbf{H}$ based on effective procedures in [36]

5. $\quad$ if $\left(\left\| \mathbf{q}_i + \mu_{i,i\text{-}1}\mathbf{q}_{i\text{-}1} \right\|^2 < \delta \left\| \mathbf{q}_{i\text{-}1} \right\|^2 \right)$, then

6. $\quad\quad$ swap $\mathbf{h}_{i\text{-}1}$ and $\mathbf{h}_i$, swap $\mathbf{t}_{i\text{-}1}$ and $\mathbf{t}_i$

7. $\quad\quad$ update GSO of $\mathbf{H}$ based on effective procedures in [36]

8. $\quad\quad i = \max\{2, i\text{-}1\}$

9. $\quad$ else

10. $\quad\quad$ for $j = i\text{-}2$ to 1 do

11. $\quad\quad\quad \mathbf{h}_i = \mathbf{h}_i - [\![\mu_{i,j}]\!]\mathbf{h}_j, \ \mathbf{t}_j = \mathbf{t}_j + [\![\mu_{i,j}]\!]\mathbf{t}_i$

12. $\quad\quad\quad$ update GSO of $\mathbf{H}$ based on effective procedures in [36]

13. $\quad\quad$ end for

14. $\quad\quad i = i+1$

15. $\quad$ end if

16. end while

17. $\widetilde{\mathbf{H}} = \mathbf{H}$

has a similar performance as that of LLL applied to the dual lattice, as to be shown later. Very

recently, it was reported in [35] that the LLL algorithm applying on the dual lattice $\underline{\mathbf{H}}^{\#}$ and the

SA algorithm on $\underline{\mathbf{H}}$ give the best performance if the MMSE detector is used as the low-complexity in Figure 2.2 to obtain the initial estimate $\hat{\mathbf{z}}$. Any reduced-complexity detector, denoted by the function $f(\mathbf{y})$ in Figure 2.2, can be used to obtain the initial estimate $\hat{\mathbf{z}}$. For example, ZF-LD and MMSE-LD in Equation (2.4), or SIC in Equation (2.6) can be used with $\mathbf{H}$ replaced by $\widetilde{\mathbf{H}}$ and $\mathbf{x}$ by $\mathbf{z}$. Furthermore, the slicer is used to lower the detection complexity [32], which is perfectly fine for an infinite constellation because $\mathbf{z} = \mathbf{Dx} \in Z^{m}$ for $\mathbf{x} \in Z^{m}$. For a finite constellation, however, there is boundary error effect; that is, $\mathbf{D}^{-1}\hat{\mathbf{z}}$ may not belong to Ω^{m}. This explains why Equation (2.8) is needed for the final detection.

2.3 Proposed Factorization Algorithms for CFAD Detectors

Traditionally, the LLL and Seysen's algorithms are used in CFAD for the channel factorization $\mathbf{H} = \widetilde{\mathbf{H}}\mathbf{D}$ with no consideration of which type of low-complexity detector is used in the $\mathbf{z}$-domain detection. In this section, we propose a different approach: channel factorization is designed specifically for the CFAD-MMSE detector, and thus improve the detector performance of the detector either in bit error rate or detector complexity over other channel factorization methods in the literature. Furthermore, a low-complexity element-wise candidate list detector is proposed that along with the new MMSE-based channel factorization can be used to approach to within fractional dB of the performance of ML detection.

2.3.1 MMSE Criterion

Let $\mathbf{G}_{MMSE}$ be the MMSE filter for the initial detection in the $\mathbf{z}$-domain, given the

factorization $\mathbf{H} = \widetilde{\mathbf{H}}\mathbf{D}$. It can be shown that

$$\mathbf{G}_{MMSE} = \arg\min_{\mathbf{G}} E\left[\|\mathbf{Gy} - \mathbf{z}\|^2\right] = \mathbf{D}\left(\mathbf{H}^H\mathbf{H} + \frac{\sigma_w^2}{\sigma_x^2}\mathbf{I}_m\right)^{-1}\mathbf{H}^H \tag{2.9}$$

From Appendix A, the covariance matrix of the error vector $\mathbf{G}_{MMSE}\mathbf{y} - \mathbf{z}$ is

$$\begin{aligned}
\mathbf{\Phi}_{MMSE} &\doteq E\left[(\mathbf{G}_{MMSE}\mathbf{y} - \mathbf{z})(\mathbf{G}_{MMSE}\mathbf{y} - \mathbf{z})^H\right] \\
&= \sigma_w^2\mathbf{D}\left(\mathbf{H}^H\mathbf{H} + \frac{\sigma_w^2}{\sigma_x^2}\mathbf{I}_m\right)^{-1}\mathbf{D}^H \\
&= \mathbf{D}\mathbf{A}\mathbf{D}^H
\end{aligned} \tag{2.10}$$

where $\mathbf{A} = \sigma_w^2\left(\mathbf{H}^H\mathbf{H} + \frac{\sigma_w^2}{\sigma_x^2}\mathbf{I}_m\right)^{-1}$ is a positive definite matrix, and the sum MSE (mean square error) is

$$tr(\mathbf{\Phi}_{MMSE}) = tr(\mathbf{D}\mathbf{A}\mathbf{D}^H). \tag{2.11}$$

where $tr(\cdot)$ denotes the sum of the diagonal elements of a square matrix. Using Equations (2.10) and (2.11), our goal is to find the factorization $\mathbf{H} = \widetilde{\mathbf{H}}\mathbf{D}_{opt}$ by solving the following optimization problem

$$\mathbf{D}_{opt} = \arg\min_{\mathbf{D}}\left[tr(\mathbf{D}\mathbf{A}\mathbf{D}^H)\right], \quad \text{s.t. } \mathbf{D} \text{ is a unimodular matix}. \tag{2.12}$$

Note that there are infinite numbers of unimodular matrices in Equation (2.12), and thus finding the optimal solution by exhaustive search is not possible. Here, two types algorithms are proposed to obtain approximate solutions efficiently: one is LLL-based, and the other is greedy-search based with column-wise optimization.

2.3.2 Type-I Algorithms (LLL based)

By applying singular-value-decomposition (SVD), the channel matrix $\mathbf{H}$ can be expressed

as

$$\mathbf{H} = \mathbf{U} \begin{bmatrix} \mathbf{\Delta} \\ \mathbf{0} \end{bmatrix} \mathbf{V}^H, \tag{2.13}$$

where $\mathbf{U}$ and $\mathbf{V}$ are unitary matrices with dimension of $n \times n$ and $m \times m$, respectively, and

$\mathbf{\Delta} = \mathrm{diag}(\Delta_1, \Delta_2, \cdots, \Delta_m)$ is an $m \times m$ diagonal matrix with the singular values

$\Delta_k > 0, \ k = 1, ..., m$. Using Equation (2.13), the matrix $\mathbf{A}$ becomes

$$\mathbf{A} = \mathbf{\Upsilon}^H \mathbf{\Upsilon}, \tag{2.14}$$

where $\mathbf{\Upsilon} = \mathbf{\Gamma}^{1/2} \mathbf{V}^H$ is an $m \times m$ nonsingular matrix, and

$$\mathbf{\Gamma} = \mathrm{diag}\left(\frac{\sigma_w^2 \sigma_x^2}{\Delta_1^2 \sigma_x^2 + \sigma_w^2}, \frac{\sigma_w^2 \sigma_x^2}{\Delta_2^2 \sigma_x^2 + \sigma_w^2}, \cdots, \frac{\sigma_w^2 \sigma_x^2}{\Delta_m^2 \sigma_x^2 + \sigma_w^2} \right). \tag{2.15}$$

More generally, we have the following lemma.

Lemma 1: With $\mathbf{\Upsilon}$ in Equation (2.14), $\mathbf{A} = \mathbf{C}^H \mathbf{C}$ if and only if $\mathbf{C} = \mathbf{P}\mathbf{\Upsilon}$, where $\mathbf{P}^H \mathbf{P} = \mathbf{I}_m$ is

an $l \times m$ matrix with $l \geq m$.

Proof: For the if part, $\mathbf{C}^H \mathbf{C} = (\mathbf{P}\mathbf{\Upsilon})^H \mathbf{P}\mathbf{\Upsilon} = \mathbf{\Upsilon}^H \mathbf{\Upsilon} = \mathbf{A}$. For the only if part, using Equation (2.14),

one gets $\mathbf{C}^H \mathbf{C} = \mathbf{\Upsilon}^H \mathbf{\Upsilon}$. Since $\mathbf{\Upsilon}$ is nonsingular, $\mathbf{\Upsilon}^{-H} \mathbf{C}^H \mathbf{C} \mathbf{\Upsilon}^{-1} = \mathbf{I}_m$. Identify $\mathbf{P} = \mathbf{C}\mathbf{\Upsilon}^{-1}$, the

proof is done.

In addition, $\mathbf{C} = \mathbf{P}\mathbf{\Upsilon}$ is full column-ranked due to that $\mathbf{\Upsilon}$ is nonsingular and $\mathbf{P}$ is full

column-ranked.

Define $\mathbf{D}^H = [\mathbf{d}_1 \mathbf{d}_2 \cdots \mathbf{d}_m]$, that is $\mathbf{d}_k$ is k-th column vector of matrix $\mathbf{D}^H$. Using

$\mathbf{A} = \mathbf{C}^H \mathbf{C}$, the sum MSE becomes

$$\begin{aligned} tr(\mathbf{\Phi}_{MMSE}) &= \sum_{k=1}^{m} \mathbf{d}_k^H \mathbf{C}^H \mathbf{C} \mathbf{d}_k \\ &= \sum_{k=1}^{m} \left\| \mathbf{C}\mathbf{d}_k \right\|^2 \end{aligned}, \tag{2.16}$$

where $\mathbf{Cd}_k, k = 1, \cdots, m$ are lattice points of the lattice $\Lambda_{\mathbf{C}} = \left\{ \mathbf{v} \mid \mathbf{v} = \sum_{k=1}^{m} \mathbf{c}_k x_k, x_k \in \mathbb{Z} \right\}$, generated

by the generator matrix $\mathbf{C} \doteq [\mathbf{c}_1 \cdots \mathbf{c}_m]$. Furthermore, $\mathbf{Cd}_k, k = 1, \cdots, m$ are linearly independent

since $\mathbf{D}^H$ is unimodular and $\mathbf{C}$ is full column-ranked, and therefore $\left\{ \mathbf{Cd}_k \right\}_{k=1}^{m}$ is a basis of the

lattice $\Lambda_{\mathbf{C}}$. Consequently, the optimization problem in Equation (2.12) becomes to find the basis

of $\Lambda_{\mathbf{C}}$ that has the smallest sum squared norm $\sum_{k=1}^{m} \left\| \mathbf{Cd}_k \right\|^2$, which is a well-known lattice

reduction problem. Let $\left\{ \mathbf{c}_{\mathrm{opt},k} \right\}_{k=1}^{m}$ be a basis of $\Lambda_{\mathbf{C}}$ that has the smallest sum squared norm, and

$\mathbf{C}_{\mathrm{opt}} = \left[\mathbf{c}_{\mathrm{opt},1}, \cdots, \mathbf{c}_{\mathrm{opt},m} \right]$. Since $\mathbf{C}_{\mathrm{opt}}$ and $\mathbf{C}$ generate the same lattice, $\mathbf{C} = \mathbf{C}_{\mathrm{opt}} \mathbf{T}_{\mathrm{opt}}$ for a

unimodular matrix $\mathbf{T}_{\mathrm{opt}}$. In addition, $\mathbf{C}_{\mathrm{opt}} = \mathbf{CD}_{\mathrm{opt}}^{H}$, thus $\mathbf{D}_{\mathrm{opt}} = \left(\mathbf{T}_{\mathrm{opt}}^{-1} \right)^{H}$. Given $\mathbf{D}_{\mathrm{opt}}$, the

desirable factorization is $\mathbf{H} = \widetilde{\mathbf{H}}_{\mathrm{opt}} \mathbf{D}_{\mathrm{opt}}$.

The LLL lattice-reduction algorithm will be adopted here as a practical way to search for

$\mathbf{D}_{\mathrm{opt}}$. In this case, if $\widetilde{\mathbf{C}}$ denotes the reduced basis by the LLL algorithm, that is $\mathbf{C} \stackrel{LLL}{=} \widetilde{\mathbf{C}} \mathbf{T}$,

where $\mathbf{T}$ is a unimodular matrix, then the approximate solution is obtained as $\widehat{\mathbf{D}} = \left(\mathbf{T}^{-1} \right)^{H}$ and

$\mathbf{H} = \widetilde{\mathbf{H}} \widehat{\mathbf{D}}$. From Appendix B, it is shown that $\widehat{\mathbf{D}}$ is the same for any decomposition $\mathbf{A} = \mathbf{C}^H \mathbf{C}$,

and thus the detection performance is independent of what particular decomposition result $\mathbf{C}$ is

used. The complete algorithm is summarized in Table 2.2.

Notice that the matrix $\mathbf{A}$ can also be rewritten as

$$\mathbf{A} = \sigma_w^2 \left(\mathbf{H}^H \mathbf{H} + \frac{\sigma_w^2}{\sigma_x^2} \mathbf{I}_m \right)^{-1} = \sigma_w^2 \left(\underline{\mathbf{H}}^H \underline{\mathbf{H}} \right)^{-1} = \sigma_w^2 \left(\underline{\mathbf{H}}^H \underline{\mathbf{H}} \right)^{-1} \underline{\mathbf{H}}^H \underline{\mathbf{H}} \left(\underline{\mathbf{H}}^H \underline{\mathbf{H}} \right)^{-1} = \mathbf{E}^H \mathbf{E},$$

(2.17)

<div align="center">Table 2.2: The Proposed Type-I Algorithm</div>

Input: $\mathbf{H}$, σ_x^2, σ_w^2

Output: $\mathbf{D}$, a unimodular matrix.

1: Compute $\mathbf{A} = \sigma_w^2 \left(\mathbf{H}^H \mathbf{H} + \dfrac{\sigma_w^2}{\sigma_x^2} \mathbf{I}_m \right)^{-1}$.

2: Perform the decomposition $\mathbf{A} = \mathbf{C}^H \mathbf{C}$ (for example by Cholesky decomposition).

3: Perform the LLL algorithm to obtain $\mathbf{C} \overset{LLL}{=} \widetilde{\mathbf{C}} \mathbf{T}$.

4: Identify $\mathbf{D} = \left(\mathbf{T}^{-1} \right)^H$.

---

where $\mathbf{E} = \sigma_w \underline{\mathbf{H}} \left(\underline{\mathbf{H}}^H \underline{\mathbf{H}} \right)^{-1}$ and $\underline{\mathbf{H}}$ is extended channel matrix in [30], [35]. In fact, $\mathbf{E}$ is the

dual matrix of $\underline{\mathbf{H}}$ scaled by σ_w, i.e., $\mathbf{E} = \sigma_w \left(\left(\underline{\mathbf{H}}^H \underline{\mathbf{H}} \right)^{-1} \underline{\mathbf{H}}^H \right)^H = \sigma_w \underline{\mathbf{H}}^\#$. Therefore, applying the

LLL algorithm, we have $\mathbf{E} \overset{LLL}{=} \widetilde{\mathbf{E}} \underline{\mathbf{T}}$ and $\underline{\mathbf{H}}^\# \overset{LLL}{=} \widetilde{\underline{\mathbf{H}}} \underline{\mathbf{T}}$. In other words, the scheme $\underline{\mathbf{H}}^\# \overset{LLL}{=} \widetilde{\underline{\mathbf{H}}} \underline{\mathbf{T}}$

used in [35] is a member of the proposed Type-I algorithms. But, since $\underline{\mathbf{H}}^\#$ has the dimension of

$(n+m) \times m$, the complexity of applying LLL algorithm on $\underline{\mathbf{H}}^\#$ is more complex than the one on

$\mathbf{C}$, which has the dimension $m \times m$.

2.3.3 Type-II Algorithms (greedy-search based)

A greedy-search algorithm is proposed here as an alternative to Type-I to obtain an

approximate solution of Equation (2.12). As to be shown later, this algorithm performs better than

Type-I and has a fixed computational complexity which is considered to be advantageous in

hardware implementation.

Using $\mathbf{D}^H = \begin{bmatrix} \mathbf{d}_1 \mathbf{d}_2 \cdots \mathbf{d}_m \end{bmatrix}$, the sum MSE can be rewritten as

$$tr(\boldsymbol{\Phi}_{MMSE}) = \sum_{k=1}^{m} \mathbf{d}_k^H \mathbf{A} \mathbf{d}_k = \sum_{k=1}^{m} mse_k , \qquad (2.18)$$

where $mse_k \doteq \mathbf{d}_k^H \mathbf{A} \mathbf{d}_k$. In this algorithm, firstly we observe that $mse_k \doteq \mathbf{d}_k^H \mathbf{A} \mathbf{d}_k$ depending only

on $\mathbf{d}_k$, $k = 1, ..., m$. Therefore, the updating of the matrix $\mathbf{D}^H$ can be done one column at a time

to minimize mse_k, from the first to the last column. This iteration can be repeated again and

again until no improvement is possible, starting from $\mathbf{D}^H = \mathbf{I}_m$.

Without loss of generality, consider that the kth-column of $\mathbf{D}^H$ is to be updated. A new

column vector $\mathbf{d}_{k,\text{new}}$ is proposed as

$$\mathbf{d}_{k,\text{new}} = \alpha_1 \mathbf{d}_1 + \cdots + \alpha_{k-1} \mathbf{d}_{k-1} + \mathbf{d}_k + \alpha_{k+1} \mathbf{d}_{k+1} + \cdots + \alpha_m \mathbf{d}_m , \qquad (2.19)$$

where $\{\alpha_m\}_{m \neq k}$ are parameters to be optimized to lower mse_k. It is shown in Appendix C that

$\mathbf{D}_{\text{new}}^H = \begin{bmatrix} \mathbf{d}_1, ..., \mathbf{d}_{k-1}, \mathbf{d}_{k,\text{new}}, \mathbf{d}_{k+1}, ..., \mathbf{d}_m \end{bmatrix}$ is unimodular provided that $\mathbf{D}^H$ is unimodular, and $\{\alpha_m\}_{m \neq k}$

are complex integers. With this new $\mathbf{d}_{k,\text{new}}$, $mse_{k,\text{new}}$ is given by

$$\begin{aligned} mse_{k,\text{new}} &= \mathbf{d}_{k,\text{new}}^H \mathbf{A} \mathbf{d}_{k,\text{new}} \\ &= \begin{bmatrix} \boldsymbol{\alpha}_1^H & 1 & \boldsymbol{\alpha}_2^H \end{bmatrix} \mathbf{R} \begin{bmatrix} \boldsymbol{\alpha}_1 \\ 1 \\ \boldsymbol{\alpha}_2 \end{bmatrix} , \end{aligned} \qquad (2.20)$$

where $\boldsymbol{\alpha}_1 = \begin{bmatrix} \alpha_1 \cdots \alpha_{k-1} \end{bmatrix}^T$, $\boldsymbol{\alpha}_2 = \begin{bmatrix} \alpha_{k+1} \cdots \alpha_m \end{bmatrix}^T$, and $\mathbf{R} = \mathbf{DAD}^H$. Define $\mathbf{D}_1 = \begin{bmatrix} \mathbf{d}_1^H \\ \vdots \\ \mathbf{d}_{k-1}^H \end{bmatrix}$ and

$\mathbf{D}_2 = \begin{bmatrix} \mathbf{d}_{k+1}^H \\ \vdots \\ \mathbf{d}_m^H \end{bmatrix}$. The matrix $\mathbf{R}$ can be partitioned as

$$
\mathbf{R} = \begin{bmatrix} \mathbf{D}_1\mathbf{A}\mathbf{D}_1^H & \mathbf{D}_1\mathbf{A}\mathbf{d}_k & \mathbf{D}_1\mathbf{A}\mathbf{D}_2^H \\ \mathbf{d}_k^H\mathbf{A}\mathbf{D}_1^H & \mathbf{d}_k^H\mathbf{A}\mathbf{d}_k & \mathbf{d}_k^H\mathbf{A}\mathbf{D}_2^H \\ \mathbf{D}_2\mathbf{A}\mathbf{D}_1^H & \mathbf{D}_2\mathbf{A}\mathbf{d}_k & \mathbf{D}_2\mathbf{A}\mathbf{D}_2^H \end{bmatrix} = \begin{bmatrix} \mathbf{R}_{1,1} & \mathbf{R}_{1,2} & \mathbf{R}_{1,3} \\ \mathbf{R}_{2,1} & \mathbf{R}_{2,2} & \mathbf{R}_{2,3} \\ \mathbf{R}_{3,1} & \mathbf{R}_{3,2} & \mathbf{R}_{3,3} \end{bmatrix},
\tag{2.21}
$$

And Equation (2.20) becomes

$$
\begin{aligned}
mse_{k,new} &= \begin{bmatrix} \boldsymbol{\alpha}_1^H & 1 & \boldsymbol{\alpha}_2^H \end{bmatrix} \begin{bmatrix} \mathbf{R}_{1,1} & \mathbf{R}_{1,2} & \mathbf{R}_{1,3} \\ \mathbf{R}_{2,1} & \mathbf{R}_{2,2} & \mathbf{R}_{2,3} \\ \mathbf{R}_{3,1} & \mathbf{R}_{3,2} & \mathbf{R}_{3,3} \end{bmatrix} \begin{bmatrix} \boldsymbol{\alpha}_1 \\ 1 \\ \boldsymbol{\alpha}_2 \end{bmatrix} \\
&= \begin{bmatrix} \boldsymbol{\alpha}_1^H & \boldsymbol{\alpha}_2^H \end{bmatrix} \begin{bmatrix} \mathbf{R}_{1,1} & \mathbf{R}_{1,3} \\ \mathbf{R}_{3,1} & \mathbf{R}_{3,3} \end{bmatrix} \begin{bmatrix} \boldsymbol{\alpha}_1 \\ \boldsymbol{\alpha}_2 \end{bmatrix} + \begin{bmatrix} \boldsymbol{\alpha}_1^H & \boldsymbol{\alpha}_2^H \end{bmatrix} \begin{bmatrix} \mathbf{R}_{1,2} \\ \mathbf{R}_{3,2} \end{bmatrix} + \begin{bmatrix} \mathbf{R}_{2,1} & \mathbf{R}_{2,3} \end{bmatrix} \begin{bmatrix} \boldsymbol{\alpha}_1 \\ \boldsymbol{\alpha}_2 \end{bmatrix} + \mathbf{R}_{2,2}, \\
&= \boldsymbol{\alpha}_{\underline{k}}^H \mathbf{S}_{2,2}\boldsymbol{\alpha}_{\underline{k}} + \boldsymbol{\alpha}_{\underline{k}}^H \mathbf{S}_{2,1} + \mathbf{S}_{1,2}\boldsymbol{\alpha}_{\underline{k}} + \mathbf{S}_{1,1}
\end{aligned}
$$

$$
\tag{2.22}
$$

where $\boldsymbol{\alpha}_{\underline{k}} = \begin{bmatrix} \boldsymbol{\alpha}_1 \\ \boldsymbol{\alpha}_2 \end{bmatrix}$, $\mathbf{S}_{2,2} = \begin{bmatrix} \mathbf{R}_{1,1} & \mathbf{R}_{1,3} \\ \mathbf{R}_{3,1} & \mathbf{R}_{3,3} \end{bmatrix}$, $\mathbf{S}_{2,1} = \begin{bmatrix} \mathbf{R}_{1,2} \\ \mathbf{R}_{3,2} \end{bmatrix}$, $\mathbf{S}_{1,2} = \begin{bmatrix} \mathbf{R}_{2,1} & \mathbf{R}_{2,3} \end{bmatrix}$ and $\mathbf{S}_{1,1} = \mathbf{R}_{2,2}$.

By differentiating $mse_{k,new}$ with respect to $\boldsymbol{\alpha}_{\underline{k}}$ and setting the result equal to zero, the optimal vector of $\boldsymbol{\alpha}_{\underline{k}}$, $\boldsymbol{\alpha}_{\underline{k},opt}$, is obtained by

$$
\mathbf{S}_{2,2}\boldsymbol{\alpha}_{\underline{k},opt} = -\mathbf{S}_{2,1}.
\tag{2.23}
$$

Furthermore, define $\mathbf{D}_{\underline{k}} \doteq \begin{bmatrix} \mathbf{D}_1 \\ \mathbf{D}_2 \end{bmatrix}$ be the matrix obtained by deleting the k-th row of the matrix $\mathbf{D}$.

Then

$$
\mathbf{S}_{2,2} = \begin{bmatrix} \mathbf{R}_{1,1} & \mathbf{R}_{1,3} \\ \mathbf{R}_{3,1} & \mathbf{R}_{3,3} \end{bmatrix} = \mathbf{D}_{\underline{k}}\mathbf{A}\mathbf{D}_{\underline{k}}^H.
\tag{2.24}
$$

Since $\mathbf{D}_{\underline{k}}$ has full row-rank (because $\mathbf{D}$ has full row-rank), from Appendix D, $\mathbf{S}_{2,2}$ is positive definite. Thus,

$$
\boldsymbol{\alpha}_{\underline{k},opt} = \begin{bmatrix} \boldsymbol{\alpha}_{1,opt} \\ \boldsymbol{\alpha}_{2,opt} \end{bmatrix} = -\mathbf{S}_{2,2}^{-1}\mathbf{S}_{2,1},
\tag{2.25}
$$

and

$$\mathbf{d}_{k,\text{new}} = \mathbf{D}^H \begin{bmatrix} \boldsymbol{\alpha}_{1,\text{opt}} \\ 1 \\ \boldsymbol{\alpha}_{2,\text{opt}} \end{bmatrix}. \tag{2.26}$$

Generally, the elements of $\boldsymbol{\alpha}_{k,\text{opt}}$ are not complex integers and thus need to be rounded to ones in order to keep $\mathbf{D}_{new}^H$ a unimodular matrix (see Appendix C). Denote $[\![\boldsymbol{\alpha}_{\underline{k},\text{opt}}]\!]_j$ be the rounding operation on the jth element of the vector $\boldsymbol{\alpha}_{\underline{k},\text{opt}}$, where more than one rounded values can be retained in order to improve performance, $\psi_{[\boldsymbol{\alpha}_{\underline{k}}]_j}$ be the set of retained complex integers in the rounding $[\![\boldsymbol{\alpha}_{\underline{k},\text{opt}}]\!]_j$, and $\Psi_{\boldsymbol{\alpha}_{\underline{k}}} = \left\{ \boldsymbol{\alpha}_{\underline{k}} = [\alpha_1 \cdots \alpha_{k-1} \alpha_{k+1} \cdots \alpha_m]^T, \ \alpha_j \in \psi_{[\boldsymbol{\alpha}_{\underline{k}}]_j} \right\}$. Then, the final $\boldsymbol{\alpha}$ to be used in updating can be obtained by

$$\boldsymbol{\alpha}^{\text{upd}} = \arg \min_{\boldsymbol{\alpha}_{\underline{k}} \in \Psi_{\boldsymbol{\alpha}_{\underline{k}}}} \begin{bmatrix} \boldsymbol{\alpha}_1^H & 1 & \boldsymbol{\alpha}_2^H \end{bmatrix} \mathbf{R} \begin{bmatrix} \boldsymbol{\alpha}_1 \\ 1 \\ \boldsymbol{\alpha}_2 \end{bmatrix} \tag{2.27}$$

In our experience with extensive simulations, $\left| \psi_{[\boldsymbol{\alpha}_{\underline{k}}]_j} \right| > 2$ provides very little improvement, where $\left| \psi_{[\boldsymbol{\alpha}_{\underline{k}}]_j} \right|$ is the cardinality of the set $\psi_{[\boldsymbol{\alpha}_{\underline{k}}]_j}$. Therefore, $\left| \psi_{[\boldsymbol{\alpha}_{\underline{k}}]_j} \right| = 2, \ \forall j$ will be used in all discussions regarding Type-II algorithms. Consider the example of $m = n = 4$. If $\boldsymbol{\alpha}_{\underline{k},\text{opt}} = [-0.3 + 0.6i, \ 0.4 - 0.1i, \ 0.7 + 0.9i]^T$, where $i = \sqrt{-1}$, then $\psi_{[\boldsymbol{\alpha}_{\underline{k}}]_1} = \{i, \ 0\}$, and $\psi_{[\boldsymbol{\alpha}_{\underline{k}}]_2} = \{0, \ 1\}$, and $\psi_{[\boldsymbol{\alpha}_{\underline{k}}]_3} = \{1 + i, \ i\}$, and it leads to

$$\Psi_{\boldsymbol{\alpha}_{\underline{k}}} = \left\{ \begin{bmatrix} i \\ 0 \\ 1+i \end{bmatrix}, \begin{bmatrix} i \\ 0 \\ i \end{bmatrix}, \begin{bmatrix} i \\ 1 \\ 1+i \end{bmatrix}, \begin{bmatrix} i \\ 1 \\ i \end{bmatrix}, \begin{bmatrix} 0 \\ 0 \\ 1+i \end{bmatrix}, \begin{bmatrix} 0 \\ 0 \\ i \end{bmatrix}, \begin{bmatrix} 0 \\ 1 \\ 1+i \end{bmatrix}, \begin{bmatrix} 0 \\ 1 \\ i \end{bmatrix} \right\}. \tag{2.28}$$

Finally, the new update of $\mathbf{d}_k$ is given by $\mathbf{d}_{k,\text{upd}} = \mathbf{D}^H \left[\left(\boldsymbol{\alpha}_1^{\text{upd}} \right)^H \ 1 \ \left(\boldsymbol{\alpha}_2^{\text{upd}} \right)^H \right]^H$, and $mse_{k,\text{upd}} = \mathbf{d}_{k,\text{upd}}^H \mathbf{A} \mathbf{d}_{k,\text{upd}}$, if $mse_{k,\text{upd}} < mse_k$. Otherwise, no update is performed and $\mathbf{d}_k$ remains

no change. The complete algorithm is summarized in Table 2.3, where the algorithm is terminated if the maximum number of iteration N_I is reached. It is worthy to note that since at each step of updating $mse_{k,\mathrm{upd}} \leq mse_k$ and the minimal mse_k is bounded below, the algorithm converges, although it may not converge to the minimal mse_k.

2.3.4 Complexity Analysis for Channel Factorization Algorithms

The complexity of different channel factorization algorithms, including LLL, SA, and the proposed algorithms, is analyzed in this sub-section based on the parameters of m, n, , N_I, $\left| \psi_{\left[a_{\underline{k}}\right]_j} \right| = \kappa$, and $|\Omega|$. Since the detailed complexity calculation is quite tedious, only the final results are summarized here. Table 2.4 summaries the complexity analysis along with that of other algorithms considered in this work. In this analysis, the complexity of an algorithm is divided into two parts: the initialization and main-body parts, where the complexity of Cholesky decomposition, Gram Schmidt Orthogonalization (GSO) and matrix inversion are those given in [69]. Note that for Type-I algorithm, because the QR decomposition [64] for the upper triangular matrix $\mathbf{C}$ is readily available with $\mathbf{Q} = \mathbf{I}_m$, and $\mathbf{R} = \mathbf{C}$, the complexity of GSO operation is reduced significantly. Table 2.5 gives the complexity for obtaining $\mathbf{d}_{k,\mathrm{upd}}$ in Type-II algorithms which is used to calculate the main-body complexity of the Type-II algorithm. Since the updating needs to be done m times in each iteration, the complexity of the main-body part is $m \cdot N_I$ times of that given in Table 2.5. The complexity of the MMSE detector is also calculated where the calculation is divided into three parts as given in Table 2.6.

Table 2.3: The Proposed Type-II Algorithm

Input: $\mathbf{H}$, σ_x^2, σ_w^2, $\mathbf{A}$, $\mathbf{D}^H = \mathbf{I}_m$ and N_I, the maximum number of iterations.

Output: $\mathbf{D}^H$, a unimodular matrix.

1: $i = 0$

2: while $\left(i < N_I \right)$ do

3:      for $k = 1$ to m do

4:          $\boldsymbol{\alpha}_{\underline{k},\mathrm{opt}} = -\mathbf{S}_{2,2}^{-1}\mathbf{S}_{2,1}$, and $\boldsymbol{\alpha}^{\mathrm{upd}} = \arg \min_{\boldsymbol{\alpha}_{\underline{k}} \in \Psi_{\boldsymbol{\alpha}_{\underline{k}}}} \begin{bmatrix} \boldsymbol{\alpha}_1^H & 1 & \boldsymbol{\alpha}_2^H \end{bmatrix} \mathbf{R} \begin{bmatrix} \boldsymbol{\alpha}_1 \\ 1 \\ \boldsymbol{\alpha}_2 \end{bmatrix}$

5:          $\mathbf{d}_{k,\mathrm{upd}} = \mathbf{D}^H \left[\left(\boldsymbol{\alpha}_1^{\mathrm{upd}} \right)^H \ 1 \ \left(\boldsymbol{\alpha}_2^{\mathrm{upd}} \right)^H \right]^H$, and $mse_{k,\mathrm{upd}} = \mathbf{d}_{k,\mathrm{upd}}^H \ \mathbf{A} \ \mathbf{d}_{k,\mathrm{upd}}$

6:          if $\left(mse_{k,\mathrm{upd}} < mse_k \right)$, then

7:             $\mathbf{d}_k = \mathbf{d}_{k,\mathrm{upd}}$, $mse_k = mse_{k,\mathrm{upd}}$

8:          end if

9:      end for

10:    if (no update for all $k = 1$ to m), then

11:       $i = N_I$

12:    else

13:       $i = i + 1$

14:    end if

15: end while

27

Table 2.4: Computational complexity of different channel factorization algorithms.

Algorithms	Computational Complexity					
	Initialization			Main-body of the Algorithm		
	Operations	Number of real multiplications	Number of real additions	Operations	Number of real multiplications	Number of real additions
LLL-extended	GSO for $\underline{\mathbf{H}}$	$4n \cdot m^2 + 4m^3$ $+2m^2 + 6m$	$4n \cdot m^2 + 4m^3$ $+m^2 + 3m$	LLL	variable	variable
SA-extended	Calculation of $\underline{\mathbf{H}}^H \underline{\mathbf{H}}$ and $\left(\underline{\mathbf{H}}^H \underline{\mathbf{H}}\right)^{-1}$	$2n \cdot m^2 + 2n \cdot m$ $2m^3 + 2m^2$	$2n \cdot m^2 + 2n \cdot m$ $2m^3 + 2m^2$	SA	variable	variable
DLLL-extended	Calculation of $\underline{\mathbf{H}}^{\#}$	$6n \cdot m^2 + 2n \cdot m$ $2m^3 + 2m^2$	$6n \cdot m^2 + 2n \cdot m$ $2m^3 + 2m^2$	LLL	variable	variable
	GSO for $\underline{\mathbf{H}}^{\#}$	$4n \cdot m^2 + 4m^3$ $+2m^2 + 6m$	$4n \cdot m^2 + 4m^3$ $+m^2 + 3m$	Calculation of $\left(\underline{\mathbf{T}}^{-1}\right)^H$	$2m^3 + 2m^2$	$2m^3 + 2m^2$
Type-I Algorithms	Calculation of $\mathbf{A}$	$2n \cdot m^2 + 2n \cdot m$ $2m^3 + 2m^2$	$2n \cdot m^2 + 2n \cdot m$ $2m^3 + 2m^2$	LLL	variable	variable
	Calculation of $\mathbf{C}$	$\dfrac{2m^3}{3}$	$\dfrac{2m^3}{3}$			
	GSO for $\mathbf{C}$	$2m^2 + 6m$	$m^2 + 3m$	Calculation of $\left(\mathbf{T}^{-1}\right)^H$	$2m^3 + 2m^2$	$2m^3 + 2m^2$
Type-II Algorithms	Calculation of $\mathbf{A}$	$2n \cdot m^2 + 2n \cdot m$ $2m^3 + 2m^2$	$2n \cdot m^2 + 2n \cdot m$ $2m^3 + 2m^2$	N_I and $\left\|\psi_{\left[\boldsymbol{a}_{\underline{k}}\right]_j}\right\| = \kappa$	$\dfrac{N_I}{3}\left(\begin{array}{l}2m^4 + 6m^3 + \\ 6m^2 - 14m\end{array}\right)$	$\dfrac{N_I}{3}\left(\begin{array}{l}2m^4 + 18m^3 - 6m^2 - \\ 14m + 18m \cdot \left(\kappa^{m-1} - 1\right)\end{array}\right)$

2.3.5 Element-Wise Candidate-List (EWCL) Detection

Here, a simple EWCL detection is proposed that along with the proposed channel factorization can be used to approach closely to the ML performance. Specifically, the K most closest complex integers to $[\mathbf{G}_{MMSE}\mathbf{y}]_k$, denoted as the set Ψ_k, are retained as the candidate symbols for detecting z_k, $k = 1, \cdots, m$, where $\mathbf{G}_{MMSE} = \mathbf{D}\left(\mathbf{H}^H\mathbf{H} + \dfrac{\sigma_w^2}{\sigma_x^2}\mathbf{I}_m\right)^{-1}\mathbf{H}^H$, that is, MMSE-LD is employed as the low-complexity detector. Let $\Psi_\mathbf{z}$ be the corresponding set of candidate signal vectors in the transform domain; that is $\Psi_\mathbf{z} = \left\{\tilde{\mathbf{z}} = \begin{bmatrix}\tilde{z}_1 & \tilde{z}_2 & \cdots & \tilde{z}_m\end{bmatrix}^T, \tilde{z}_k \in \Psi_k\right\}$. Then, the decision for the EWCL detection is given by

$$\hat{\mathbf{x}} = \arg \min_{\mathbf{x} \in \Psi_\mathbf{x}} \|\mathbf{y} - \mathbf{H}\mathbf{x}\|^2, \tag{2.29}$$

where $\Psi_\mathbf{x} = \left\{\tilde{\mathbf{x}} \mid \tilde{\mathbf{x}} = \arg \min_{\mathbf{x} \in \Omega^m} \|\mathbf{D}^{-1}\tilde{\mathbf{z}} - \mathbf{x}\|^2, \text{ and } \tilde{\mathbf{z}} \in \Psi_\mathbf{z}\right\}$. As to be shown in the next section, $K = 2$ is enough to approach closely to the ML performance.

Table 2.5: Computational complexity for obtaining $\mathbf{d}_{k,\text{upd}}$ in Type-II algorithms with $\left|\psi_{[\mathbf{\alpha}_k]_j}\right| = \kappa$

Algorithm	Computational complexity of $\mathbf{d}_{k,\text{upd}}$		
	Operations	Number of real multiplications	Number of real additions
Type-II Algorithms	Solve linear equation set for $\mathbf{\alpha}_{k,\text{opt}}$ in (21)	$\dfrac{2(m-1)^3}{3}$	$\dfrac{2(m-1)^3}{3}$
	Obtain $\mathbf{\alpha}^{\text{upd}}$ in (25)	$4m^2 - 4$	$4m^2 - 4 + 6 \cdot (\kappa^{m-1} - 1)$
	Obtain integer vector $\mathbf{d}_{k,\text{upd}}$	0	$4m^2 - 4m$

Table 2.6: Computational complexity of MIMO detector

Algorithm	Computational complexity of MIMO detector		
	Operations	Number of real multiplications	Number of real additions
MIMO detector in Figure 2.2	Calculation of $\mathbf{G}_{MMSE}$ in (7) and $\mathbf{D}^{-1}$	$8n \cdot m^2 + 2m^3 + 2m^2$	$8n \cdot m^2 + 2m^3 + 2m^2$
	Calculation of $\mathbf{G}_{MMSE}\mathbf{y}$ and $\mathbf{D}^{-1}\hat{\mathbf{z}}$:	$4n \cdot m + 4m^2$	$4n \cdot m + 4m^2$
	Obtain $\hat{\mathbf{x}}$ by (6)	$4m \cdot |\Omega|$	$4m \cdot |\Omega|$

2.4 Simulation Results

This section provides simulations to compare the proposed algorithms and those in the literature in the aspects of performance and complexity for the CFAD detectors. In the simulations, the data vectors $\mathbf{x}$ are transmitted on a frame-by-frame basis, with 200 data vectors per frame. Total of 10^4 frames are simulated. Signal constellation is fixed to 16QAM for easy comparisons between cases with different antenna numbers, although similar conclusions can be drawn for other constellation sizes according to our results not shown here. The channel is block faded; that is, $\mathbf{H}$ remains unchanged over a frame and changes independently from frame to frame. Signal to noise power ratio (SNR) is defined as $m \cdot \sigma_x^2 / \sigma_w^2$. A total of five factorization algorithms are considered, including the LLL (LLL-extended [30]) and Syesen's algorithms

(SA-extended [35], [39]) working on $\underline{\mathbf{H}}$, the LLL algorithm working on the dual matrix of $\underline{\mathbf{H}}$ (DLLL-extended [34][35][34,35]), and the proposed Type-I and Type-II algorithms. It has been shown in [35] that reduction working on $\underline{\mathbf{H}}$ outperforms that on $\mathbf{H}$. Therefore, only those algorithms working on $\underline{\mathbf{H}}$ are compared here. The complex version of the LLL algorithm in Table 2.1 (with $\delta = 0.999$) is used in all channel factorization methods that use LLL, where $\llbracket \cdot \rrbracket$ stands for the operation of rounding its element to the nearest complex integer. The Cholesky decomposition is used to obtain $\mathbf{A} = \mathbf{C}^H \mathbf{C}$ in Type-I algorithm, and $\left| \psi_{\left[\boldsymbol{a}_k \right]_j} \right| = \kappa = 2$ in Type-II algorithm.

The bit-error-rate (BER) for CFAD-MMSE-LD in uncorrelated MIMO channels ($\rho = 0.0$) are compared first. Figure 2.4 shows the effect of iteration number N_I on the BER performance of Type-II Algorithm for the case of $m = n = 6$. As can be seen, there is almost no performance improvement with $N_I > 3$. Consequently, we use $N_I = 3$ for the subsequent comparisons. Figure 2.5, Figure 2.6, Figure 2.7, and Figure 2.8 show the comparisons between different channel factorizations for the cases of $m = n = 2$, $m = n = 4$, $m = n = 6$, and $m = n = 8$ respectively. In these figures, the performance of conventional (non-factorized) MMSE detector is also provided for reference. With smaller numbers of antennas, e.g., $m = n = 2, 4$, all the considered channel factorization algorithms perform similarly especially for $m = n = 2$; the CFAD, however, provides significant improvement over the conventional MMSE detector. As expected, DLLL-extended and Type-I have the same performance because DLLL-extended is a member of the Type-I algorithms, as discussed in the previous Section. SA-extended performs closely to Type-I and outperforms LLL-extended by about 1.5-2.5 dB at $\mathrm{BER} = 10^{-4}$ for $m = n = 6, 8$. Type-II has the best performance with a 0.5 dB gain margin over Type-I (DLLL-extended) and SA-extended. In Figure 2.6, Figure 2.7, and Figure 2.8, the performance of the best-performed pre-coder for un-coded[1] system proposed in [72] is also given for comparison purpose. Clearly, the pre-coder's performance is inferior to that of the proposed CFAD methods.

In [71], [72], the performance improvement with pre-coding was shown to be much higher for the cases of $m > n$.

The comparisons over the correlated MIMO channels ($\rho = 0.6$) are shown in Figure 2.9 for the case of $m = n = 8$. As shown in the figure, the channel correlation degrades the performance of the conventional MMSE detector very dramatically. In addition, Type-II outperforms Type-I (DLLL-extended) and SA-extended by about 0.7 dB. In Figure 2.10, we compare $E_{\mathbf{H}}[mse_{\max}]$ between different algorithms, where $mse_{\max} = \max_k\{mse_k\}$ is the worst square error among all the receive branches, and $E_{\mathbf{H}}[\cdot]$ denotes the average operation over $\mathbf{H}$. $mse_{\max}$ dominates the BER performance. As is shown, Type-II shows its superiority over others.

Figure 2.11 is an example of computational complexity comparison between different channel factorizations, where the empirical CDF (cumulative density function) of the number of real multiplications is shown for $m = n = 6$, SNR = 28 dB, ρ=0.0 . Since the hardware implementation cost of a multiplication is much higher than that of an addition [70], only multiplications is taken into consideration here for complexity comparison. Noticeably, the LLL-based methods (LLL-extended, DLLL-extended and Type-I) and SA-extended all have a variable complexity; Type-I has the less complexity, then, LLL-extended, DLLL-extended and SA-extended. The same order of complexity is observed for other cases not shown here. In this specific example, Type-II is more complex than LLL and SA-based algorithms for about 35% of the channel realizations. Nevertheless, Type-II has a fixed computational complexity which is considered to be advantageous in hardware implementation.

---

1. Note that the "code" of "pre-coder" and "pre-coding" means spatial beam-forming at the transmitter. On the other hand, the "code" of "un-coded system" means forward error correction coding.

In this following, the complexity of MIMO receiver (channel factorization plus MMSE detection) is compared specifically when Type-I, SA-extended and DLLL-extended are employed as the factorization algorithm. Recall that these algorithms have a similar BER performance as shown in Figure 2.5-Figure 2.9. The comparison is made from two aspects: *hardware complexity* and *computational complexity per data vector*. For data vectors where pilots are located, both channel factorization and MMSE detection are required to be performed, and, therefore, for a fixed hardware clock rate, extra circuitry is needed for the computation of the factorization algorithm, and that increases hardware complexity. Table 2.7 shows the hardware complexity ratio of channel factorization to overall MIMO receiver for the considered factorization algorithms. As is seen, the ratio ranges from 44% to 74%. Therefore, how to reduce the complexity of channel factorization algorithm is an important issue. In addition, from Table 2.7, it can be shown that the saving of *hardware complexity* of overall MIMO receiver offered by Type-I ranges from 21% to 43 %. For example, the saving for SA-extended for the case of $P\{Q \le q\} = 0.5$ is $\frac{(5804 + 2904) - (2772 + 2904)}{5804 + 2904} = 34\%$.

The *computational complexity per data vector*, evaluated by the number of real multiplications per data vector $\frac{N_{cf}}{p} + N_{MIMO}$, is also employed for comparisons, where N_{cf} and N_{MIMO} are the number of real multiplication for the channel factorization algorithm and the MMSE MIMO detector, respectively, and p is the number of data vectors in a frame. Figure 2.12 is such a comparison for $P\{Q \le q\} = 0.9$. Similar results are observed for 10 and 50 percentiles although they are not shown here for brevity. As is shown, the complexity saving by Type-I is quite significant for small p. For example, for $p = 6$ the savings are $\frac{4307 - 3479}{4307} = 19\%$ and $\frac{3887 - 3479}{3887} = 11\%$ for SA-extended, and DLLL-extended respectively. As expected, the complexity saving becomes smaller for larger p.

In practical mobile cellular systems, channel estimation is usually done for every 0.5 to 1 ms

in order to cover mobility up to 350 km/hour [75]-[76]. For example, in the 3GPP-LTE specification, there are 7 (OFDM) symbols in a slot (0.5 ms) where time-frequency multiplexed pilots are used for the cell-specific channel estimation [75]. Also, in the IEEE 802.16m specification, there are 5 to 7 (OFDM) symbols in a sub-frame (around 1ms) where time-frequency multiplexed pilots are used for channel estimation. In this type of systems, Type-I algorithm is particular useful. In wireless LAN systems, on the other hand, the so-called preamble-based training is employed where pilot signals are placed at the beginning of a data packet. In this case, if the packet size p is large, says over 30, the saving provided by Type-I becomes quite small.

Table 2.7: Hardware complexity ratio of channel factorization algorithm to overall MIMO receiver, i.e., $\dfrac{N_{cf}}{N_{cf} + N_{MIMO}}$, for the case of $m = n = 6$, 16QAM, SNR = 28 dB, ρ=0.0

Comparison points	SA-extended	DLLL-extended	Type-I
$P\{Q \leq q\} = 0.1$	$\dfrac{3686}{3686 + 2904} = 56\%$	$\dfrac{4735}{4735 + 2904} = 62\%$	$\dfrac{2287}{2287 + 2904} = 44\%$
$P\{Q \leq q\} = 0.5$	$\dfrac{5804}{5804 + 2904} = 67\%$	$\dfrac{5220}{5220 + 2904} = 64\%$	$\dfrac{2772}{2772 + 2904} = 49\%$
$P\{Q \leq q\} = 0.9$	$\dfrac{8415}{8415 + 2904} = 74\%$	$\dfrac{5897}{5897 + 2904} = 67\%$	$\dfrac{3449}{3449 + 2904} = 54\%$
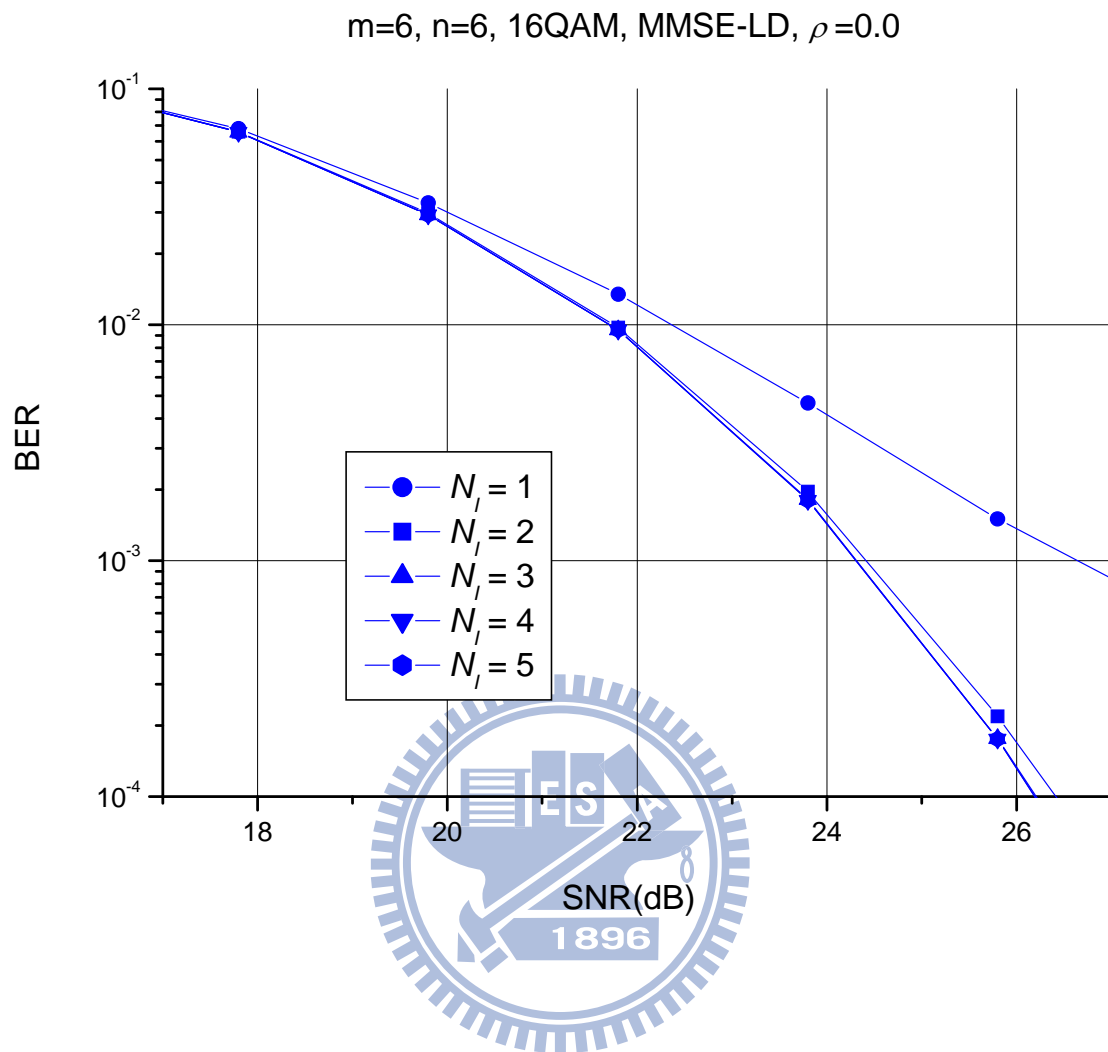
Figure 2.4: The effect of N_I of Type-II algorithm on BER for the case of

$m = 6, n = 6,$ 16QAM, ρ=0.0
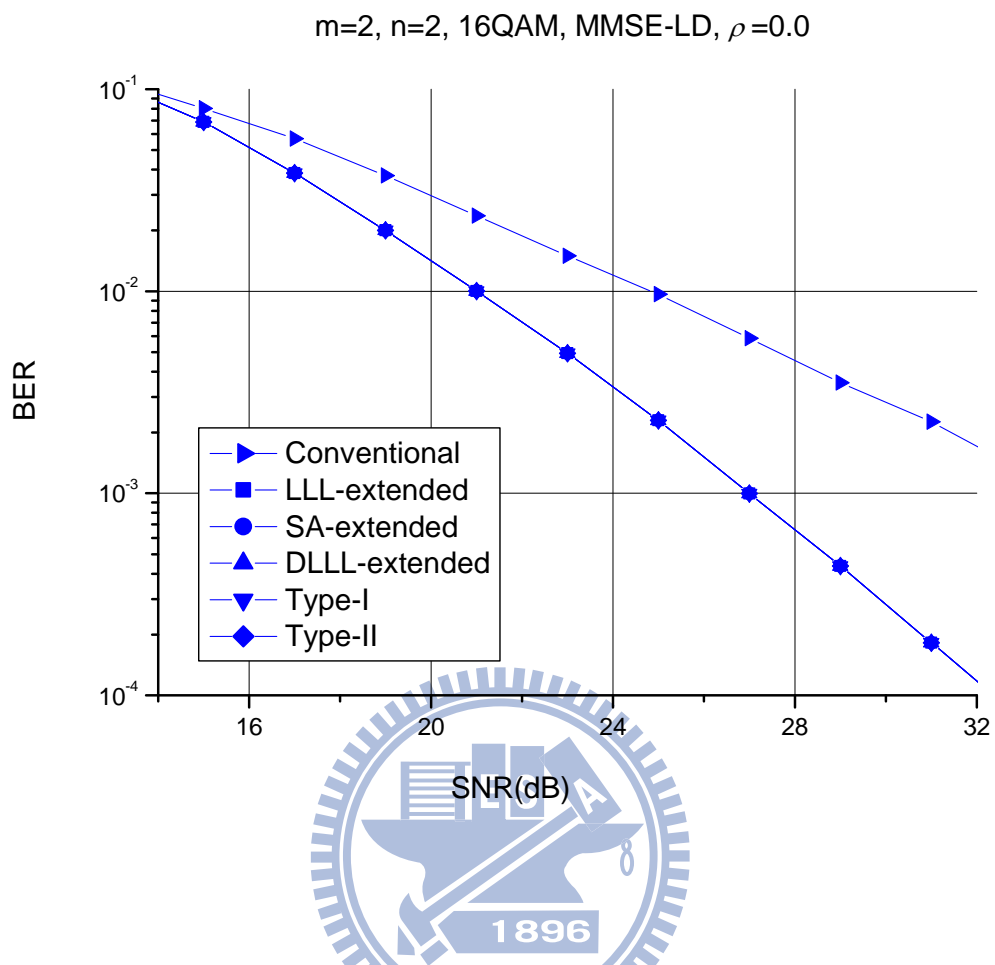
Figure 2.5: BER comparisons of different channel factorizations for CFAD-MMSE in the case of

$m = 2, n = 2,$ 16QAM, ρ=0.0 .
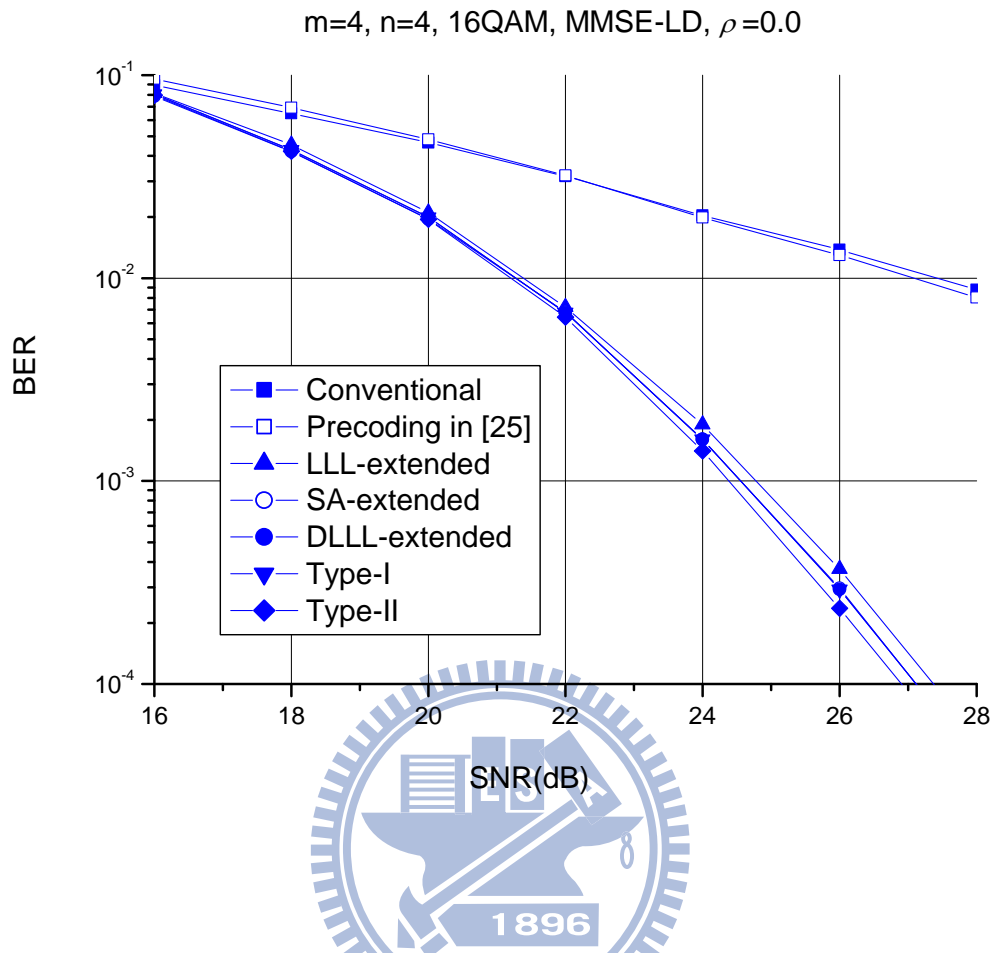
Figure 2.6: BER comparisons of different channel factorizations for CFAD-MMSE in the case of

$m = 4, n = 4,$ 16QAM, ρ=0.0 .
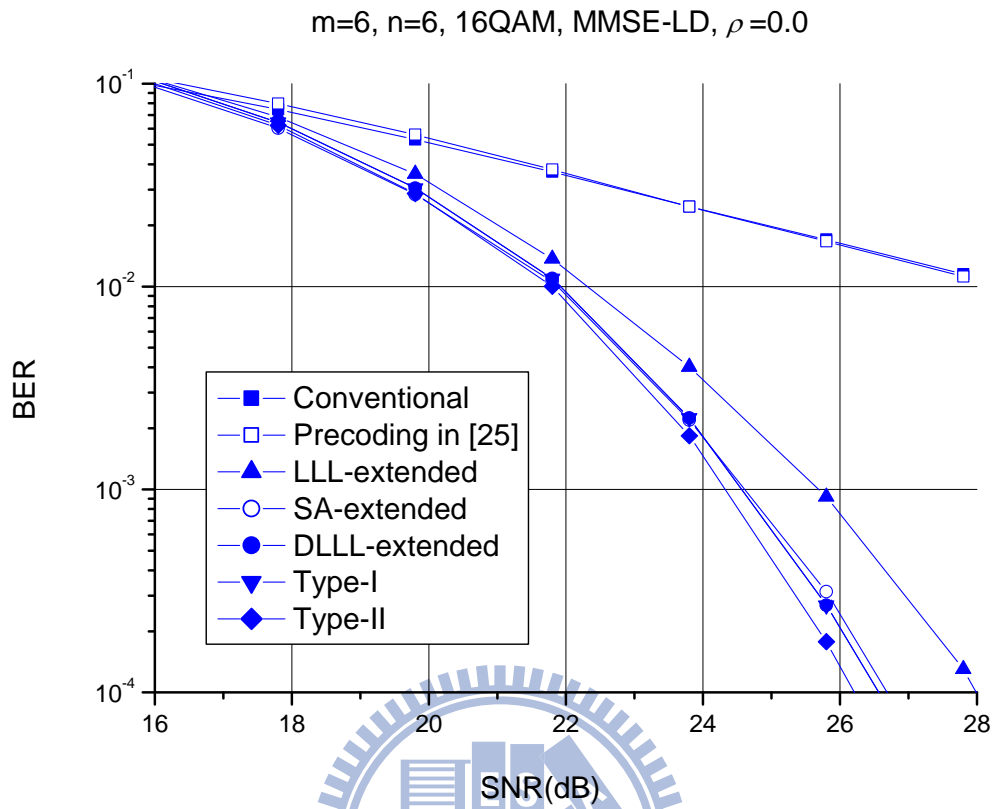
Figure 2.7: BER comparisons of different channel factorizations for CFAD-MMSE in the case of $m = 6, n = 6,$ 16QAM, ρ=0.0 .
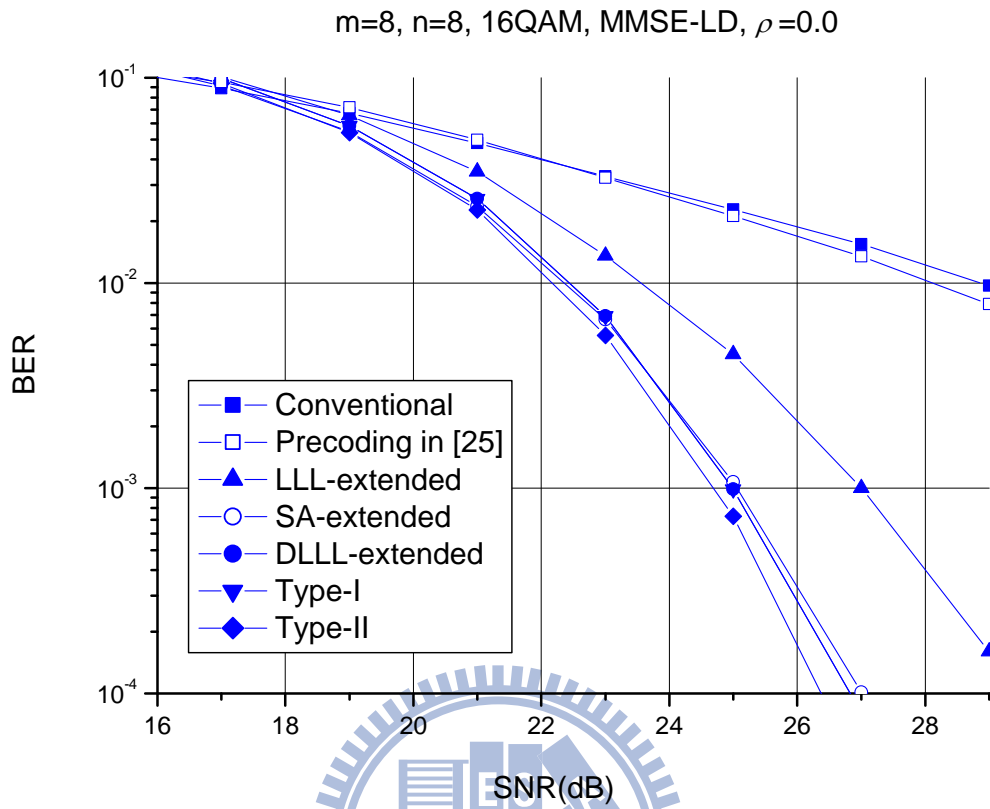
Figure 2.8: BER comparisons of different channel factorizations for CFAD-MMSE in the case of

$m = 8, n = 8,$ 16QAM, $\rho = 0.0$.
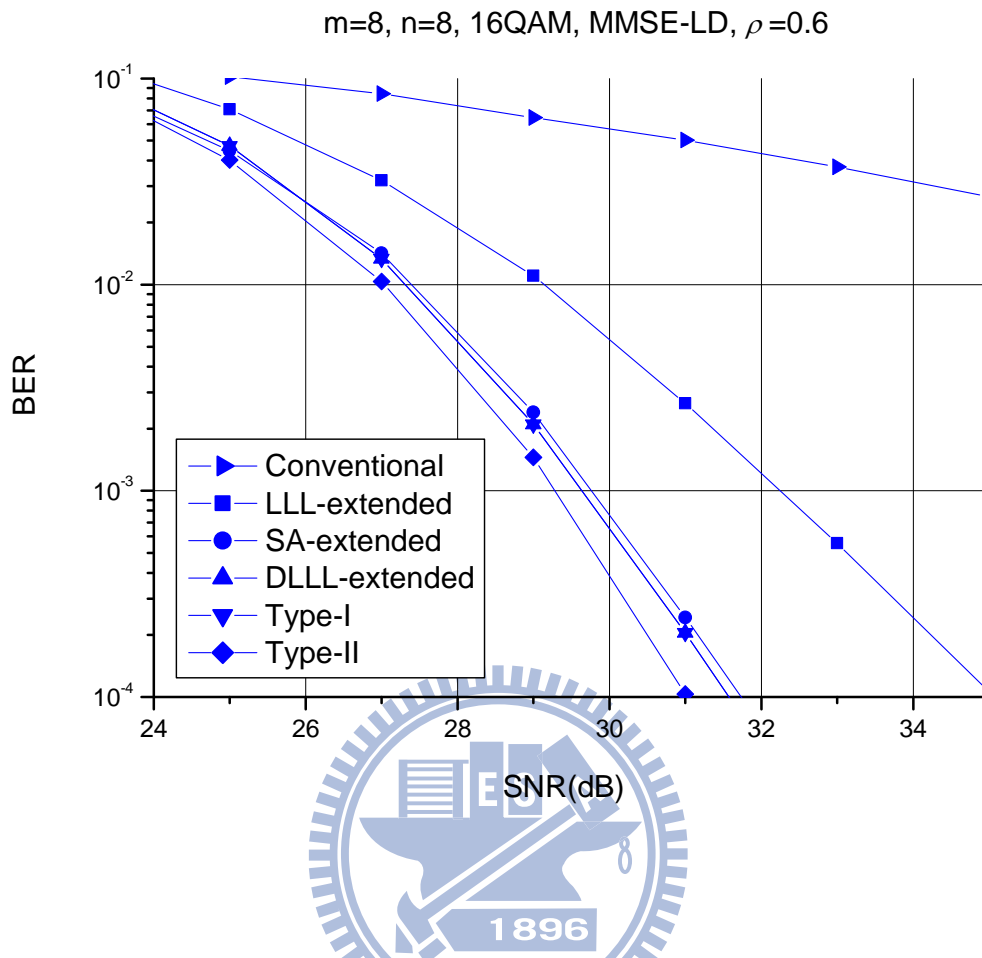
Figure 2.9: BER comparisons of different channel factorizations for CFAD-MMSE in the case of

$m = 8, n = 8,$ 16QAM, ρ=0.6 .

m=8, n=8, 16QAM, MMSE-LD, ρ =0.6
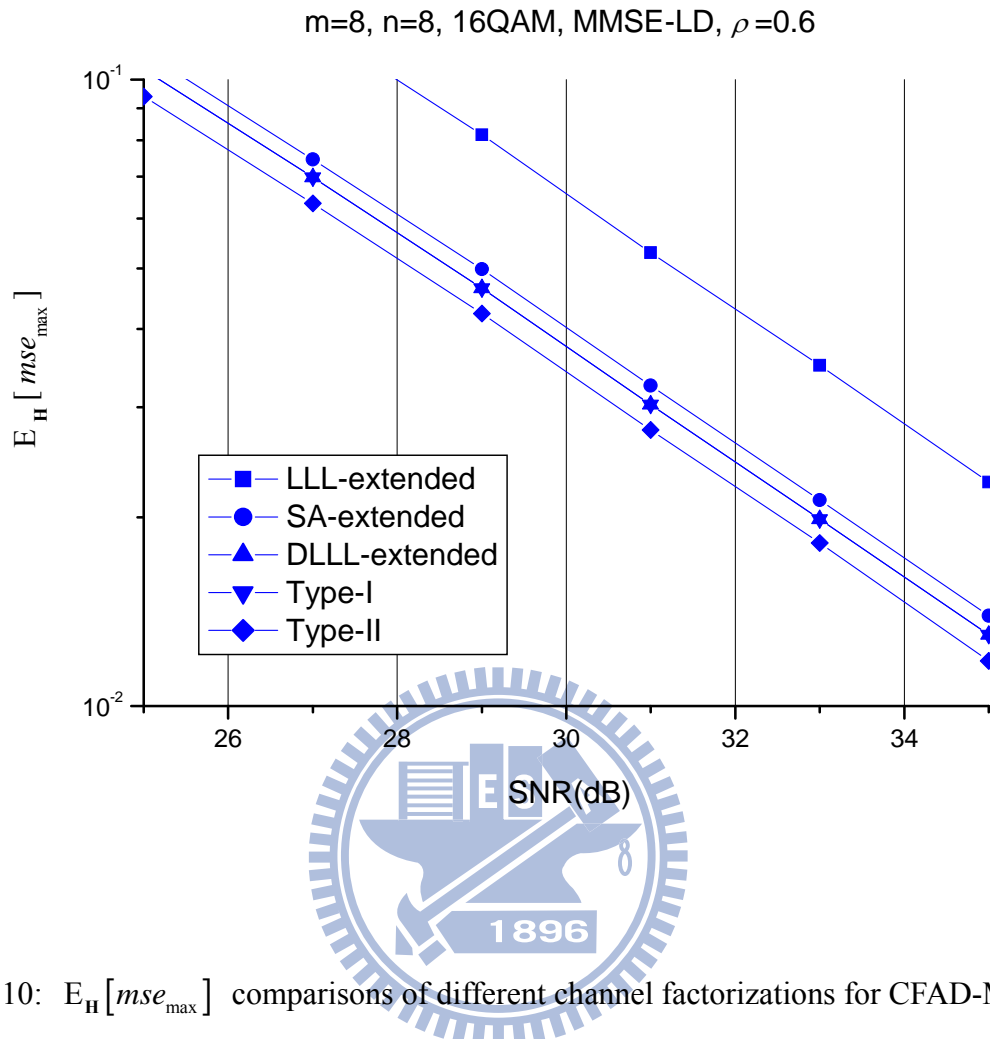
Figure 2.10: $\mathrm{E_H}\left[mse_{\max}\right]$ comparisons of different channel factorizations for CFAD-MMSE in the case of $m = 8, n = 8,$ 16QAM, ρ=0.6.
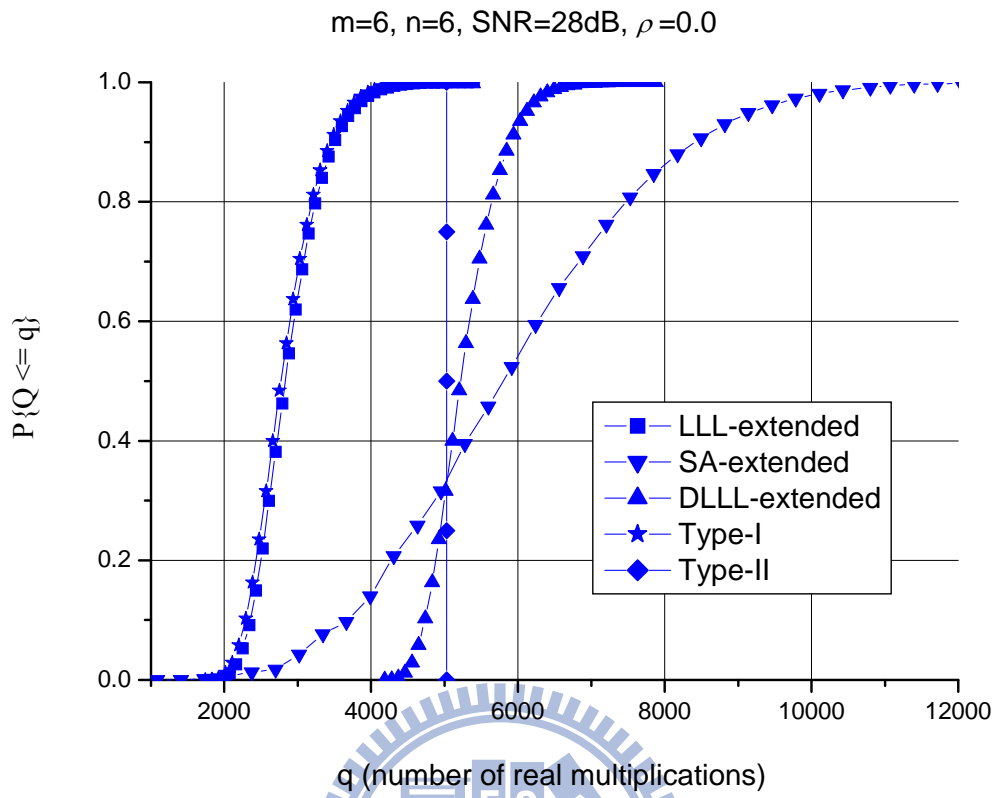
Figure 2.11: Complexity comparisons of different channel factorization algorithms.
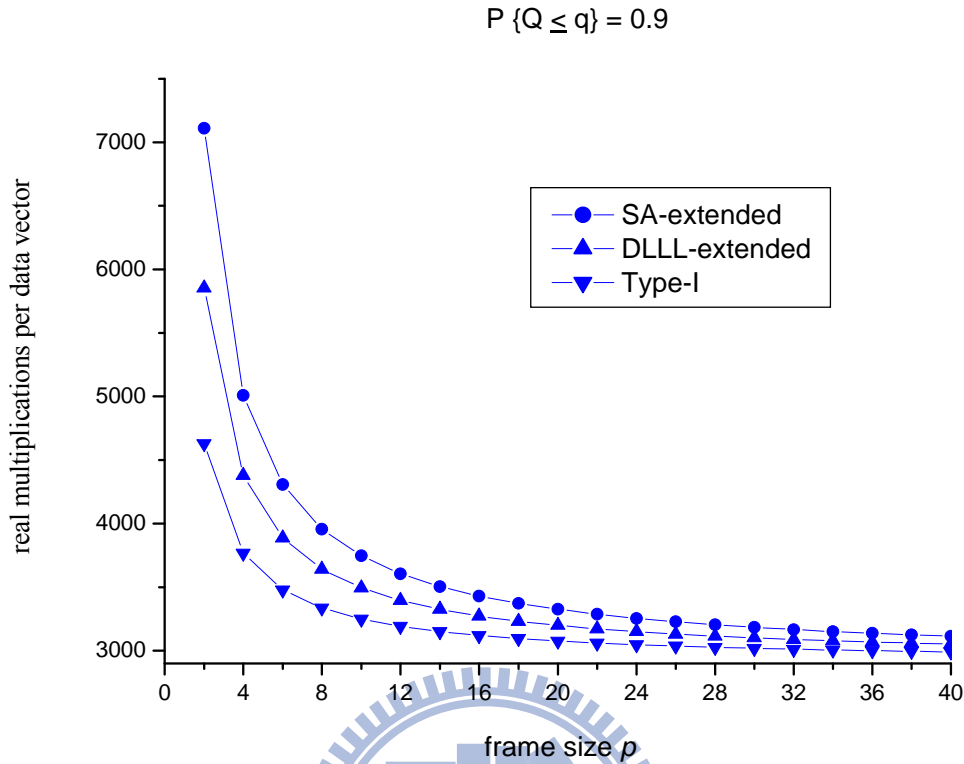
Figure 2.12: Number of real multiplications per data vector for different channel factorization algorithms with $m = n = 6$, 16QAM, SNR = 28 dB, ρ=0.0 and $P\{Q \leq q\} = 0.9$.

Next, the bit-error-rate (BER) for CFAD-MMSE-SIC and CFAD-MMSE-EWCL in uncorrelated MIMO channels ($\rho = 0.0$) are compared. As shown in Figure 2.13, the performance improvement is diminishing when the SIC detector is used instead. This might be attributed to the fact that in the nonlinear SIC detector the noise enhancement is not as significant as in the linear MMSE detector, and the performance improvement provided by the traditional LRAD is less prominent. In Figure 2.14, we show the performance of CFAD-MMSE-EWCL detectors for the case of $m = 6, n = 6, 16QAM$. Again, the proposed methods outperform conventional LLL and SA algorithms. Furthermore, as can be seen, using EWCL along with the proposed MMSE

channel factorization can approach very closely to the ML performance (within a fractional dB).
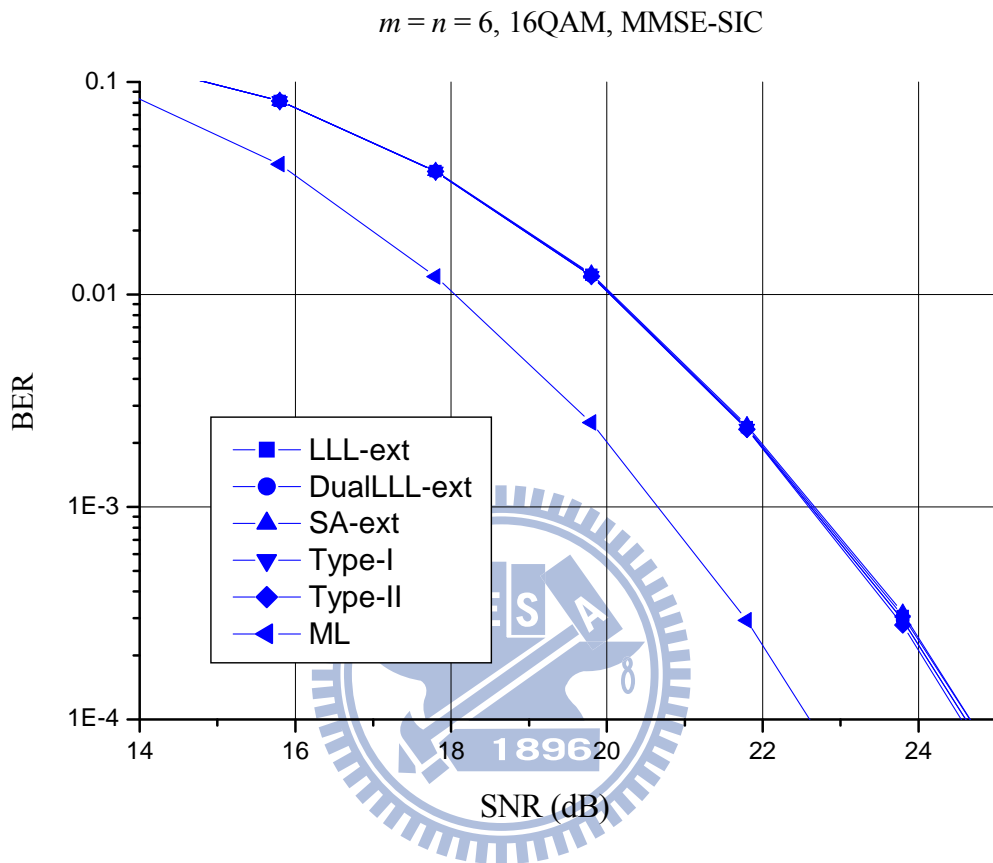
Figure 2.13: Comparison of the BER performance of different channel factorization methods
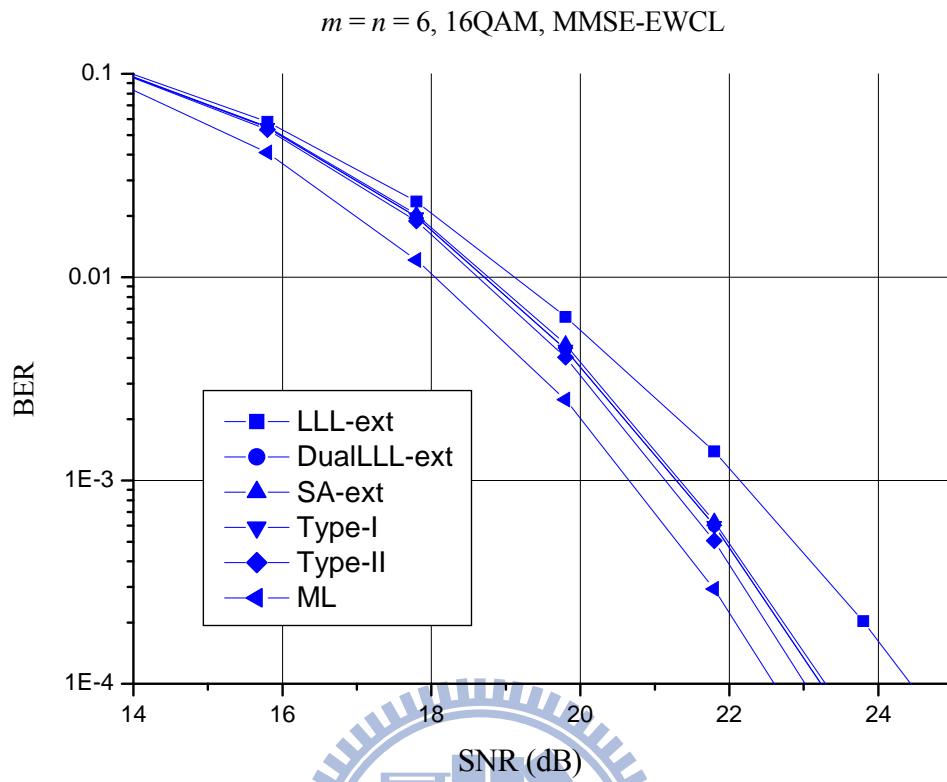
Figure 2.14: Comparison of bit-error-rate performance for different factorization algorithms with

$m = n = 6$, 16QAM .

2.5 Conclusions

A new design on channel factorization is proposed for the channel-factorization aided detectors, where effective factorization algorithms are sought to minimize the sum mean-squared-error of the MMSE detector. Two new types of factorization algorithms are devised; the first type is LLL based, where the best-performed factorization algorithm found in the literature, i.e., the DLLL-extended algorithm, is a member of this type but with a higher complexity. The second type is greedy-search based which can provide around 0.5-1.0 dB gain over the first type and has a fixed computational complexity which is advantageous in hardware implementation. The computational complexity of the proposed methods are analyzed and compared to the existing methods. In addition, combining proposed MMSE channel factorization algorithm with the element-wise, candidate-list (EWCL) detector can approach to within a fractional dB of the ML performance.

Chapter 3

MIMO-OFDM Systems with In-phase/ Quadrature-phase Imbalances

In this Chapter, receiver designs are investigated for the MIMO-OFDM systems with the presence of I-Q imbalances. I-Q imbalance is one of the key radio impairments in the direct-conversion architecture that will degrade significantly the communication performance if left uncompensated. Both frequency-dependent and independent I/Q imbalances at the transmitter and receiver are considered.
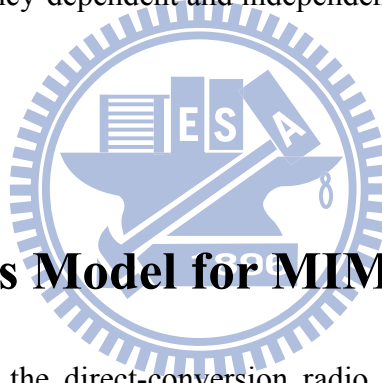
3.1 I/Q Imbalances Model for MIMO-OFDM Systems

Figure 3.1 shows the model of the direct-conversion radio transmitter and receiver with the presence of I-Q imbalances. The equivalent low-pass signal after transmit filter imbalance (frequency-dependent imbalance), $v(t) = v_I(t) + jv_Q(t)$, is expressed as

$$v(t) = x(t) \otimes \left(\frac{h_{TI}(t) + h_{TQ}(t)}{2} \right) + x^*(t) \otimes \left(\frac{h_{TI}(t) - h_{TQ}(t)}{2} \right) \qquad (3.1)$$

where $x(t) = x_I(t) + jx_Q(t)$ is the baseband signal for transmission. In addition, the equivalent low-pass signal after frequency–independent I-Q imbalance, $s(t)$, is expressed as
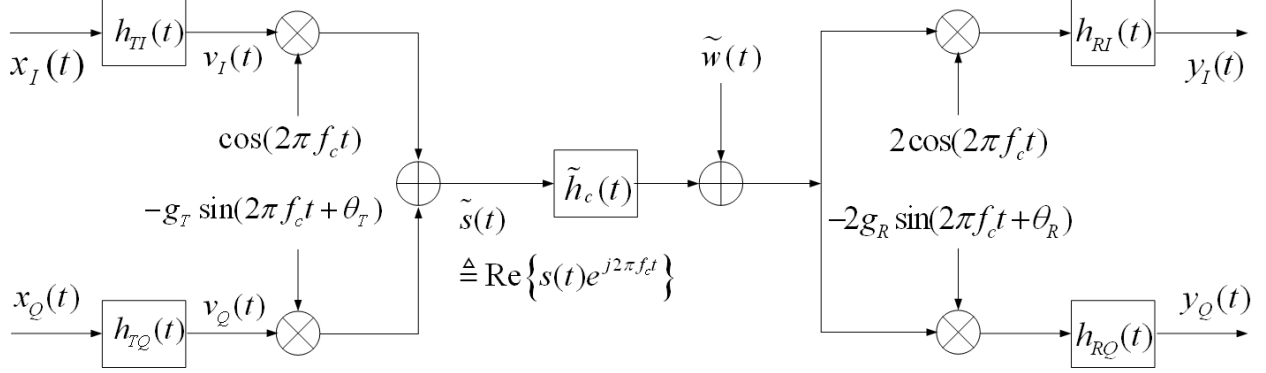
Figure 3.1: I/Q imbalances model at transmitter and receiver sides

$$s(t) = \frac{1}{2}v(t)\left(1 + g_T e^{j\theta_T}\right) + \frac{1}{2}v^*(t)\left(1 - g_T e^{j\theta_T}\right) \tag{3.2}$$

where g_T and θ_T are the gain and phase imbalances due to imperfection of the local oscillator. Using Equations (3.1) and (3.2), we have

$$s(t) = x(t) \otimes h_{T+}(t) + x^*(t) \otimes h_{T-}(t) \tag{3.3}$$

where $h_{T+}(t) = \frac{1}{2}\left[h_{TI}(t) + g_T e^{j\theta_T} h_{TQ}(t)\right]$, and $h_{T-}(t) = \frac{1}{2}\left[h_{TI}(t) - g_T e^{j\theta_T} h_{TQ}(t)\right]$. For discrete-time signal model, Equation (3.3) becomes

$$s[n] = x[n] \otimes h_{T+}[n] + x^*[n] \otimes h_{T-}[n] \tag{3.4}$$

where $h_{T+}[n] = \frac{1}{2}\left(h_{TI}[n] + g_T e^{j\theta_T} h_{TQ}[n]\right)$, and $h_{T-}[n] = \frac{1}{2}\left(h_{TI}[n] - g_T e^{j\theta_T} h_{TQ}[n]\right)$. Noticeably, for the case of no I-Q imbalances, i.e., $h_{TI}[n] = h_{TQ}[n]$, $g_T = 1$, and $\theta_T = 0$, Equation (3.4) degenerate to the ideal case

$$s[n] = x[n] \otimes h_{TI}[n] \tag{3.5}$$

Similarly, with the presence of receiver I-Q imbalance, the demodulated baseband signal, $y[n]$, is expressed as

$$y[n] = \left(s[n] \otimes h_c[n] + w[n] \right) \otimes h_{R+}[n] + \left(s[n] \otimes h_c[n] + w[n] \right)^* \otimes h_{R-}[n] \tag{3.6}$$

where $h_c[n]$ and $w[n]$ are baseband channel response and received noise, respectively, and

$h_{R+}[n] \triangleq \frac{1}{2}\left(h_{RI}[n] + h_{RQ}[n] g_R e^{-j\theta_R} \right)$ and $h_{R-}[n] \triangleq \frac{1}{2}\left(h_{RI}[n] - h_{RQ}[n] g_R e^{j\theta_R} \right)$ result from I/Q

imbalances at receiver side. g_R and θ_R are the receiver gain and phase imbalances.

Substitute Equation (3.4) into (3.6), the received signal, under the effects of transmitter and receiver I-Q imbalances, is

$$y[n] = \left[\left(x[n] \otimes h_{T+}[n] + x^*[n] \otimes h_{T-}[n] \right) \otimes h_c[n] + w[n] \right] \otimes h_{R+}[n]$$
$$+ \left[\left(x[n] \otimes h_{T+}[n] + x^*[n] \otimes h_{T-}[n] \right) \otimes h_c[n] + w[n] \right]^* \otimes h_{R-}[n] \tag{3.7}$$

Further, it can be rewritten as

$$y[n] = \begin{Bmatrix} x[n] \otimes \left(h_{T+}[n] \otimes h_c[n] \otimes h_{R+}[n] + h_{T-}^*[n] \otimes h_c^*[n] \otimes h_{R-}[n] \right) + \\ x^*[n] \otimes \left(h_{T-}[n] \otimes h_c[n] \otimes h_{R+}[n] + h_{T+}^*[n] \otimes h_c^*[n] \otimes h_{R-}[n] \right) \end{Bmatrix}$$
$$+ \begin{Bmatrix} w[n] \otimes h_{R+}[n] + \\ w^*[n] \otimes h_{R-}[n] \end{Bmatrix} \tag{3.8}$$

Equation (3.8) can be easily generalized to MIMO systems with m transmit and n receive antennas. In this case, for example, the received signal at i-th antenna, $y_i[n]$, is expressed as

$$y_i[n] = \sum_{j=1}^{m} \begin{Bmatrix} x_j[n] \otimes \left(h_{T+,j}[n] \otimes h_{c,ij}[n] \otimes h_{R+,i}[n] + h_{T-,j}^*[n] \otimes h_{c,ij}^*[n] \otimes h_{R-,i}[n] \right) + \\ x_j^*[n] \otimes \left(h_{T-,j}[n] \otimes h_{c,ij}[n] \otimes h_{R+,i}[n] + h_{T+,j}^*[n] \otimes h_{c,ij}^*[n] \otimes h_{R-,i}[n] \right) \end{Bmatrix}$$
$$+ \begin{Bmatrix} w_i[n] \otimes h_{R+,i}[n] + \\ w_i^*[n] \otimes h_{R-,i}[n] \end{Bmatrix}, \text{ for } i = 1, 2, ..., n \tag{3.9}$$

Consider the MIMO-OFDM systems where the length of overall channel response is not

larger than that of cyclic-prefix (CP) of an OFDM symbol, i.e., the case with inter-symbol interference (ISI) and inter-carrier interference (ICI) free. After Fast-Fourier Transform (FFT), the signals at k-th sub-carrier of the i-th receive antenna , $Y_i[k]$, is

$$
Y_i[k] = \sum_{j=1}^{m} \left\{ \begin{array}{l} X_j[k]\left(H_{T+,j}[k]H_{c,ij}[k]H_{R+,i}[k] + H^*_{T-,j}[-k]H^*_{c,ij}[-k]H_{R-,i}[k]\right) + \\ X^*_j[-k]\left(H_{T-,j}[k]H_{c,ij}[k]H_{R+,i}[k] + H^*_{T+,j}[-k]H^*_{c,ij}[-k]H_{R-,i}[k]\right) \end{array} \right\} + \widehat{W}_i[k] \qquad (3.10)
$$

where $\left\{\widehat{W}_i[k]\right\}_k = DFT\left\{w_i[n]\otimes h_{R+,i}[n] + w^*_i[n]\otimes h_{R-,i}[n]\right\}_n = DFT\left\{\mathbf{H}_{R+,i}\mathbf{w}_i + \mathbf{H}_{R-,i}\mathbf{w}^*_i\right\}_n$ with

$\mathbf{w}_i = \left[w_{i,1},...,w_{i,N+L-1}\right]^T$, and

$$
\mathbf{H}_{R\pm,i} = \begin{bmatrix} h_{R\pm,i,L_R} & \cdots & h_{R\pm,i,2} & h_{R\pm,i,1} & & 0 \\ & h_{R\pm,i,L_R} & \cdots & h_{R\pm,i,2} & h_{R\pm,i,1} & \\ & & \ddots & & \ddots & \\ 0 & & h_{R\pm,i,L_R} & \cdots & h_{R\pm,i,2} & h_{R\pm,i,1} \end{bmatrix}_{N\times(N+L_R-1)} , \qquad (3.11)
$$

Where L_R is the length of receive filters $h_{R\pm}[n]$. It turns out that $\widehat{W}_i = \left\{\widehat{W}_i[k]\right\}_k = \mathbf{F}\left(\mathbf{H}_{R+,i}\mathbf{w}_i + \mathbf{H}_{R-,i}\mathbf{w}^*_i\right)$, where $\mathbf{F}$ is N-point DFT matrix.

Similarly, the received signals at the mirror frequency, i.e., $-k$ -th sub-carrier, from i-th receive antenna, $Y_i[-k]$, is

$$
Y^*_i[-k] = \sum_{j=1}^{m} \left\{ \begin{array}{l} X^*_j[-k]\left(H^*_{T+,j}[-k]H^*_{c,ij}[-k]H^*_{R+,i}[-k] + H_{T-,j}[k]H_{c,ij}[k]H^*_{R-,i}[-k]\right) + \\ X_j[k]\left(H^*_{T-,j}[-k]H^*_{c,ij}[-k]H^*_{R+,i}[-k] + H_{T+,j}[k]H_{c,ij}[k]H^*_{R-,i}[-k]\right) \end{array} \right\} + \widehat{W}^*_i[-k]
$$

$$
(3.12)
$$

It is worth to notice from Equations (3.10) and (3.12) that the transmitted signal at the mirror sub-carrier, i.e., $X^*_j[-k]$, will interfere with the desired symbol $X_j[k]$ due to I-Q imbalances. Accordingly, the received signals at mirror sub-carrier should be jointly processed to attain better

performance.

Next, Equations (3.10) and (3.12) can be rewritten as

$$Y_i[k] = \sum_{j=1}^{m} \left(X_j[k] H_{ij}^{11}[k] + X_j^*[-k] H_{ij}^{12}[k] \right) + \widehat{W}_i[k]$$

$$Y_i^*[-k] = \sum_{j=1}^{m} \left(X_j[k] H_{ij}^{21}[-k] + X_j^*[-k] H_{ij}^{22}[-k] \right) + \widehat{W}_i^*[-k]$$

(3.13)
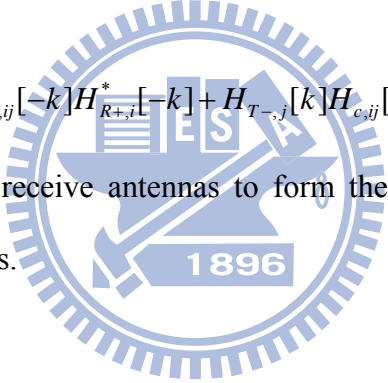
where

$$H_{ij}^{11}[k] = H_{T+,j}[k] H_{c,ij}[k] H_{R+,i}[k] + H_{T-,j}^*[-k] H_{c,ij}^*[-k] H_{R-,i}[k],$$

$$H_{ij}^{12}[k] = H_{T-,j}[k] H_{c,ij}[k] H_{R+,i}[k] + H_{T+,j}^*[-k] H_{c,ij}^*[-k] H_{R-,i}[k],$$

$$H_{ij}^{21}[-k] = H_{T-,j}^*[-k] H_{c,ij}^*[-k] H_{R+,i}^*[-k] + H_{T+,j}[k] H_{c,ij}[k] H_{R-,i}^*[-k],$$

and

$$H_{ij}^{22}[-k] = H_{T+,j}^*[-k] H_{c,ij}^*[-k] H_{R+,i}^*[-k] + H_{T-,j}[k] H_{c,ij}[k] H_{R-,i}^*[-k].$$

We collect the signals from all receive antennas to form the composite signal model for the MIMO-OFDM systems as follows.

$$\begin{bmatrix} Y_1[k] \\ \vdots \\ Y_n[k] \\ Y_1^*[-k] \\ \vdots \\ Y_n^*[-k] \end{bmatrix} = \begin{bmatrix} H_{1,1}^{11}[k] & \cdots & H_{1,m}^{11}[k] & H_{1,1}^{12}[k] & \cdots & H_{1,m}^{12}[k] \\ \vdots & \ddots & \vdots & \vdots & \ddots & \vdots \\ H_{n,1}^{11}[k] & \cdots & H_{n,m}^{11}[k] & H_{n,1}^{12}[k] & \cdots & H_{n,m}^{12}[k] \\ H_{1,1}^{21}[-k] & \cdots & H_{1,m}^{21}[-k] & H_{1,1}^{22}[-k] & \cdots & H_{1,m}^{22}[-k] \\ \vdots & \ddots & \vdots & \vdots & \ddots & \vdots \\ H_{n,1}^{21}[-k] & \cdots & H_{n,m}^{21}[-k] & H_{n,1}^{22}[-k] & \cdots & H_{n,m}^{22}[-k] \end{bmatrix} \begin{bmatrix} X_1[k] \\ \vdots \\ X_m[k] \\ X_1^*[-k] \\ \vdots \\ X_m^*[-k] \end{bmatrix} + \begin{bmatrix} \widehat{W}_1[k] \\ \vdots \\ \widehat{W}_n[k] \\ \widehat{W}_1^*[-k] \\ \vdots \\ \widehat{W}_n^*[-k] \end{bmatrix}$$

(3.14)

Define $\mathbf{Y} = \begin{bmatrix} \mathbf{Y}[k] \\ \mathbf{Y}^*[-k] \end{bmatrix}$, we have

$$\mathbf{Y} = \begin{bmatrix} \mathbf{H}^{11}[k] & \mathbf{H}^{12}[k] \\ \mathbf{H}^{21}[-k] & \mathbf{H}^{22}[-k] \end{bmatrix} \begin{bmatrix} \mathbf{x}[k] \\ \mathbf{x}^*[-k] \end{bmatrix} + \begin{bmatrix} \widehat{\mathbf{W}}[k] \\ \widehat{\mathbf{W}}^*[-k] \end{bmatrix} = \mathbf{Hx} + \widehat{\mathbf{W}}$$

where

$$\mathbf{H}^{11}[k] = \mathbf{H}_{R+}[k]\mathbf{H}_c[k]\mathbf{H}_{T+}[k] + \mathbf{H}_{R-}[k]\mathbf{H}_c^*[-k]\mathbf{H}_{T-}^*[-k],$$

$$\mathbf{H}^{12}[k] = \mathbf{H}_{R+}[k]\mathbf{H}_c[k]\mathbf{H}_{T-}[k] + \mathbf{H}_{R-}[k]\mathbf{H}_c^*[-k]\mathbf{H}_{T+}^*[-k],$$

$$\mathbf{H}^{21}[-k] = \mathbf{H}_{R+}^*[-k]\mathbf{H}_c^*[-k]\mathbf{H}_{T-}^*[-k] + \mathbf{H}_{R-}^*[-k]\mathbf{H}_c[k]\mathbf{H}_{T+}[k],$$

and

$$\mathbf{H}^{22}[-k] = \mathbf{H}_{R+}^*[-k]\mathbf{H}_c^*[-k]\mathbf{H}_{T+}^*[-k] + \mathbf{H}_{R-}^*[-k]\mathbf{H}_c[k]\mathbf{H}_{T-}[k]$$

with

$$\mathbf{H}_c[\pm k] = \begin{bmatrix} H_{c,1,1}[\pm k] & \cdots & H_{c,1,m}[\pm k] \\ \vdots & \ddots & \vdots \\ H_{c,n,1}[\pm k] & \cdots & H_{c,n,m}[\pm k] \end{bmatrix},$$

$$\mathbf{H}_{T\pm}[\pm k] = \begin{bmatrix} H_{T\pm,1}[\pm k] & & 0 \\ & \ddots & \\ 0 & & H_{T\pm,m}[\pm k] \end{bmatrix},$$

and

$$\mathbf{H}_{R\pm}[\pm k] = \begin{bmatrix} H_{R\pm,1}[\pm k] & & 0 \\ & \ddots & \\ 0 & & H_{R\pm,n}[\pm k] \end{bmatrix}.$$

3.2 Receiver Structure Design for MIMO-OFDM Systems with I/Q Imbalances

As is shown in Equation (3.14), the size of MIMO signal model is doubled due to jointly consider

the signals at the desired and mirror sub-carriers. Though performance improvement may be obtained with this type of joint detection, the complexity may increase tremendously. In this section, the different detection algorithms are examined based on the compromise between performance and complexity for MIMO-OFDM systems with I-Q imbalances.

First type of receiver structure considered, denoted as Type-I, is the joint detection of the desired and mirror signals $\mathbf{x}$ in Equation (3.14). Detection algorithms employed and compared in this Chapter are MMSE, MMSE-SIC, CF-I, and CF-II, which are low-complexity algorithms in practice. Note that CF-I and CF-II are the two newly proposed types of channel-factorization-aided detectors described in Chapter 2. Another type of receiver structure, denoted as Type-II, is composed of two-step processing, including the mirror interference cancellation (MIC) followed by a detection of mirror signals. In particular, firstly, multiply $\mathbf{Y}$ by MIC matrix $\mathbf{G}$ to obtain

$$\widetilde{\mathbf{Y}} = \mathbf{GY} = \begin{bmatrix} \mathbf{G}^{11} & \mathbf{G}^{12} \\ \mathbf{G}^{21} & \mathbf{G}^{22} \end{bmatrix} \begin{bmatrix} \mathbf{Y}[k] \\ \mathbf{Y}^*[-k] \end{bmatrix} = \begin{bmatrix} \mathbf{G}^{11}\mathbf{Y}[k] + \mathbf{G}^{12}\mathbf{Y}^*[-k] \\ \mathbf{G}^{21}\mathbf{Y}[k] + \mathbf{G}^{22}\mathbf{Y}^*[-k] \end{bmatrix} \tag{3.15}$$

then, carry out the detections of $\mathbf{x}[k]$ and $\mathbf{x}[-k]$ by making use of $\mathbf{G}^{11}\mathbf{Y}[k] + \mathbf{G}^{12}\mathbf{Y}^*[-k]$ and $\mathbf{G}^{21}\mathbf{Y}[k] + \mathbf{G}^{22}\mathbf{Y}^*[-k]$, respectively.

In this Chapter, only the MIMO-OFDM systems with equal number of transmit and receive antenna is concerned. The MIC matrix can be $\mathbf{G}_{ZF} = \mathbf{H}^{-1}$, $\mathbf{G}_{MMSE} = \mathbf{H}^H \left(\mathbf{H}\mathbf{H}^H + \frac{1}{\sigma_s^2} \mathbf{C}_{\widehat{\mathbf{w}}} \right)^{-1}$, or

$$\mathbf{G}_{BZF} = \begin{bmatrix} \mathbf{I}_n & -\mathbf{\Phi}[-k] \\ -\mathbf{\Phi}[k] & \mathbf{I}_n \end{bmatrix}, \text{ with } \begin{cases} \mathbf{\Phi}[-k] = \mathbf{H}^{12}[k]\left(\mathbf{H}^{22}[-k]\right)^{-1} \\ \mathbf{\Phi}[k] = \mathbf{H}^{21}[-k]\left(\mathbf{H}^{11}[k]\right)^{-1} \end{cases} \text{ based on ZF, MMSE, and}$$

block-ZF (BZF) algorithms, respectively, where $\mathbf{C}_{\widehat{\mathbf{w}}} = E\left[\widehat{\mathbf{W}}\widehat{\mathbf{W}}^H \right]$. Also, it is easy to show that

$$C_{\widehat{\mathbf{W}}} = E\left\{\begin{bmatrix}\widehat{\mathbf{W}}[k] \\ \widehat{\mathbf{W}}^*[-k]\end{bmatrix}\begin{bmatrix}\widehat{\mathbf{W}}^H[k] & \widehat{\mathbf{W}}^T[-k]\end{bmatrix}\right\} = E\left\{\begin{bmatrix}\widehat{\mathbf{W}}[k] \\ \widehat{\mathbf{W}}^*[k']\end{bmatrix}\begin{bmatrix}\widehat{\mathbf{W}}^H[k] & \widehat{\mathbf{W}}^T[k']\end{bmatrix}\right\}$$

$$= \sigma_n^2 \begin{bmatrix}\mathbf{\Psi}_{k,k} & \mathbf{\Psi}_{k,k'} \\ \mathbf{\Psi}_{k',k} & \mathbf{\Psi}_{k',k'}\end{bmatrix}, \quad k' = N - k + 2 \tag{3.16}$$

where k' is the index of the mirror sub-carrier of the k-th sub-carrier, and

$$\mathbf{\Psi}_{k,k} = \begin{bmatrix}\varphi_{1,k,k} & & 0 \\ & \ddots & \\ 0 & & \varphi_{n,k,k}\end{bmatrix},$$

and

$$\mathbf{\Psi}_{k,k'} = \begin{bmatrix}\varphi_{1,k,k'} & & 0 \\ & \ddots & \\ 0 & & \varphi_{n,k,k'}\end{bmatrix} = \mathbf{\Psi}_{k',k}^H$$

with

$$\varphi_{i,k,k} = \left\| \left[\mathbf{F}\mathbf{H}_{R+,i}\right]_{[k,:]} \right\|^2 + \left\| \left[\mathbf{F}\mathbf{H}_{R-,i}\right]_{[k,:]} \right\|^2, \quad i = 1,\dots,n$$

$$\varphi_{i,k,k'} = \left[\mathbf{F}\mathbf{H}_{R+,i}\right]_{[k,:]} \left[\mathbf{F}\mathbf{H}_{R-,i}\right]_{[k',:]}^T + \left[\mathbf{F}\mathbf{H}_{R-,i}\right]_{[k,:]} \left[\mathbf{F}\mathbf{H}_{R+,i}\right]_{[k',:]}^T, \quad i = 1,\dots,n \tag{3.17}$$

Note that if I/Q is matched at receiver side, i.e., $\mathbf{H}_{R-,i} = \mathbf{0}_{N \times (N+L-1)}, \forall i$, then $C_{\widehat{\mathbf{W}}}$ is diagonalized.

Note that for Type-II receiver with ZF-MIC,

$$\widetilde{\mathbf{Y}}_{ZF} = \mathbf{G}_{ZF}\mathbf{Y} = \begin{bmatrix}\mathbf{G}_{ZF}^{11} & \mathbf{G}_{ZF}^{12} \\ \mathbf{G}_{ZF}^{21} & \mathbf{G}_{ZF}^{22}\end{bmatrix}\begin{bmatrix}\mathbf{Y}[k] \\ \mathbf{Y}^*[-k]\end{bmatrix} = \begin{bmatrix}\mathbf{x}[k] + \mathbf{G}_{ZF}^{11}\widehat{\mathbf{W}}[k] + \mathbf{G}_{ZF}^{12}[k]\widehat{\mathbf{W}}^*[-k] \\ \mathbf{x}^*[-k] + \mathbf{G}_{ZF}^{21}\widehat{\mathbf{W}}[k] + \mathbf{G}_{ZF}^{22}[k]\widehat{\mathbf{W}}^*[-k]\end{bmatrix}$$

where $\mathbf{G}_{ZF} = \mathbf{H}^{-1} = \begin{bmatrix}\mathbf{H}^{11}[k] & \mathbf{H}^{12}[k] \\ \mathbf{H}^{21}[-k] & \mathbf{H}^{22}[-k]\end{bmatrix}^{-1} = \begin{bmatrix}\mathbf{G}_{ZF}^{11} & \mathbf{G}_{ZF}^{12} \\ \mathbf{G}_{ZF}^{21} & \mathbf{G}_{ZF}^{22}\end{bmatrix}$, with

$$\begin{cases} \mathbf{G}_{ZF}^{11} = \left(\mathbf{H}^{11}[k] - \mathbf{H}^{12}[k] \left(\mathbf{H}^{22}[-k] \right)^{-1} \mathbf{H}^{21}[-k] \right)^{-1} \\[2ex] \mathbf{G}_{ZF}^{12} = -\left(\mathbf{H}^{11}[k] - \mathbf{H}^{12}[k] \left(\mathbf{H}^{22}[-k] \right)^{-1} \mathbf{H}^{21}[-k] \right)^{-1} \mathbf{H}^{12}[k] \left(\mathbf{H}^{22}[-k] \right)^{-1} \\[2ex] \mathbf{G}_{ZF}^{21} = -\left(\mathbf{H}^{22}[k] - \mathbf{H}^{21}[k] \left(\mathbf{H}^{11}[-k] \right)^{-1} \mathbf{H}^{12}[-k] \right)^{-1} \mathbf{H}^{21}[-k] \left(\mathbf{H}^{11}[k] \right)^{-1} \\[2ex] \mathbf{G}_{ZF}^{22} = \left(\mathbf{H}^{22}[k] - \mathbf{H}^{21}[k] \left(\mathbf{H}^{11}[-k] \right)^{-1} \mathbf{H}^{12}[-k] \right)^{-1} \end{cases}$$

(3.18)

In addition, it is easy to show that

$$\mathbf{G}_{ZF} = \begin{bmatrix} \left(\mathbf{H}^{11}[k] - \mathbf{H}^{12}[k] \left(\mathbf{H}^{22}[-k] \right)^{-1} \mathbf{H}^{21}[-k] \right)^{-1} & \mathbf{0}_{m \times m} \\[2ex] \mathbf{0}_{m \times m} & \left(\mathbf{H}^{22}[k] - \mathbf{H}^{21}[k] \left(\mathbf{H}^{11}[-k] \right)^{-1} \mathbf{H}^{12}[-k] \right)^{-1} \end{bmatrix} \mathbf{G}_{BZF}$$

where

$$\mathbf{G}_{BZF} = \begin{bmatrix} \mathbf{I}_n & -\mathbf{\Phi}[-k] \\ -\mathbf{\Phi}[k] & \mathbf{I}_n \end{bmatrix}$$

with

$$\mathbf{\Phi}[-k] = \mathbf{H}^{12}[k] \left(\mathbf{H}^{22}[-k] \right)^{-1}$$

and

$$\mathbf{\Phi}[k] = \mathbf{H}^{21}[-k] \left(\mathbf{H}^{11}[k] \right)^{-1}$$

(3.19)

Based on the relationships between $\mathbf{G}_{ZF}$ and $\mathbf{G}_{BZF}$ described in Equation (3.19), and the results shown in Appendix E, it is clear later that the identical BER performance can be attained for ZF-MIC and BZF-MIC, if the same detection algorithms are employed. In addition, the computational complexity of BZF-MIC is less complexity than that of ZF-MIC while comparing the expressions of $\mathbf{G}_{ZF}$ and $\mathbf{G}_{BZF}$ in Equations (3.18) and (3.19).

3.3 Case Study and Simulation Results

In this section, different cases with TX and/or RX I/Q imbalances for MIMO-OFDM systems with equal number of transmit and receive antenna, i.e., $m = n$, are studied and compared by simulations. Table 3.1 gives the system and I/Q imbalance parameters which are typical values in real systems [73], [74]. In the sequel of this chapter, "TX_Imb = 1" stands for transmitter side I-Q imbalance with parameters $\left\{ g_{T,j}, \theta_{T,j}, f_j^{TI}, f_j^{TQ} \right\}_{j=1}^{m}$ indicated in Table 3.1. By contrast, "TX_Imb = 0" means ideal transmitter, i.e., $\left\{ g_{T,j} = 1, \theta_{T,j} = 0^o, f_j^{TI} = f_j^{TQ} \right\}_{j=1}^{m}$. Similar meanings are also used for "RX_Imb". The transmission is done on a frame-by-frame basis. For each case, different strategies may be adopted for receiver structure design to compromise between BER performance and computational complexity. Furthermore, discrete-time, wide-sense stationary uncorrelated scattering (WSSUS) Rayleigh channel model, described in Chapter 4, is used for each pair of transmit and receive antennas. The power delay profile of the multi-path channel follows the exponential decay model

$$\sigma_l^2 = \sigma_0^2 \cdot \exp\left(-lT_s/T_{rms}\right), \quad l = 1, 2, ..., L \quad , \tag{3.20}$$

with $\sigma_0^2 = 1 - \exp\left(-T_s/T_{rms}\right)$, $L = 6T_{rms}/T_s$, such that $\sum_{l=0}^{L} \sigma_l^2 \approx 1$, where T_{rms} and T_s are root mean square delay spread and sampling period, respectively. The channel remains unchanged during a frame. Also, the multi-path channels between different pair of transmit and receive antennas is uncorrelated to each other.

Table 3.1: System Parameters

System Parameter and Radio Impairments	Parameter Value
Channel Bandwidth	20 MHz
FFT length $\left(N\right)$, cyclic prefix length $\left(N_g\right)$	$N=64$, $N_g=16$
OFDM-Symbol Time $\left(T_{OFDM}\right)$, Symbol Time $\left(T_s\right)$	$T_{OFDM}=4\ \mu s$, $T_s=50\ ns$
Sub-carrier Spacing $\left(\dfrac{1}{NT_s}\right)$	0.3125 MHz
Number of Transmit and Receive Antenna $\left(m,n\right)$	$m=n=2$
Frequency independent I-Q Imbalance $\left(g_{T,j},\theta_{T,j}\right)$, $\left(g_{R,i},\theta_{R,i}\right)$	$\left(g_{T,1}=1.05,\theta_{T,1}=4^o\right),\left(g_{T,2}=0.94,\theta_{T,2}=-5^o\right)$ $\left(g_{R,1}=0.96,\theta_{R,1}=5^o\right),\left(g_{R,2}=0.94,\theta_{R,2}=4^o\right)$
$\left\{h_{TI,j}[n],h_{TQ,j}[n],h_{RI,i}[n],h_{RQ,i}[n]\right\}$: 2rd order FIR with cut-off frequency $\left(f_j^{TI},f_j^{TQ},f_i^{RI},f_i^{RQ}\right)$ MHz	$\left(f_1^{TI}=8,f_1^{TQ}=8.3\right),\left(f_2^{TI}=8,f_2^{TQ}=8.2\right)$ $\left(f_1^{RI}=8.1,f_1^{RQ}=8.4\right),\left(f_2^{RI}=8.1,f_2^{RQ}=7.9\right)$

3.3.1 Complexity Analysis

In this subsection, the averaged computational complexity for different receiver structures concerned in this chapter is presented and compared. Related complexities of matrix computations are the same as those used in Chapter 2 [69]. Firstly, Table 3.2 gives the averaged computational complexity of Type-I receivers, where $NM_{CF-I(II),2m}$ and $NA_{CF-I(II),2m}$ are number of real multiplication and addition needed for CF-I (II) algorithms with channel matrix

size *2m*. These results can be found by referring to subsection 2.3.4. Also, *p* is frame size, that is, channel factorization algorithms need to be performed once per *p* OFDM symbols.

Table 3.2: Averaged computational complexity of Type-I receivers

Type-I receiver	Number of real multiplications	Number of real additions
Joint-MMSE	$64m^3 + 32m^2 + 8m \cdot |\Omega|$	$64m^3 + 32m^2 + 8m \cdot |\Omega|$
Joint-MMSESIC	$16m^3 + 24m^2 + 2\sum_{k=1}^{2m} k^3 + 8m|\Omega| + 2(1+4m)\sum_{k=1}^{2m} k^2$	$16m^3 + 24m^2 + 2\sum_{k=1}^{2m} k^3 + 8m|\Omega| + 2(1+4m)\sum_{k=1}^{2m} k^2$
Joint-CF-I	$\dfrac{NM_{CF-I,2m}}{p} + 80m^3 + 40m^2 + 8m \cdot |\Omega|$	$\dfrac{NA_{CF-I,2m}}{p} + 80m^3 + 40m^2 + 8m \cdot |\Omega|$
Joint-CF-II	$\dfrac{NM_{CF-II,2m}}{p} + 80m^3 + 40m^2 + 8m \cdot |\Omega|$	$\dfrac{NA_{CF-II,2m}}{p} + 80m^3 + 40m^2 + 8m \cdot |\Omega|$

Next, the averaged computational complexities of Type-II receivers are evaluated. As mentioned in previous section and shown in Appendix E that the BER performance of BZF-MIC is identical to that of ZF-MIC while the same detection algorithms are employed. Also, BZF-MIC is less complex than ZF-MIC in MIC stage. Accordingly, the averaged computational complexity of ZF-MIC isn't compared in this subsection. Table 3.3 provides the averaged computational complexity of Type-II receivers. As the expressions of MIC matrices of BZF and MMSE, i.e., $\mathbf{G}_{BZF}$ and $\mathbf{G}_{MMSE}$ shown in previous subsection, the computation of $\mathbf{G}_{BZF}$ is less complex than that of $\mathbf{G}_{MMSE}$, which leads to that the complexity of BZF-MIC is much smaller. In addition, the BER performance of BZF-MIC is nearly identical to that of MMSE-MIC if the same detection

algorithm is used, which will be shown in the following subsections. It is therefore concluded that BZF-MIC is preferable to employ for detection than MMSE-MIC, if Type-II receiver is considered.

Table 3.3: Averaged computational complexity of Type-II receivers

Type-II receiver	Number of real multiplications	Number of real additions
BZF-MMSE	$28m^3 + 36m^2 + 8m \cdot |\Omega|$	$28m^3 + 36m^2 + 8m \cdot |\Omega|$
BZF-MMSESIC	$16m^3 + 32m^2 + 4\sum_{k=1}^{m} k^3 +$ $8m|\Omega| + 4(1+2m)\sum_{k=1}^{m} k^2$	$16m^3 + 32m^2 + 4\sum_{k=1}^{m} k^3 +$ $8m|\Omega| + 4(1+2m)\sum_{k=1}^{m} k^2$
BZF-CF-I	$\dfrac{2 \cdot NM_{CF-I,m}}{p} + 32m^3 + 40m^2 + 8m \cdot |\Omega|$	$\dfrac{2 \cdot NA_{CF-I,m}}{p} + 32m^3 + 40m^2 + 8m \cdot |\Omega|$
BZF-CF-II	$\dfrac{2 \cdot NM_{CF-II,m}}{p} + 32m^3 + 40m^2 + 8m \cdot |\Omega|$	$\dfrac{2 \cdot NA_{CF-II,m}}{p} + 32m^3 + 40m^2 + 8m \cdot |\Omega|$
MMSE-MMSESIC	$68m^3 + 44m^2 + 4\sum_{k=1}^{m} k^3 +$ $8m|\Omega| + 4(1+2m)\sum_{k=1}^{m} k^2$	$68m^3 + 44m^2 + 4\sum_{k=1}^{m} k^3 +$ $8m|\Omega| + 4(1+2m)\sum_{k=1}^{m} k^2$
MMSE-CF-I	$\dfrac{2 \cdot NM_{CF-I,m}}{p} + 84m^3 + 52m^2 + 8m \cdot |\Omega|$	$\dfrac{2 \cdot NA_{CF-I,m}}{p} + 84m^3 + 52m^2 + 8m \cdot |\Omega|$
MMSE-CF-II	$\dfrac{2 \cdot NM_{CF-II,m}}{p} + 84m^3 + 52m^2 + 8m \cdot |\Omega|$	$\dfrac{2 \cdot NA_{CF-II,m}}{p} + 84m^3 + 52m^2 + 8m \cdot |\Omega|$

Figure 3.2 compares the averaged number of real multiplications required by two receiver structures, i.e., Type-I and Type-II with BZF-MIC, with different detection algorithms for the case of $m = n = 2, 64\text{QAM}, \text{SNR} = 20\text{dB}, p = 6$. Aforementioned, BZF-MIC outperforms over

ZF-MIC and MMSE-MIC in complexity, and attains comparable BER performance, which will be shown later. It can be seen by Figure 3.2, the complexity increases while replacing BZF-MIC (Type-II) with Type-I receiver are $\dfrac{1664-1392}{1392}=20\%$, $\dfrac{1988-1416}{1416}=40\%$, $\dfrac{1970-1485}{1485}=33\%$, and $\dfrac{2033-1481}{1481}=37\%$ for MMSE, MMSESIC, CF-I at $P\{Q\leq q\}=0.5$, and CF-II detection algorithms, respectively.
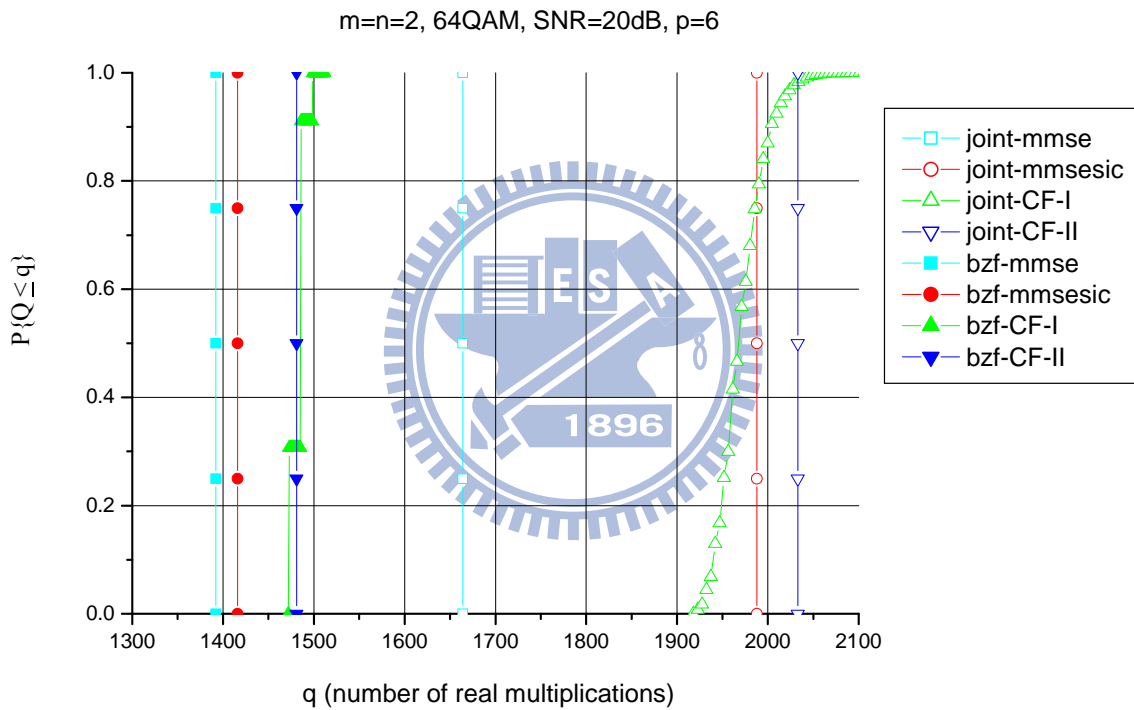
Figure 3.2: Averaged computational complexity comparisons of two receiver structures with different detection algorithms

3.3.2 BER Performance with TX_Imb = RX_Imb = 0 (Ideal)

In this case, signals model in Equation (3.14) can be simplified as

$$\mathbf{Y} = \begin{bmatrix} \mathbf{Y}[k] \\ \mathbf{Y}^*[-k] \end{bmatrix} = \begin{bmatrix} \mathbf{H}^{11}[k] & \mathbf{0}_{m \times m} \\ \mathbf{0}_{m \times m} & \mathbf{H}^{22}[-k] \end{bmatrix} \begin{bmatrix} \mathbf{x}[k] \\ \mathbf{x}^*[-k] \end{bmatrix} + \begin{bmatrix} \widehat{\mathbf{W}}[k] \\ \widehat{\mathbf{W}}^*[-k] \end{bmatrix} = \mathbf{Hx} + \widehat{\mathbf{W}}$$

$$= \begin{bmatrix} \mathbf{H}^{11}[k]\mathbf{x}[k] + \widehat{\mathbf{W}}[k] \\ \mathbf{H}^{22}[-k]\mathbf{x}^*[-k] + \widehat{\mathbf{W}}^*[-k] \end{bmatrix}$$

(3.21)

due to $\mathbf{H}_{T-}[k] = \mathbf{H}_{T-}[-k] = \mathbf{0}_{m \times m}$, and $\mathbf{H}_{R-}[k] = \mathbf{H}_{R-}[-k] = \mathbf{0}_{m \times m}$. Because the noise in $\mathbf{Y}[k]$ and $\mathbf{Y}^*[-k]$ are uncorrelated to each other owing to $\mathbf{H}_{R-,i} = \mathbf{0}_{N \times (N+L-1)}, \forall i$, $\mathbf{C}_{\widehat{\mathbf{W}}}$ is diagonal mentioned before, the BER performance of Type-I receiver is identical to that of Type-II receiver while the same detection algorithm is applied. Accordingly, Type-II receiver is preferred thanks to its less computational complexity by reducing the size of MIMO signal model processed. This can be demonstrated by the results shown in Figure 3.3 for the case of $m = n = 2$, $64QAM$, and $T_{rms}/T_s = 2, L = 12$ (indoor environment). Note that MMSE detection roughly attains the performance of diversity one, and MMSE-SIC outperforms MMSE, but can't achieve full diversity. By contrast, both CF-I and CF-II perform the best and obtain full diversity, as shown in Chapter 2.

Figure 3.3: Comparison of BER performance for the case of TX_Imb = RX_Imb = 0.

3.3.3 BER Performance with TX_Imb = 1, RX_Imb = 0

Received signals can be expressed as:

$$\mathbf{Y} = \begin{bmatrix} \mathbf{Y}[k] \\ \mathbf{Y}^*[-k] \end{bmatrix} = \begin{bmatrix} \mathbf{H}^{11}[k] & \mathbf{H}^{12}[k] \\ \mathbf{H}^{21}[-k] & \mathbf{H}^{22}[-k] \end{bmatrix} \begin{bmatrix} \mathbf{x}[k] \\ \mathbf{x}^*[-k] \end{bmatrix} + \begin{bmatrix} \widehat{\mathbf{W}}[k] \\ \widehat{\mathbf{W}}^*[-k] \end{bmatrix} = \mathbf{H}\mathbf{x} + \widehat{\mathbf{W}}$$

$$\mathbf{H}^{11}[k] = \mathbf{H}_{R+}[k]\mathbf{H}_c[k]\mathbf{H}_{T+}[k], \ \mathbf{H}^{12}[k] = \mathbf{H}_{R+}[k]\mathbf{H}_c[k]\mathbf{H}_{T-}[k]$$

with $\ \mathbf{H}^{21}[-k] = \mathbf{H}_{R+}^*[-k]\mathbf{H}_c^*[-k]\mathbf{H}_{T-}^*[-k], \ \mathbf{H}^{22}[-k] = \mathbf{H}_{R+}^*[-k]\mathbf{H}_c^*[-k]\mathbf{H}_{T+}^*[-k]$ \hfill (3.22)

$$\mathbf{C}_{\widehat{\mathbf{w}}} = \sigma_n^2 \begin{bmatrix} \mathbf{\Psi}_{k,k} & \mathbf{0}_{mxm} \\ \mathbf{0}_{mxm} & \mathbf{\Psi}_{k',k'} \end{bmatrix}, \ \ k' = N - k + 2$$

62

because of $\mathbf{H}_{R-}[k]=\mathbf{H}_{R-}[-k]=\mathbf{0}_{m\times m}$ and $\mathbf{H}_{R-,i}=\mathbf{0}_{N\times(N+L-1)}$, $\forall i$. We can find from Equation (3.22) that $\mathbf{x}[k]$ experiences both $\mathbf{H}_c[k]$ and $\mathbf{H}_c^*[-k]$, which are the constituent of $\mathbf{H}^{11}[k]$ and $\mathbf{H}^{21}[-k]$, respectively, to be present in the received signals at subcarrier k and its mirror subcarrier $–k$, i.e., $\mathbf{Y}[k]$ and $\mathbf{Y}^*[-k]$, due to TX I/Q imbalance. Similar phenomenon can also be occurred for $\mathbf{x}^*[-k]$. That is to say, $\mathbf{x}[k]$ and $\mathbf{x}^*[-k]$ should be detected jointly based on received signals $\mathbf{Y}$ so as to obtain better performance, thanks to potential diversity gain provided by TX I/Q imbalance.

As shown in Figure 3.4, the performance limit of Type-II receivers with only TX I/Q imbalance is to approach to that of systems without I/Q imbalances (ideal case). On the contrary, Type-I receivers can obtain improved performance (even compare with ideal case with the same detection algorithm except for MMSE) based on the fact that TX I/Q imbalance is capable of providing additional diversity gain. For MMSE algorithm, two types of receivers perform comparable. For MMSESIC and CF-I (II), Type-I receivers outperform Type-II about 3 dB and 2.5 dB at $\text{BER}=10^{-3}$ and $\text{BER}=10^{-4}$, respectively, but at the expense of increased computational complexity discussed in subsection 3.3.1. In addition, Type-II receivers with BZF-MIC and MMSE-MIC perform comparable to ideal case if the same detection algorithms are employed.
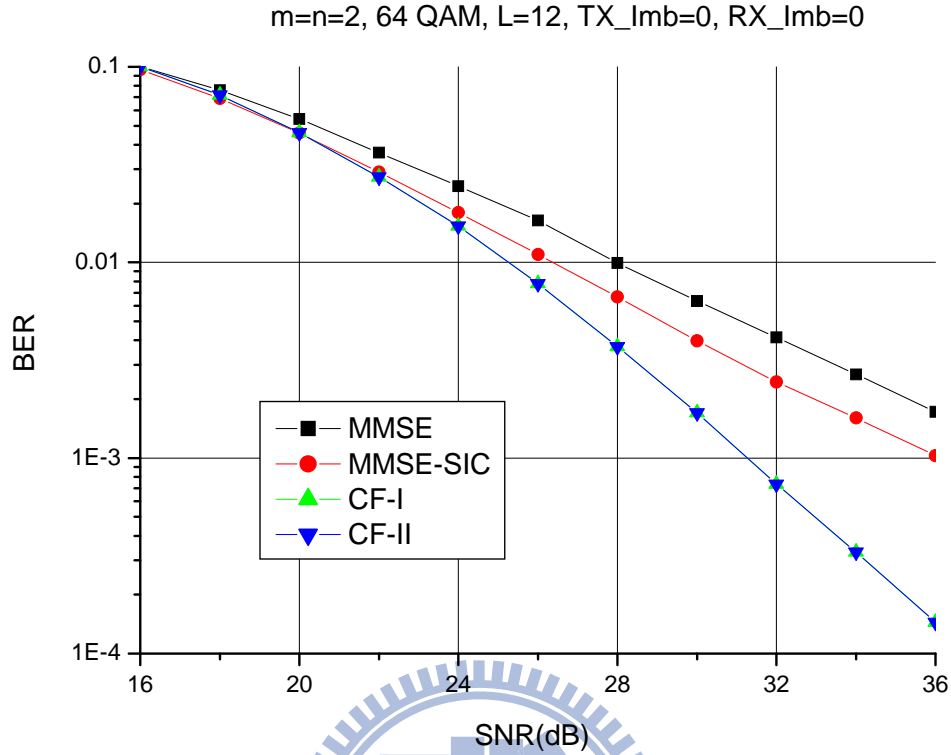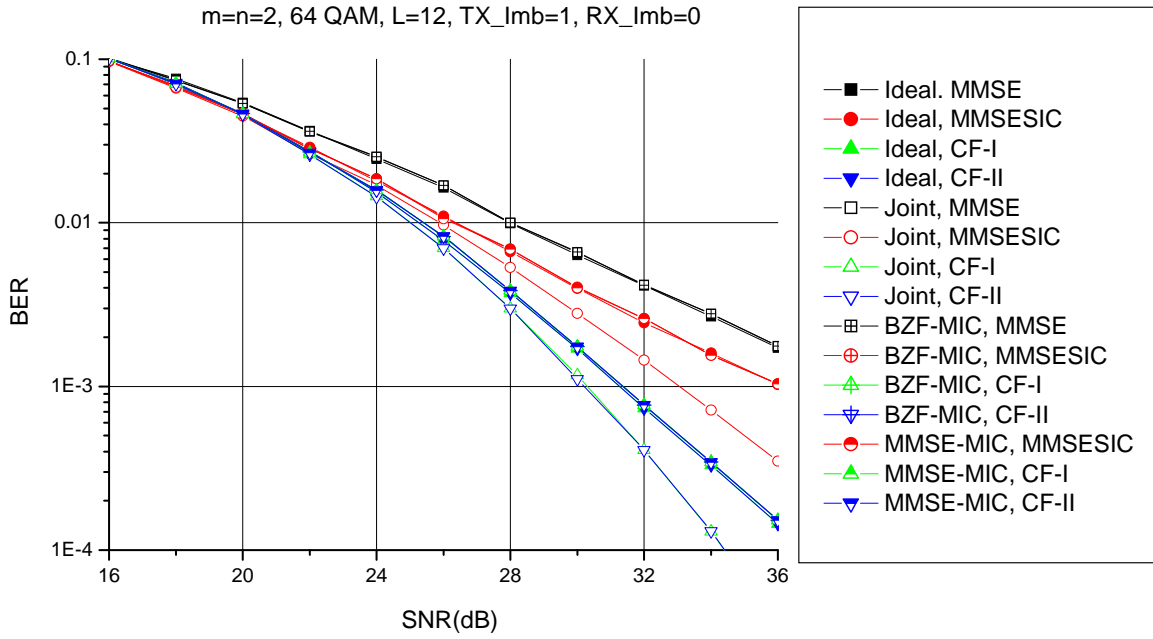
Figure 3.4: Comparison of BER performance for the case of TX_Imb = 1, RX_Imb = 0.
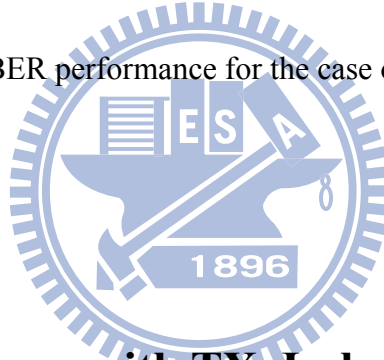
3.3.4 BER Performance with TX_Imb = 0, RX_Imb = 1

In this case, received signals can be expressed as:

$$\mathbf{Y} = \begin{bmatrix} \mathbf{Y}[k] \\ \mathbf{Y}^*[-k] \end{bmatrix} = \begin{bmatrix} \mathbf{H}^{11}[k] & \mathbf{H}^{12}[k] \\ \mathbf{H}^{21}[-k] & \mathbf{H}^{22}[-k] \end{bmatrix} \begin{bmatrix} \mathbf{x}[k] \\ \mathbf{x}^*[-k] \end{bmatrix} + \begin{bmatrix} \widehat{\mathbf{W}}[k] \\ \widehat{\mathbf{W}}^*[-k] \end{bmatrix} = \mathbf{Hx} + \widehat{\mathbf{W}}$$

$$\mathbf{H}^{11}[k] = \mathbf{H}_{R+}[k]\mathbf{H}_c[k]\mathbf{H}_{T+}[k],\ \mathbf{H}^{12}[k] = \mathbf{H}_{R-}[k]\mathbf{H}_c^*[-k]\mathbf{H}_{T+}^*[-k],$$

with $\mathbf{H}^{21}[-k] = \mathbf{H}_{R-}^*[-k]\mathbf{H}_c[k]\mathbf{H}_{T+}[k],\ \mathbf{H}^{22}[-k] = \mathbf{H}_{R+}^*[-k]\mathbf{H}_c^*[-k]\mathbf{H}_{T+}^*[-k]$ (3.23)

$$\mathbf{C}_{\widehat{\mathbf{W}}} = \sigma_n^2 \begin{bmatrix} \mathbf{\Psi}_{k,k} & \mathbf{\Psi}_{k,k'} \\ \mathbf{\Psi}_{k',k} & \mathbf{\Psi}_{k',k'} \end{bmatrix},\quad k' = N - k + 2$$

because of $\mathbf{H}_{T-}[k] = \mathbf{H}_{T-}[-k] = \mathbf{0}_{m \times m}$ and $\mathbf{H}_{T-,j} = \mathbf{0}_{N \times (N+L-1)},\ \forall j$. Note that although $\mathbf{x}[k]$ is

64

present not only at $\mathbf{Y}[k]$ but also at $\mathbf{Y}^*[-k]$ of receiver side, the potential diversity gain is not

longer available. It results from the fact that the channel gain constituent of $\mathbf{H}^{11}[k]$ and

$\mathbf{H}^{21}[-k]$ is the same, i.e., $\mathbf{H}_c[k]$. Similar phenomenon can also be found for $\mathbf{x}[-k]$.
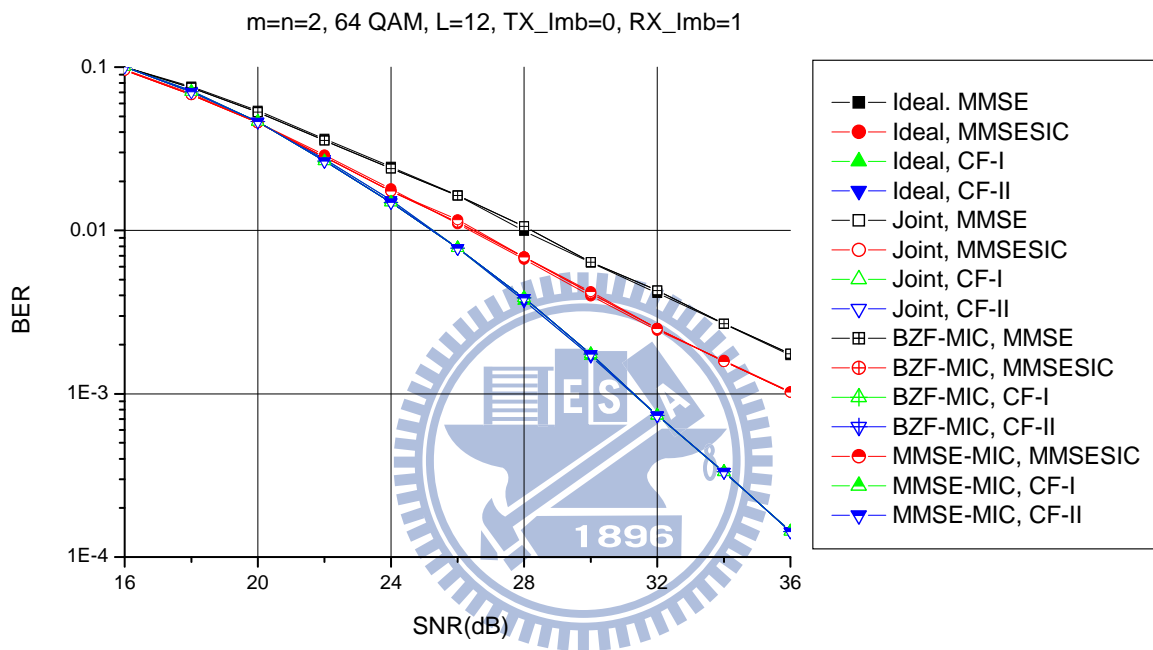
Figure 3.5: Comparison of BER performance for the case of TX_Imb = 0, RX_Imb = 1.

Figure 3.5 presents the performance comparisons. As can be seen, the performance with only RX I/Q imbalance is comparable for two types of receivers while the same detection algorithm is used, and can just approach to that of ideal case without attaining additional diversity gain.

3.3.5 BER Performance with TX_Imb = 1, RX_Imb = 1

This case is essentially the combinations of cases described in subsections 3.3.3 and 3.3.4, and the received signal model is expressed in Equation (3.14). Also its performance behavior is similar to that of systems with only TX I/Q imbalance, which can be seen by Figure 3.6.
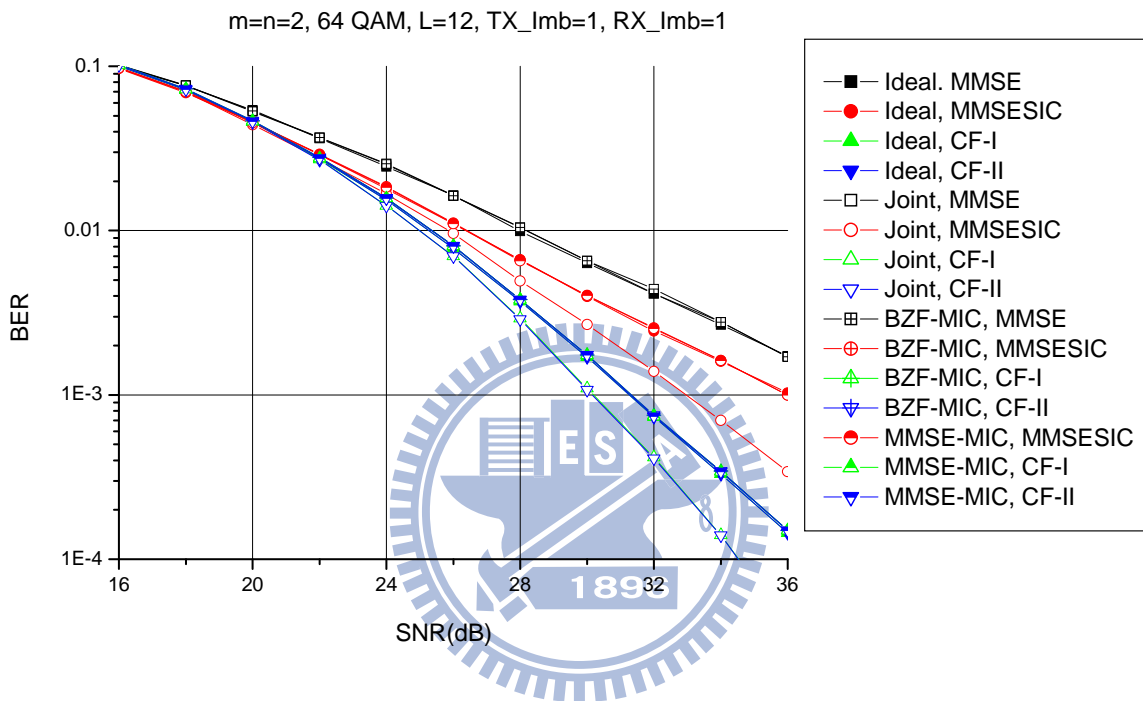
Figure 3.6: Comparison of BER performance for the case of TX_Imb = RX_Imb = 1.

3.4 Conclusions

According to the case studies and simulation results provided in previous section, receiver structures should be properly chosen based on MIMO-OFDM systems with TX and/or RX I-Q imbalances such as to compromise between performance and computational complexity. For

example, in the forward-link (down-link) of cellular systems, TX (base station) I-Q imbalance is nearly perfect, but RX (mobile unit) may have large I-Q imbalance due to its low-cost requirements. In this case (no additional receiver diversity can be exploited), Type-II receiver is recommended to enable comparable performance with Type-I and ideal case, and reduced computational complexity receiver (mobile unit). On the contrary, in the reverse-link (up-link) of cellular systems, receivers (base station) are suggested to employ Type-I structure so as to attain improved BER performance by making use of potential diversity gain provided by TX I-Q imbalance, but at the cost of increased computational complexity.
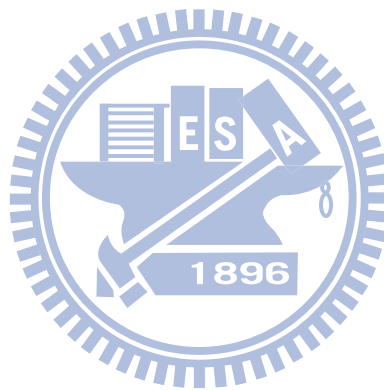
Chapter 4

Transmitter Pre-Processing for 2-D OFDM-CDMA Forward-Link Systems over Time-varying Rayleigh Fading Channels

2-D OFDM-CDMA is a promising access technology for the next–generation mobile cellular systems, thanks to its capability to exploit both the temporal and spectral characteristics of the fading channels. In this Chapter, transmitter-based pre-processing is investigated for 2-D OFDM-CDMA forward link systems over the time-variant multi-path Rayleigh fading channels, aiming to increase the system sum data rate and shift the signal processing complexity of a mobile unit to the base station. For the non-selective fading channels, the optimum pre-processing that achieves the maximum sum data rate is obtained by applying the principle of multi-user water filling under the condition of zero MAI. For the selective channels, preprocessing methods based on the traditional criteria of ZF and MMSE are investigated first, and then a new method called ZF-MWF (zero forcing with multi-user water filling) is proposed to increase the system performance.

4.1 System Model

4.1.1 Radio Resource Unit (RRU)

In order to apply 2-D spreading, the time-frequency radio resource in a frame is divided into non-overlapped $g_f \times g_t$ rectangular radio resource units (RRU) as shown in Figure 4.1 (a), where g_f and g_t are the frequency- and time-domain spreading factor, respectively. $G \doteq g_f \cdot g_t > 1$ is the overall spreading factor. In an RRU, the sub-carriers and OFDM symbols are assumed to be adjacent to each other[2]. Users with the same overall spreading factor can share an RRU in a code division fashion as shown in Figure 4.1 (b), and users with different overall spreading factor use different RRUs. Since RRUs are non-overlapping, without loss of generality only one RRU will be treated explicitly in the rest of this paper. Note that for $g_t = 1$ the system degenerates to an MC-CDMA system and for $g_f = 1$ an MC-DS-CDMA system; MC-CDMA and MC-DS-CDMA are special cases of the considered 2-D OFDM-CDMA system.

Different spreading patterns, characterized by the pair (g_f, g_t), can be employed under a fixed overall spreading factor. Figure 4.2 depicts such possibilities for $G = 16$ with different selections of g_f and g_t. For examples, $(g_f = 2, g_t = 8)$ and $(g_f = 4, g_t = 4)$ are two legitimate spreading patterns. Different spreading patterns may result in different performance depending on the frequency and time selectivity of the channel, as to shown later. In fact, how spreading patterns perform against each other under a fixed G is one of the issues that interest us in this study.

Let G be the number of users in the system. (Recall that G also is the overall

---

2. The sub-carriers and OFDM symbols in an RRU can also be scattered over the frequency and time, respectively in order to increase diversity order [9].
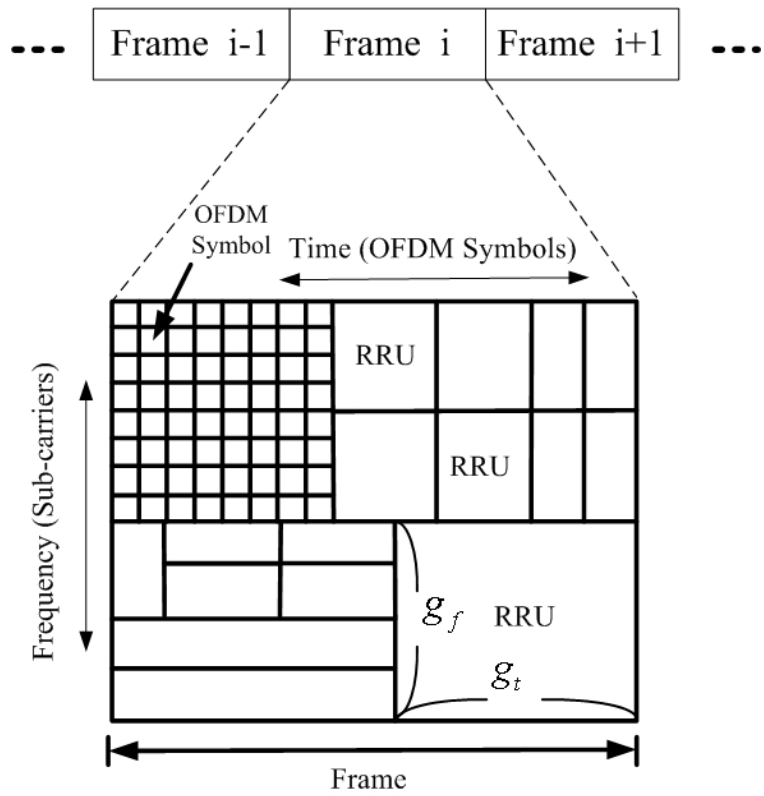
(a)
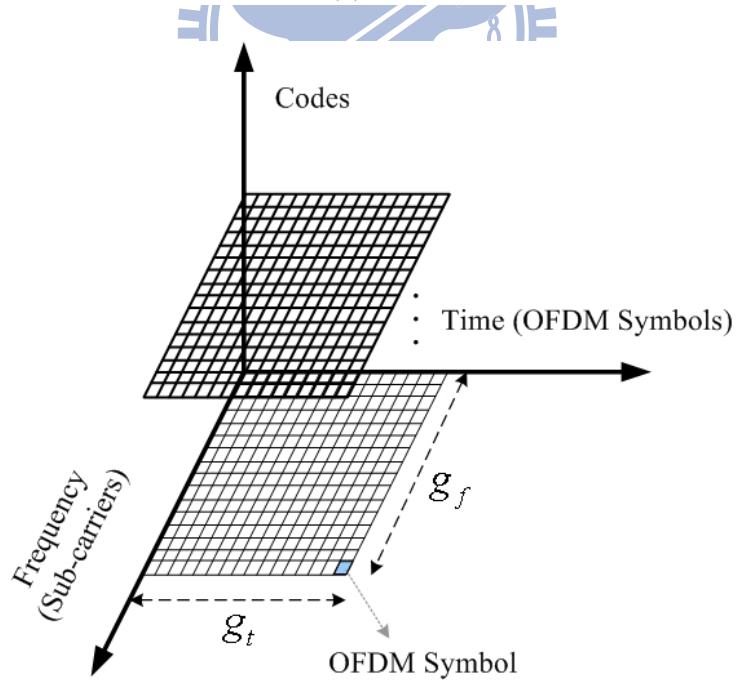
(b)

Figure 4.1: Radio Resource Units

spreading factor.) With orthogonal spreading codes, an RRU can be shared simultaneously by all the G users in a code division fashion, one code for each user. Nevertheless, it can also be shared by the G users in a time division fashion by scheduling different users in different frames; that is some users are scheduled to transmit in a frame and others are scheduled in other frames. In a time-varying fading
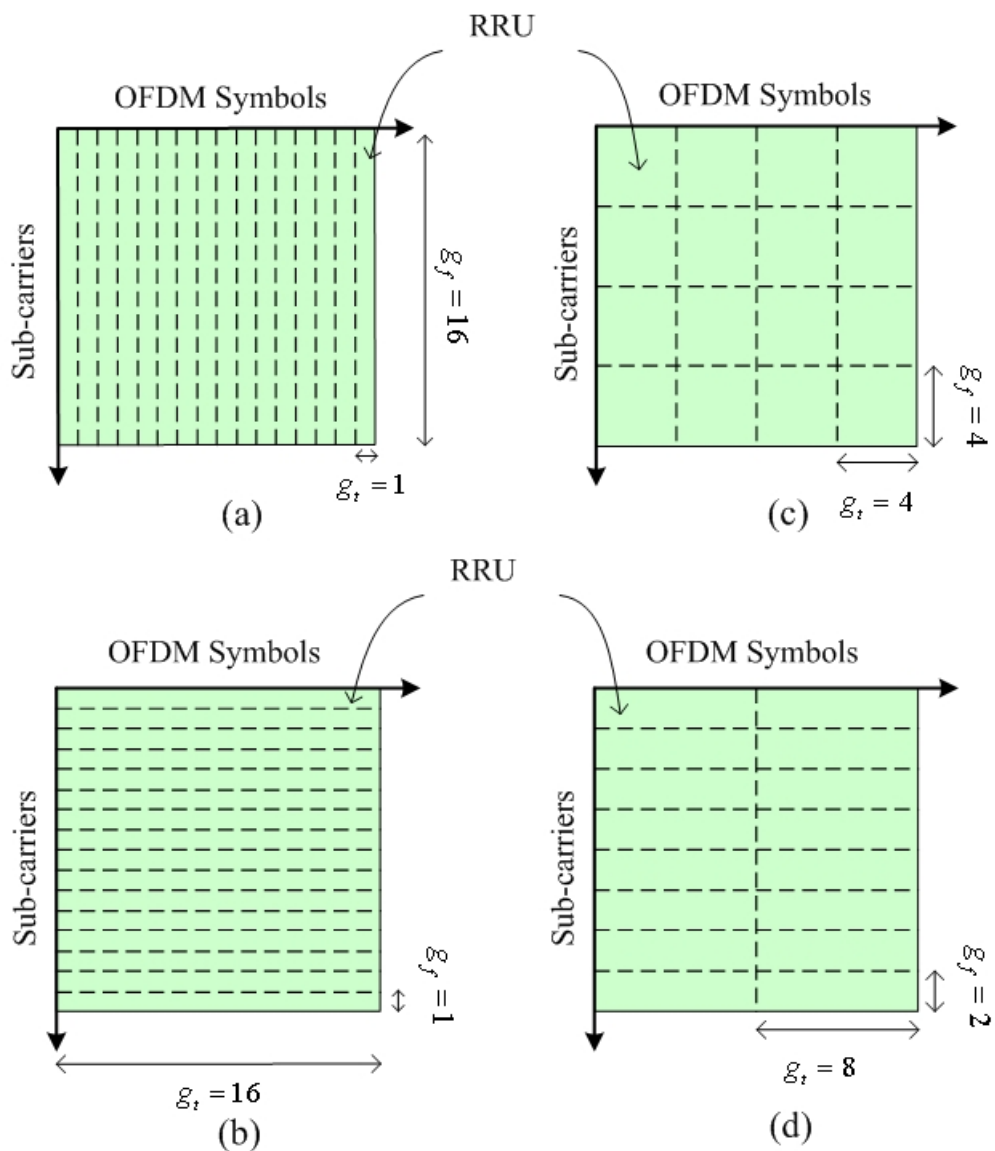
Figure 4.2: Example Spreading Patterns

environment, by scheduling those users who are in a good channel condition in a particular frame, one can take advantage of the multi-user diversity and increase the system throughput [19]. To investigate the multi-user diversity gain, we allow $K < G$ users be scheduled in a frame in our formulation. In this case, each scheduled user can use up to G/K spreading codes, where G/K is a positive integer. For a time-varying channel, it is plausible that each user has a fair access to the channel in the long run.

Anyhow, G symbols are always transmitted in an RRU, although the symbols may or may not belong to the same user. By that sense an RRU is said to support G data channels, one channel for a data symbol.

4.1.2 Channel Model

A discrete-time, wide-sense stationary uncorrelated scattering (WSSUS) Rayleigh channel is considered. The complex equivalent low-pass response for transmitting the i-th symbol $x^{(i)}$ (i-th data channel) is given by

$$h^{(i)}(t;\tau) = \sum_{l=0}^{L} h_l^{(i)}(t)\delta(\tau - lT_s), \quad i = 1,...,G, \tag{4.1}$$

where $\delta(\cdot)$ is the Dirac delta function, $h_l^{(i)}(t)$ is the lth path gain, lT_s is the propagation delay for the lth path, and T_s is the sampling duration of the system. $h_l^{(i)}(t)$ is a complex Gaussian random variable with zero mean and variance σ_l^2, and $\left\{h_l^{(i)}(t)\right\}_{l=0}^{L}$ are independent of each other for each i. In addition, $\left\{h_l^{(i)}(t)\right\}_{l=0}^{L}$ are independent of $\left\{h_l^{(j)}(t)\right\}_{l=0}^{L}$ if the ith and jth channels are not destined to the same user. The channel is assumed to be remained constant over one OFDM symbol and vary symbol-by-symbol based on channel time variation. Thus Equation (4.1) can be simplified as

72

$$h^{(i)}(n;\tau) = \sum_{l=0}^{L} h_l^{(i)}(n)\delta(\tau - lT_s), \quad i = 1,...,G, \tag{4.2}$$

where n is the OFDM symbol index. Furthermore, the power delay profile of the multi-path channel follows the exponential decay model

$$\sigma_l^2 = \sigma_0^2 \cdot \exp(-10l/L), \quad l = 1,2,....,L \quad , \tag{4.3}$$

with $\sigma_0^2 = 1 - \exp(-10/L)$, and $\sum_{l=0}^{L} \sigma_l^2 = 1$. For symbols (data channels) targeted to the same user, the channel responses are identical. Finally, the Clarke's two-dimensional isotropic scattering model for $\{h_l^{(i)}(n)\}$ will be used to model the time variation of channels in this study [61].

4.1.3 Transmitter and Receiver

The transmitter of the considered OFDM-CDMA forward-link system is sketched in Figure 4.3 (a). Recall that only one RRU will be explicitly treated. The data symbol $x^{(i)}$, $i = 1,...,G$ is first spread over time- and frequency-domain by a two-dimensional spreading code $c_{m,n}^{(i)}, m = 1,..., g_f, n = 1,..., g_t$, and the spreading *chip* is pre-processed by multiplying the complex-valued gain $p_{m,n}^{(i)}, m = 1,..., g_f, n = 1,..., g_t$, respectively. (Note that the data symbols may or may not belong to the same user.) The corresponding *chips* from all data symbols in an RRU are summed together before being allocated to the time-frequency plane which is done, along with chips from other RRUs, by the time-frequency mapping. Lastly, the allocated chips are performed IFFT and sent for further operations such as parallel-to-serial conversion, cyclic-prefix insertion and analog/RF front-end processing.
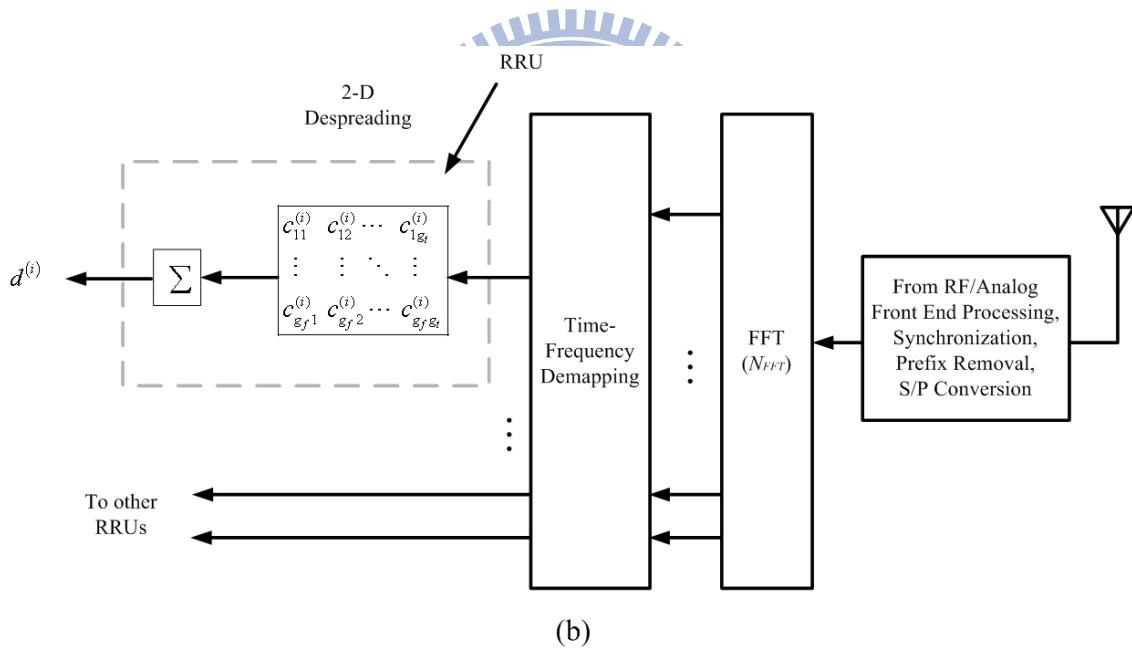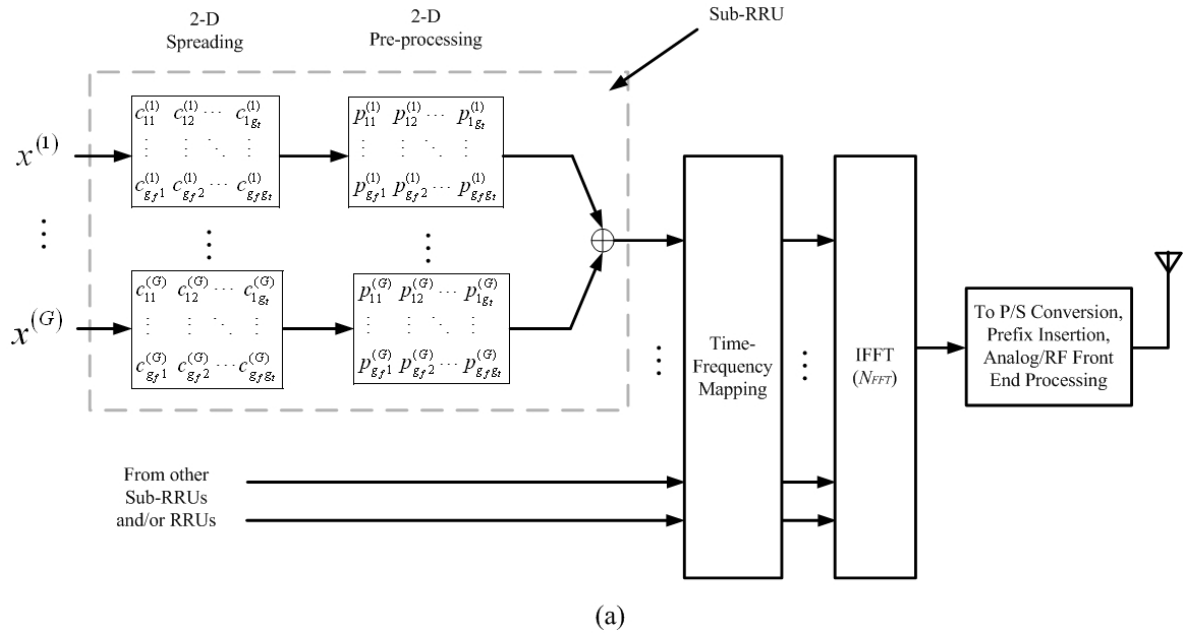
Figure 4.3: (a) Transmitter (b) Receiver

As is shown in Figure 4.3 (b), at the receive end of ith data channel, after RF/analog processing, synchronization, cyclic-prefix removal and serial to parallel conversion, the received signal is performed FFT and time-frequency de-mapping. The de-mapped chips of the considered

RRU are passed through a simple two-dimensional de-spreading because most of the signal processing has been shifted to the base station. The de-spread signals are then forwarded for further demodulation and/or decoding.

4.1.4 Signal Models

Assuming that the length of cyclic-prefix is larger than the maximum delay spread LT_s and that perfect frequency/time synchronization is achievable at the receiver, then the de-mapped signal of the (m,n)th chip of i-th data channel is given by,

$$y_{m,n}^{(i)} = \left(\sum_{j=1}^{G} x^{(j)} p_{m,n}^{(j)} c_{m,n}^{(j)} \right) H_{m,n}^{(i)} + W_{m,n}^{(i)}, m = 1,...,g_f, n = 1,...,g_t, i = 1,...,G , \qquad (4.4)$$

where

$$H_{m,n}^{(i)} = \sum_{l=0}^{L} h_l^{(i)}(n) e^{\frac{-j2\pi lm}{N_{FFT}}} , \qquad (4.5)$$

and $W_{m,n}^{(i)}$ are the associated (frequency-domain) channel gain and noise, respectively, and N_{FFT} is the size of IFFT/FFT. Note again that $H_{m,n}^{(i)} = H_{m,n}^{(j)}$, and $W_{m,n}^{(i)} = W_{m,n}^{(j)}$ if $x^{(i)}$ and $x^{(j)}$ belong to the same user. In addition, $W_{m,n}^{(i)}$ is a Gaussian variable with zero mean and variance σ_W^2.

For notation simplicity, we redefine the two-dimensional chip index (m,n) into the one-dimensional one by using $k = (n-1)g_f + m, \ n = 1,\cdots g_t, m = 1,\cdots g_f, k = 1\cdots G$. With this new indexing notation, Equation (4.5) can be rewritten as the matrix form below.

$$\mathbf{y}^{(i)} \doteq \begin{bmatrix} y_1^{(i)} \\ \vdots \\ y_k^{(i)} \\ \vdots \\ y_G^{(i)} \end{bmatrix} = \begin{bmatrix} \left(\sum_{j=1}^{G} x^{(j)} p_1^{(j)} c_1^{(j)} \right) H_1^{(i)} + W_1^{(i)} \\ \vdots \\ \left(\sum_{j=1}^{G} x^{(j)} p_k^{(j)} c_k^{(j)} \right) H_k^{(i)} + W_k^{(i)} \\ \vdots \\ \left(\sum_{j=1}^{G} x^{(j)} p_G^{(j)} c_G^{(j)} \right) H_G^{(i)} + W_G^{(i)} \end{bmatrix}$$

$$= \begin{bmatrix} H_1^{(i)} & & 0 \\ & \ddots & \\ 0 & & H_G^{(i)} \end{bmatrix} \left(\left[\mathbf{p}^{(1)}, ..., \mathbf{p}^{(G)} \right] \odot \left[\mathbf{c}^{(1)}, ..., \mathbf{c}^{(G)} \right] \right) \begin{bmatrix} x^{(1)} \\ \vdots \\ x^{(G)} \end{bmatrix} + \begin{bmatrix} W_1^{(i)} \\ \vdots \\ W_G^{(i)} \end{bmatrix}$$

(4.6)

where $\mathbf{p}^{(j)} \doteq \left[p_1^{(j)} \cdots p_G^{(j)} \right]^T$, $\mathbf{c}^{(j)} \doteq \left[c_1^{(j)} \cdots c_G^{(j)} \right]^T$, $\odot$ denotes the Hadamard product (element-by-element multiplication), and $[\bullet]^T$ the operation of transpose of a vector and/or matrix. Define $\mathbf{x} = \left[x^{(1)} \cdots x^{(G)} \right]^T$, $\mathbf{w}^{(i)} = \left[W_1^{(i)} \cdots W_G^{(i)} \right]^T$, $\mathbf{P} = \left[\mathbf{p}^{(1)} \mathbf{p}^{(2)} \cdots \mathbf{p}^{(G)} \right]$, $\mathbf{C} = \left[\mathbf{c}^{(1)} \mathbf{c}^{(2)} \cdots \mathbf{c}^{(G)} \right]$ and $\mathbf{H}^{(i)} = \begin{bmatrix} H_1^{(i)} & & 0 \\ & \ddots & \\ 0 & & H_G^{(i)} \end{bmatrix}$,

Equation (4.6) becomes

$$\mathbf{y}^{(i)} = \mathbf{H}^{(i)} \left(\mathbf{P} \odot \mathbf{C} \right) \mathbf{x} + \mathbf{w}^{(i)},$$

(4.7)

where $\mathbf{x}$ is the symbol vector with the covariance matrix $\sigma_x^2 \mathbf{I}_G$, $\mathbf{w}^{(i)}$ is a complex Gaussian vector with the covariance matrix $\sigma_W^2 \mathbf{I}_G$, σ_x^2 and σ_W^2 are the average transmit power, and noise power for each sub-carrier, respectively, and $\mathbf{I}_G$ is the identity matrix of dimension G.

Let $d^{(i)}$ be the decision variable of i-th data channel. Then,

$$d^{(i)} \doteq \mathbf{c}^{(i)^H} \mathbf{y}^{(i)} = \mathbf{c}^{(i)^H} \mathbf{H}^{(i)} \left(\mathbf{P} \odot \mathbf{C} \right) \mathbf{x} + \mathbf{c}^{(i)^H} \mathbf{w}^{(i)},$$

(4.8)

where $[\bullet]^H = [\bullet]^{*^T}$ denotes conjugate transpose operation, and $\left\{ \mathbf{c}^{(i)^H} \mathbf{w}^{(i)} \right\}_{i=1}^{G}$ are i.i.d. Gaussian variables provided that orthogonal codes are used.

4.2 Transmitter-Based Pre-Processing

4.2.1 Sum Data Rate

For a multiple access system, sum data rate is the maximum achievable reliable data rate of all users supported by the system [19]. It is a measure of system throughput from the information-theoretical point of view. Sum data rate will be adopted here as the performance index for the design and comparison of different pre-processing methods.

From Equation (4.8), the decision variable for i-th symbol can be rewritten as

$$d^{(i)} = \underbrace{\mathbf{c}^{(i)^H} \mathbf{H}^{(i)} \left(\mathbf{p}^{(i)} \odot \mathbf{c}^{(i)} \right) x^{(i)}}_{\text{desired signal}} + \underbrace{\sum_{\substack{j=1 \\ j \neq i}}^{G} \mathbf{c}^{(i)^H} \mathbf{H}^{(i)} \left(\mathbf{p}^{(j)} \odot \mathbf{c}^{(j)} \right) x^{(j)} + \underbrace{\mathbf{c}^{(i)^H} \mathbf{w}^{(i)}}_{\text{noise}}}_{\text{MAI}} . \qquad (4.9)$$

The MAI term can be approximated as a zero-mean Gaussian variable under the assumption of large G [62]. Therefore, the achievable maximum reliable data rate $\mathcal{C}^{(i)}$ for i-th data channel, given $\mathbf{H}^{(i)}$, is given by [19], [63]

$$\mathcal{C}^{(i)} = \frac{1}{G} \log_2 \left\{ 1 + \frac{E\left[\left| \mathbf{c}^{(i)^H} \mathbf{H}^{(i)} \mathbf{q}^{(i)} x^{(i)} \right|^2 \right]}{E\left[\left| \sum_{\substack{j=1 \\ j \neq i}}^{G} \mathbf{c}^{(i)^H} \mathbf{H}^{(i)} \mathbf{q}^{(j)} x^{(j)} + \mathbf{c}^{(i)^H} \mathbf{w}^{(i)} \right|^2 \right]} \right\}$$

$$= \frac{1}{G} \log_2 \left\{ 1 + \frac{\sigma_x^2 \cdot \mathbf{q}^{(i)^H} \mathbf{H}^{(i)^H} \mathbf{c}^{(i)} \mathbf{c}^{(i)^H} \mathbf{H}^{(i)} \mathbf{q}^{(i)}}{\sigma_x^2 \sum_{\substack{j=1 \\ j \neq i}}^{G} \mathbf{q}^{(j)^H} \mathbf{H}^{(i)^H} \mathbf{c}^{(i)} \mathbf{c}^{(i)^H} \mathbf{H}^{(i)} \mathbf{q}^{(j)} + \sigma_w^2} \right\} \text{ b/s/Hz,} \qquad (4.10)$$

where $\mathbf{q}^{(i)} \doteq \mathbf{p}^{(i)} \odot \mathbf{c}^{(i)}$, and $\left\| \mathbf{c}^{(i)} \right\|^2 = 1$ for $i=1,2,\ldots,G$. As a result, the sum data rate $\mathcal{C}$ which is the sum of individual rate is obtained by

$$\mathcal{C} = \sum_{i=1}^{G} \mathcal{C}^{(i)} = \frac{1}{G} \sum_{i=1}^{G} \log_2 \left\{ 1 + \frac{\sigma_x^2 \cdot \mathbf{q}^{(i)^H} \mathbf{H}^{(i)^H} \mathbf{c}^{(i)} \mathbf{c}^{(i)^H} \mathbf{H}^{(i)} \mathbf{q}^{(i)}}{\sigma_x^2 \sum_{\substack{j=1 \\ j \neq i}}^{G} \mathbf{q}^{(j)^H} \mathbf{H}^{(i)^H} \mathbf{c}^{(i)} \mathbf{c}^{(i)^H} \mathbf{H}^{(i)} \mathbf{q}^{(j)} + \sigma_W^2} \right\} \quad \text{b/s/Hz} \qquad (4.11)$$

With the performance index in Equation (4.11), our problem becomes to find the set of optimum pre-processing weight vectors $\left\{ \hat{\mathbf{q}}^{(i)} \right\}$, for a given $\left\{ \mathbf{H}^{(i)} \right\}$, to obtain the maximum sum data rate by solving the following constrained optimization problem

$$\left\{ \hat{\mathbf{q}}^{(i)} \right\} = \arg \left\{ \max_{\left\{ \mathbf{q}^{(i)} \right\}} \mathcal{C} \right\}, \quad \text{s.t.} \sum_{i=1}^{G} \left\| \mathbf{q}^{(i)} \right\|^2 = G. \qquad (4.12)$$

After obtaining the sum data rate for a particular $\left\{ \mathbf{H}^{(i)} \right\}$, the average sum data rate, called ergodic sum data rate in [19][3], is evaluated by $\mathcal{C}_{erg} = \mathrm{E}[\mathcal{C}]$, where the expectation is taken over all channels $\left\{ \mathbf{H}^{(i)} \right\}$.
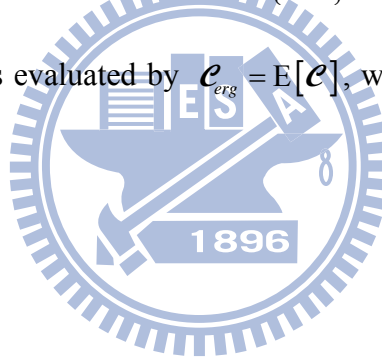
4.2.2 Non-selective Fading Channels

For the non-selective (both time and frequency) fading channels, $\mathbf{H}^{(i)} = H^{(i)} \mathbf{I}_G$ for all i. In this case, as to be shown, the optimization in Equation (4.12) can be carried out easily in two steps, thanks to the nice property of orthogonality among different data channels in this channel condition. Firstly, from Equation (4.10), it is observed that if a set of $\left\{ \mathbf{q}^{(i)} \right\}$ which is able to

---

3. ε-outage data rate is a more appropriate performance measure for a very slow fading channel [19, chapter 6] which is not the case considered here.

maximize the respective signal power $E\left[\left|\mathbf{c}^{(i)^H}\mathbf{H}^{(i)}\mathbf{q}^{(i)}x^{(i)}\right|^2\right]$ while completely eliminating the

MAI $\sigma_x^2\sum\limits_{\substack{j=1\\j\neq i}}^{G}\mathbf{q}^{(j)^H}\mathbf{H}^{(i)^H}\mathbf{c}^{(i)}\mathbf{c}^{(i)^H}\mathbf{H}^{(i)}\mathbf{q}^{(j)},\forall i$, then it will be the optimal one. Such a $\{\mathbf{q}^{(i)}\}$ is indeed

available as derived as follows. According to the results of Rayleigh Quotient [64],

$\mathbf{q}^{(i)^H}\mathbf{H}^{(i)^H}\mathbf{c}^{(i)}\mathbf{c}^{(i)^H}\mathbf{H}^{(i)}\mathbf{q}^{(i)}\leq\lambda_{\max}\left\|\mathbf{q}^{(i)}\right\|^2$ with equality if $\mathbf{q}^{(i)}$ is the eigenvector associated with the

maximum eigenvalue $\lambda_{\max}$ of the Hermitian matrix $\mathbf{H}^{(i)^H}\mathbf{c}^{(i)}\mathbf{c}^{(i)^H}\mathbf{H}^{(i)}$. In addition, it is easy to

see that $\operatorname{rank}\left(\mathbf{H}^{(i)^H}\mathbf{c}^{(i)}\mathbf{c}^{(i)^H}\mathbf{H}^{(i)}\right)=1$ with $\lambda_{\max}=\left\|\mathbf{H}^{(i)^H}\mathbf{c}^{(i)}\right\|^2$ and the corresponding eigenvector

$t_i\cdot\mathbf{H}^{(i)^H}\mathbf{c}^{(i)}$, where t_i is a non-zero complex value. Setting $\mathbf{q}^{(i)}=t_i\cdot\mathbf{H}^{(i)^H}\mathbf{c}^{(i)},\forall i$ in Equation

(4.10), it is clear that MAI can be removed completely because all the spreading codes are

orthogonal, and therefore $\tilde{\mathbf{q}}^{(i)}=t_i\cdot\mathbf{H}^{(i)^H}\mathbf{c}^{(i)},\forall i$ is the set of optimum pre-processing vectors that

maximizes $\mathcal{C}^{(i)}$ given the transmit power $\sigma_x^2\left\|\tilde{\mathbf{q}}^{(i)}\right\|^2,\forall i$. The next step is to apply the principle

of multi-user water filling so as to maximize the sum data rate. This can be done by solving the

following constrained optimization problem,

$$\left\{\left\|\hat{\mathbf{q}}^{(i)}\right\|^2\right\}=\arg\left\{\max_{\left\{\left\|\tilde{\mathbf{q}}^{(i)}\right\|^2\right\}}\sum_{i=1}^{G}\log_2\left[1+\frac{\sigma_x^2\left\|\mathbf{H}^{(i)^H}\mathbf{c}^{(i)}\right\|^2\left\|\tilde{\mathbf{q}}^{(i)}\right\|^2}{\sigma_W^2}\right]\right\},\text{ s.t. }\sum_{i=1}^{G}\left\|\tilde{\mathbf{q}}^{(i)}\right\|^2=G.\qquad(4.13)$$

Equation (4.13) can be solved by applying the theory of Lagrange Multiplier as follows [65].

Since the objective function is lower bounded by zero, there exists at least one solution in

Equation (4.13). Define the Lagrange function

$$f\left(\left\|\tilde{\mathbf{q}}^{(1)}\right\|^2,...,\left\|\tilde{\mathbf{q}}^{(G)}\right\|^2,\lambda\right)=\sum_{i=1}^{G}\log_2\left\{1+\frac{\sigma_x^2\left\|\mathbf{H}^{(i)^H}\mathbf{c}^{(i)}\right\|^2\left\|\tilde{\mathbf{q}}^{(i)}\right\|^2}{\sigma_W^2}\right\}+\lambda\left(\sum_{i=1}^{G}\left\|\tilde{\mathbf{q}}^{(i)}\right\|^2-G\right),\quad(4.14)$$

where λ is the real Lagrange multiplier. The necessary conditions for the solutions are given by

$$\frac{\partial}{\partial \left\| \tilde{\mathbf{q}}^{(i)} \right\|^2} f\left(\left\| \hat{\mathbf{q}}^{(1)} \right\|^2, \dots, \left\| \hat{\mathbf{q}}^{(G)} \right\|^2, \hat{\lambda} \right) = 0, \ \forall i, \tag{4.15}$$

and

$$\frac{\partial}{\partial \lambda} f\left(\left\| \hat{\mathbf{q}}^{(1)} \right\|^2, \dots, \left\| \hat{\mathbf{q}}^{(G)} \right\|^2, \hat{\lambda} \right) = 0 \tag{4.16}$$

These equations lead to

$$\left\| \hat{\mathbf{q}}^{(i)} \right\|^2 = -\frac{1}{\hat{\lambda} \cdot \ln 2} - \frac{\sigma_w^2}{\sigma_x^2 \left\| \mathbf{H}^{(i)^H} \mathbf{c}^{(i)} \right\|^2}, \ \forall i \tag{4.17}$$

and

$$\sum_{i=1}^{G} \left\| \hat{\mathbf{q}}^{(i)} \right\|^2 = G \tag{4.18}$$

From Equations (4.17) and (4.18) we have

$$\left\| \hat{\mathbf{q}}^{(i)} \right\|^2 = \left[1 + \frac{\sigma_w^2}{G \cdot \sigma_x^2} \sum_{j=1}^{G} \frac{1}{\left\| \mathbf{H}^{(j)^H} \mathbf{c}^{(j)} \right\|^2} - \frac{\sigma_w^2}{\sigma_x^2 \cdot \left\| \mathbf{H}^{(i)^H} \mathbf{c}^{(i)} \right\|^2} \right]^+, \ i = 1 \cdots G, \tag{4.19}$$

where $[x]^+ = \max\{x, 0\}$. Equation (4.19) is a form of multi-user water filling.

4.2.3 Selective Fading Channels

For the selective (either time, frequency or both) fading channels, there is no easy way to solve the constrained optimization problem in Equation (4.12) because the *orthogonality* among different data channels are destroyed. In this part, we first apply the traditional ZF-PN (zero forcing with power normalization) and MMSE (minimum mean square error) criteria to design the pre-processing. Then a new method called ZF-MWF (zero forcing with multi-user water filling) is proposed.

4.2.3.1 Zero-Forcing with Power Normalization

The basic idea of this method is trying to decouple different data channels (data symbols) at the outputs of de-spreading by properly choosing matrix $\mathbf{Q} \doteq \mathbf{P} \odot \mathbf{C}$ at the base station. In other words, the MAI is eliminated completely at the outputs of the de-spreading operation of the receiver. Then, the total transmit power is normalized to meet the power constraint [12].

Define $\mathbf{d}$ be the aggregated decision variables from all data channels. From Equation (4.9),

$$\mathbf{d} \doteq \begin{bmatrix} d^{(1)} \\ \vdots \\ d^{(G)} \end{bmatrix} = \begin{bmatrix} \mathbf{c}^{(1)^H} \mathbf{H}^{(1)} \mathbf{Q} \mathbf{x} + \mathbf{c}^{(1)^H} \mathbf{w}^{(1)} \\ \vdots \\ \mathbf{c}^{(G)^H} \mathbf{H}^{(G)} \mathbf{Q} \mathbf{x} + \mathbf{c}^{(G)^H} \mathbf{w}^{(G)} \end{bmatrix} = \begin{bmatrix} \mathbf{c}^{(1)^H} \mathbf{H}^{(1)} \\ \vdots \\ \mathbf{c}^{(G)^H} \mathbf{H}^{(G)} \end{bmatrix} \mathbf{Q}\mathbf{x} + \begin{bmatrix} \mathbf{c}^{(1)^H} \mathbf{w}^{(1)} \\ \vdots \\ \mathbf{c}^{(G)^H} \mathbf{w}^{(G)} \end{bmatrix} = \underbrace{\mathbf{RQx}}_{signal} + \underbrace{\mathbf{w}}_{noise} \quad (4.20)$$

where

$$\mathbf{R} = \begin{bmatrix} \mathbf{c}^{(1)^H} \mathbf{H}^{(1)} \\ \vdots \\ \mathbf{c}^{(G)^H} \mathbf{H}^{(G)} \end{bmatrix}, \quad \text{and } \mathbf{w} = \begin{bmatrix} \mathbf{c}^{(1)^H} \mathbf{w}^{(1)} \\ \vdots \\ \mathbf{c}^{(G)^H} \mathbf{w}^{(G)} \end{bmatrix}.$$

To eliminate completely the MAI, we need the condition that $\mathbf{R}\widetilde{\mathbf{Q}}\mathbf{x} = \mathbf{x}$. That results in

$$\widetilde{\mathbf{Q}} = \mathbf{R}^H \left(\mathbf{R}\mathbf{R}^H \right)^{-1} \doteq \mathbf{R}_R^+ . \tag{4.21}$$

$\mathbf{R}_R^+$ is the right pseudo inverse of matrix $\mathbf{R}$. On the other hand, the total transmit power needs to be normalized to $\sigma_x^2 \cdot G$, that is $E\left[\left\| \hat{\mathbf{Q}}\mathbf{x} \right\|^2 \right] = \sigma_x^2 \cdot G$. Therefore, $\hat{\mathbf{Q}} = \sqrt{G}\mathbf{R}_R^+ / \left\| \mathbf{R}_R^+ \right\|_F$ where $\left\| \bullet \right\|_F$ stands for the Frobenius norm of a matrix.

4.2.3.2 Minimum Mean Square Error

In this method, $\hat{\mathbf{Q}}$ is selected to minimize mean square error between the decision vector $\mathbf{d}$ and transmitted symbol vector $\mathbf{x}$, under a fixed transmit power. The associated constrained

optimization problem can be formulated as follows.

$$\widehat{\mathbf{Q}} = \arg\left\{\min_{\mathbf{Q}} E\left[\|\mathbf{d} - \mathbf{x}\|^2\right]\right\}, \text{ s.t. } \|\mathbf{Q}\|_F^2 = tr\left\{\mathbf{Q}^H\mathbf{Q}\right\} = G \quad , \tag{4.22}$$

where

$$E\left[\|\mathbf{d} - \mathbf{x}\|^2\right] = E\left[\|\mathbf{RQx} + \mathbf{w} - \mathbf{x}\|^2\right] = \sigma_x^2 \cdot tr\left\{\left[\mathbf{Q}^H\mathbf{R}^H - \mathbf{I}_G\right]\left[\mathbf{RQ} - \mathbf{I}_G\right]\right\} + G \cdot \sigma_w^2 \quad .$$

$$\tag{4.23}$$

Therefore, Equation (4.22) can be rewritten as

$$\widehat{\mathbf{Q}} = \arg\left\{\min_{\mathbf{Q}} tr\left\{\left[\mathbf{Q}^H\mathbf{R}^H - \mathbf{I}_G\right]\left[\mathbf{RQ} - \mathbf{I}_G\right]\right\}\right\}, \text{ s.t. } \|\mathbf{Q}\|_F^2 = tr\left\{\mathbf{Q}^H\mathbf{Q}\right\} = G \tag{4.24}$$

In what follows, again, the theory of Lagrange Multiplier is employed to solve the above constrained optimization problem.

Define the Lagrange function as

$$f(\mathbf{Q}, \lambda) = tr\left\{\left[\mathbf{Q}^H\mathbf{R}^H - \mathbf{I}_G\right]\left[\mathbf{RQ} - \mathbf{I}_G\right]\right\} + \lambda\left(tr\left\{\mathbf{Q}^H\mathbf{Q}\right\} - G\right). \tag{4.25}$$

The necessary conditions for the solutions in Equation (4.24) are $\dfrac{\partial}{\partial \mathbf{Q}} f\left(\widehat{\mathbf{Q}}, \hat{\lambda}\right) = \mathbf{0}$ and

$\dfrac{\partial}{\partial \lambda} f\left(\widehat{\mathbf{Q}}, \hat{\lambda}\right) = 0$, which in turn give the conditions

$$\left(\mathbf{R}^H\mathbf{R} + \hat{\lambda} \cdot \mathbf{I}_G\right)\widehat{\mathbf{Q}} = \mathbf{R}^H \quad , \tag{4.26}$$

and

$$tr\left\{\widehat{\mathbf{Q}}^H\widehat{\mathbf{Q}}\right\} = G. \tag{4.27}$$

In Appendix F, it is shown that the square matrix $\left(\mathbf{R}^H\mathbf{R} + \hat{\lambda} \cdot \mathbf{I}_G\right)$ in Equation (4.26) is nonsingular in order for $\left(\hat{\lambda}, \widehat{\mathbf{Q}}\right)$ to become a solution. Therefore,

$$\widehat{\mathbf{Q}} = \left(\mathbf{R}^H\mathbf{R} + \hat{\lambda} \cdot \mathbf{I}_G\right)^{-1}\mathbf{R}^H , \tag{4.28}$$

and from Equation (4.27) we have

$$tr\left\{\left(\mathbf{R}^H\mathbf{R} + \hat{\lambda} \cdot \mathbf{I}_G\right)^{-1}\mathbf{R}^H\mathbf{R}\left(\mathbf{R}^H\mathbf{R} + \hat{\lambda} \cdot \mathbf{I}_G\right)^{-1}\right\} = G. \tag{4.29}$$

By applying the spectral decomposition to the Hermitian matrix $\mathbf{R}^H\mathbf{R}$, that is,

$$\mathbf{R}^H \mathbf{R} = \sum_{i=1}^{G} \lambda_i \mathbf{v}_i \mathbf{v}_i^{\mathrm{H}} \tag{4.30}$$

where λ_i and $\mathbf{v}_i$ are the eigenvalue and eigenvector of the matrix $\mathbf{R}^H \mathbf{R}$, respectively. Equation (4.29) can be simplified as

$$\sum_{i=1}^{G} \frac{\lambda_i}{\left(\hat{\lambda} + \lambda_i \right)^2} = G \tag{4.31}$$

where from the Appendix F, $\hat{\lambda} \neq -\lambda_i, \forall i$. Equation (4.31) can be solved by using numerical methods such as the one given in [66].

4.2.3.3 Zero-forcing with Multi-user Water Filling

From Equation (4.10), it is clear that the achievable data rate of a specific channel can be increased by maximizing the received signal power and/or eliminating MAI. Also, as discussed in the case of non-selective channels, the principle of multi-user water filling can be applied in a multi-user environment to increase the sum data rate. In our previous discussions, ZF with power normalization is able to remove MAI completely but with no attempt to maximize the received signal power. MMSE, on the other hand, tries to strike a balance between MAI and noise. The residual MAI, however, may limit the sum data rate in Equation (4.11) while noise is comparably small. Unfortunately, both methods do not exploit the potential gain of multi-user water filling as does in the non-selective case, in a multi-user environment. In this section, a novel two-step pre-processing method called ZF with multi-user water filling is proposed. In the first step, the received signal power is maximized for each respective data channel under the condition of zero MAI, and then the principle of multi-user water filling is applied in the second step so as to increase the sum data rate.

The first step is to find a set of $\left\{ \tilde{\mathbf{q}}^{(i)} \right\}$ such that the MAI in Equation (4.9) is eliminated

completely and at the same time the respective desired signal power is maximized. In other words,

$$\tilde{\mathbf{q}}^{(i)} = \arg\left\{\max_{\mathbf{q}^{(i)}} \ \mathbf{q}^{(i)^H} \mathbf{H}^{(i)^H} \mathbf{c}^{(i)} \mathbf{c}^{(i)^H} \mathbf{H}^{(i)} \mathbf{q}^{(i)}\right\},$$
$$\text{s.t.} \ \mathbf{q}^{(i)} \in \bigcap_{\substack{j=1 \\ j \neq i}}^{G} \mathcal{N}\left\{\mathbf{H}^{(j)^H} \mathbf{c}^{(j)} \mathbf{c}^{(j)^H} \mathbf{H}^{(j)}\right\}, \ \forall i \tag{4.32}$$

where $\mathcal{N}\{\mathbf{A}\}$ denotes the null space of the matrix $\mathbf{A}$, and $\cap$ the operation of intersection. Equivalently,

$$\tilde{\mathbf{q}}^{(i)} = \arg\left\{\max_{\mathbf{q}^{(i)}} \ \mathbf{q}^{(i)^H} \mathbf{H}^{(i)^H} \mathbf{c}^{(i)} \mathbf{c}^{(i)^H} \mathbf{H}^{(i)} \mathbf{q}^{(i)}\right\}, \ \text{s.t.} \ \mathbf{q}^{(i)} \in \mathcal{N}\{\mathcal{H}\} \ \forall i \tag{4.33}$$

where

$$\mathcal{H} \doteq \begin{bmatrix} \mathbf{H}^{(1)^H} \mathbf{c}^{(1)} \mathbf{c}^{(1)^H} \mathbf{H}^{(1)} \\ \vdots \\ \mathbf{H}^{(i-1)^H} \mathbf{c}^{(i-1)} \mathbf{c}^{(i-1)^H} \mathbf{H}^{(i-1)} \\ \mathbf{H}^{(i+1)^H} \mathbf{c}^{(i+1)} \mathbf{c}^{(i+1)^H} \mathbf{H}^{(i+1)} \\ \vdots \\ \mathbf{H}^{(G)^H} \mathbf{c}^{(G)} \mathbf{c}^{(G)^H} \mathbf{H}^{(G)} \end{bmatrix}. \tag{4.34}$$

Let $\left\{\boldsymbol{\beta}_1^{(i)}, ..., \boldsymbol{\beta}_{D_i}^{(i)}\right\}$ be an orthonormal basis of $\mathcal{N}\{\mathcal{H}\}$, and D_i be its dimension. Then, $\mathbf{q}^{(i)} = \sum_{j=1}^{D_i} \alpha_j^{(i)} \boldsymbol{\beta}_j^{(i)}$ for some $\left\{\alpha_j^{(i)}\right\}$, and $\left\|\mathbf{q}^{(i)}\right\|^2 = \left\|\boldsymbol{\alpha}^{(i)}\right\|^2$, where $\boldsymbol{\alpha}^{(i)} = \left[\alpha_1^{(i)}, ..., \alpha_{D_i}^{(i)}\right]^{\text{T}}$. Recall that the spectral decomposition of Hermitian matrix $\mathbf{H}^{(i)^H} \mathbf{c}^{(i)} \mathbf{c}^{(i)^H} \mathbf{H}^{(i)} = \sum_{m=1}^{G} \lambda_m^{(i)} \mathbf{v}_m^{(i)} \mathbf{v}_m^{(i)^H}$, where $\lambda_1^{(i)} \geq \cdots \geq \lambda_G^{(i)}$ and $\left\{\mathbf{v}_1^{(i)}, ..., \mathbf{v}_G^{(i)}\right\}$ is an orthonormal basis that spans $\mathbb{C}^{G \times 1}$. Remember that $\text{rank}\left(\mathbf{H}^{(i)^H} \mathbf{c}^{(i)} \mathbf{c}^{(i)^H} \mathbf{H}^{(i)}\right) = 1$, then $\lambda_1^{(i)} = \left\|\mathbf{H}^{(i)^H} \mathbf{c}^{(i)}\right\|^2$, $\lambda_2^{(i)} = \cdots = \lambda_G^{(i)} = 0$ results in $\mathbf{H}^{(i)^H} \mathbf{c}^{(i)} \mathbf{c}^{(i)^H} \mathbf{H}^{(i)} = \lambda_1^{(i)} \mathbf{v}_1^{(i)} \mathbf{v}_1^{(i)^H}$. Next, we can express $\boldsymbol{\beta}_j^{(i)}$ as $\boldsymbol{\beta}_j^{(i)} = \sum_{k=1}^{G} a_{j,k}^{(i)} \mathbf{v}_k^{(i)}$, for $j = 1, ..., D_i$, for some $\left\{a_{j,k}^{(i)}\right\}$ and $\mathbf{q}^{(i)} = \sum_{j=1}^{D_i} \alpha_j^{(i)} \boldsymbol{\beta}_j^{(i)} = \sum_{j=1}^{D_i} \alpha_j^{(i)} \sum_{k=1}^{G} a_{j,k}^{(i)} \mathbf{v}_k^{(i)} = \sum_{k=1}^{G} b_k^{(i)} \mathbf{v}_k^{(i)}$, where $b_k^{(i)} = \sum_{j=1}^{D_i} a_{j,k}^{(i)} \alpha_j^{(i)}$. Furthermore,

$$\mathbf{q}^{(i)^H} \mathbf{H}^{(i)^H} \mathbf{c}^{(i)} \mathbf{c}^{(i)^H} \mathbf{H}^{(i)} \mathbf{q}^{(i)} = \left(\sum_{l=1}^{G} b_l^{(i)} \mathbf{v}_l^{(i)} \right)^H \left(\lambda_1^{(i)} \mathbf{v}_1^{(i)} \mathbf{v}_1^{(i)^H} \right) \left(\sum_{n=1}^{G} b_n^{(i)} \mathbf{v}_n^{(i)} \right) \tag{4.35}$$

$$= \left| b_1^{(i)} \right|^2 \lambda_1^{(i)} = \left| b_1^{(i)} \right|^2 \left\| \mathbf{H}^{(i)^H} \mathbf{c}^{(i)} \right\|^2$$

Where $b_1^{(i)} = \sum_{j=1}^{D_i} a_{j,1}^{(i)} \alpha_j^{(i)} = \left\langle \mathbf{a}_1^{(i)}, \boldsymbol{\alpha}^{(i)} \right\rangle$ is the inner product of vectors $\mathbf{a}_1^{(i)} = \left[a_{1,1}^{(i)*}, \dots, a_{D_i,1}^{(i)*} \right]^T$ and $\boldsymbol{\alpha}^{(i)}$.

By applying Cauchy-Schwarz Inequality [64], $\left| b_1^{(i)} \right|^2 \leq \left\| \mathbf{a}_1^{(i)} \right\|^2 \left\| \boldsymbol{\alpha}^{(i)} \right\|^2$ with equality if $\boldsymbol{\alpha}^{(i)} = t_i \mathbf{a}_1^{(i)}$

for some value t_i. Accordingly, let $\tilde{\mathbf{q}}^{(i)} = t_i \cdot \sum_{j=1}^{D_i} a_{j,1}^{(i)*} \boldsymbol{\beta}_j^{(i)}$ we have

$$\max \left\{ \mathbf{q}^{(i)^H} \mathbf{H}^{(i)^H} \mathbf{c}^{(i)} \mathbf{c}^{(i)^H} \mathbf{H}^{(i)} \mathbf{q}^{(i)} \right\} = \left\| \mathbf{a}_1^{(i)} \right\|^2 \left\| \boldsymbol{\alpha}^{(i)} \right\|^2 \left\| \mathbf{H}^{(i)^H} \mathbf{c}^{(i)} \right\|^2 = \left\| \mathbf{a}_1^{(i)} \right\|^2 \left\| \mathbf{H}^{(i)^H} \mathbf{c}^{(i)} \right\|^2 \left\| \tilde{\mathbf{q}}^{(i)} \right\|^2, \tag{4.36}$$

And the sum data rate in Equation (4.11) becomes

$$\mathcal{C} = \sum_{i=1}^{G} \log_2 \left\{ 1 + \frac{\sigma_x^2 \left\| \mathbf{a}_1^{(i)} \right\|^2 \left\| \mathbf{H}^{(i)^H} \mathbf{c}^{(i)} \right\|^2 \left\| \tilde{\mathbf{q}}^{(i)} \right\|^2}{\sigma_W^2} \right\} \tag{4.37}$$

In the second step, the principle of multi-user water filling is applied in Equation (4.37) in order to obtain the maximum sum data rate. That is, we are seeking for

$$\left\{ \left\| \hat{\mathbf{q}}^{(i)} \right\|^2 \right\} = \arg \left\{ \max_{\left\{ \left\| \tilde{\mathbf{q}}^{(i)} \right\|^2 \right\}} \sum_{i=1}^{G} \log_2 \left[1 + \frac{\sigma_x^2 \left\| \mathbf{a}_1^{(i)} \right\|^2 \left\| \mathbf{H}^{(i)^H} \mathbf{c}^{(i)} \right\|^2 \left\| \tilde{\mathbf{q}}^{(i)} \right\|^2}{\sigma_W^2} \right] \right\}, \text{ s.t. } \sum_{i=1}^{G} \left\| \tilde{\mathbf{q}}^{(i)} \right\|^2 = G \tag{4.38}$$

With an application of the theory of Lagrange Multiplier, it can be shown that

$$\left\| \hat{\mathbf{q}}^{(i)} \right\|^2 = \left[1 + \frac{1}{G} \sum_{j=1}^{G} \frac{\sigma_W^2}{\sigma_x^2 \left\| \mathbf{a}_1^{(j)} \right\|^2 \left\| \mathbf{H}^{(j)^H} \mathbf{c}^{(j)} \right\|^2} - \frac{\sigma_W^2}{\sigma_x^2 \cdot \left\| \mathbf{a}_1^{(i)} \right\|^2 \left\| \mathbf{H}^{(i)^H} \mathbf{c}^{(i)} \right\|^2} \right]^+ \forall i. \tag{4.39}$$

The complete algorithm for ZF-MWF is summarized in Table 4.1.

Table 4.1: Zero-forcing with Multi-user Water Filling

Input: channel responses $\{\mathbf{H}^{(i)}\}$ and spreading codes $\{\mathbf{c}^{(i)}\}$.

Output: pre-processing weight vectors $\{\hat{\mathbf{q}}^{(i)}\}$.

---

1. for $i = 1$ to G do

2. obtain orthonormal basis $\{\boldsymbol{\beta}_1^{(i)},...,\boldsymbol{\beta}_{D_i}^{(i)}\}$ of null space of matrix $\mathcal{H}$, defined in Equation (2.34)

3. determine $\mathbf{a}_1^{(i)} = \left[a_{1,1}^{(i)},...., a_{D_i,1}^{(i)} \right]^H$ based on the relations between $\{\boldsymbol{\beta}_1^{(i)},...,\boldsymbol{\beta}_{D_i}^{(i)}\}$ and $\{\mathbf{v}_1^{(i)},...,\mathbf{v}_G^{(i)}\}$, i.e., $\boldsymbol{\beta}_j^{(i)} = \sum_{k=1}^{G} a_{j,k}^{(i)} \mathbf{v}_k^{(i)}$, for $j = 1,...,D_i$, where $\{\mathbf{v}_1^{(i)},...,\mathbf{v}_G^{(i)}\}$ are the orthonormal eigenvector set of Hermitian matrix $\mathbf{H}^{(i)^H}\mathbf{c}^{(i)}\mathbf{c}^{(i)^H}\mathbf{H}^{(i)}$.

4. end for

5. determine power allocation results $\left\{ \left\| \hat{\mathbf{q}}^{(i)} \right\|^2 \right\}$ based on Equation (2.39)

6. obtain t_i by $t_i = \dfrac{\left\| \hat{\mathbf{q}}^{(i)} \right\|}{\left\| \mathbf{a}_1^{(i)} \right\|}$ for $i = 1,2,...,G$, since $\left\| \hat{\mathbf{q}}^{(i)} \right\|^2 = \left\| \boldsymbol{\alpha}^{(i)} \right\|^2 = \left\| t_i \mathbf{a}_1^{(i)} \right\|^2$

7. determine $\hat{\mathbf{q}}^{(i)} = \sum_{j=1}^{D_i} \alpha_j^{(i)} \boldsymbol{\beta}_j^{(i)}$ for $i = 1,2,...,G$ with $\boldsymbol{\alpha}^{(i)} = t_i \mathbf{a}_1^{(i)}$

4.3 Numerical Results

This section presents and compares the ergodic sum data rate of the considered pre-processing methods. The system parameters are summarized in Table 4.2. Recall that there are total G users in the system, but they may not all be scheduled to transmit in a frame. $K \leq G$ denotes the actual number of scheduled users. For $K < G$, G/K codes are allocated to each user (multi-code transmission), and the system can exploit the multi-user diversity gain to increase the sum data rate. The user scheduling is performed on a frame-by-frame basis. As given

in Table 4.2, a frame consists of 16 OFDM symbols. The Hadamard-Walsh orthogonal codes are used throughout this study.

Table 4.2: System parameters

Parameters	Values
Number of users in the system, G	16
Overall processing gain, G	16
Number of users scheduled in a frame, K	1, 2, 4, 8, 16
Number of spreading codes allocated to each scheduled user	G/K
OFDM symbol duration, T_{OFDM}	$10\mu s$
Useful OFDM symbol duration, T_{FFT}	$8\mu s$
Sub-carrier frequency spacing, $\Delta f = 1/T_{FFT}$	125 KHz
System sampling period, T_s	T_{FFT}/N_{FFT}
FFT size, N_{FFT}	256
Cyclic prefix size	64
Normalized frequency selectivity, $\Delta f/B_c$ B_c, coherent bandwidth of the channel	1/8, 1/4, 1/2
Frame size	16 OFDM symbols
Normalized time selectivity, T_{OFDM}/T_c T_c, coherence time of the channel	1/8, 1/4, 1/2
Spreading Codes	Hadamard-Walsh codes

In Table 4.2, $\Delta f / B_c$ and T_{OFDM} / T_c are defined as the normalized frequency and time selectivity, respectively, where B_c is the coherent bandwidth and T_c the coherent time of the channel. In this study, $B_c = 1/(50\sigma_\tau)$ and $T_c = 1/(50 f_D)$, where σ_τ is the root-mean-square delay spread and f_D the maximum Doppler spread of the channel [67]. By changing the path number L and f_D, we can obtain the desirable frequency and time selectivity designated in Table 4.2. For example, $L = 7, 13, 26$ correspond to $\Delta f / B_c = 1/8, 1/4, 1/2$, and $f_D = 250, 500, 1000$ Hz correspond to $T_{OFDM} / T_c = 1/8, 1/4, 1/2$, respectively.

Figure 4.4 shows the performance of the ergodic sum data rate for the non-selective channel, with different number of scheduled users. The number of channel samples used for evaluating the ergodic sum data rate is over 20000. Recall that for the non-selective fading channels, the pre-processing is the optimum one that achieves the maximum sum data rate. For comparison purpose, the sum data rate for AWGN channel is also included in the figure. Clearly, for $K \leq 8$ higher ergodic sum data rate is obtained for fading channels than AWGN case, thanks to the exploitation of the multi-user diversity. Nevertheless, the advantage of multi-user diversity diminishes as the number of scheduled users becomes larger. In fact, for $K = 16$ the ergodic sum data rate of the fading channel is less than that of the AWGN channel except for very low SNRs.

Figure 4.5 compares the ergodic sum data rate for the considered pre-processing methods in selective channels with $K = 16$. Frequency-domain spreading with two values of channel selectivity, that is $\Delta f / B_c = 1/2, 1/4$ is used as the example. As are shown in the figure, the channel selectivity decreases the ergodic sum data rate; the more severe the channel selectivity, the smaller the ergodic sum data rate. This phenomenon is more prominent for MMSE in the high SNR region, because in MMSE there is a residual MAI and that becomes more dominant in performance at high SNR region. The newly proposed ZF-MWF could significantly outperform the other two, depending on the channel selectivity and the operating SNR. Only a small gap is observed with this new method, as compared to the maximum ergodic sum data rate that is only

achievable with the nonselective channels. ZF-PN performs less favorable than the other two in low SNR region. Nevertheless, it outperforms MMSE in high SNR region where MAI is the dominant factor.

Figure 4.6 shows the performance of considered pre-processing methods in selective channels with two cases of scheduled number, $K = 16$ and $K = 4$. It is apparently that multi-user diversity gain can be still exploited in selective channels. In addition, the comparative results of performance between these pre-processing methods are consistent with those shown in Figure 2.5.

Figure 4.7, Figure 4.8, and Figure 4.9 show the advantage by using 2-D spreading and the importance of selection of the spreading patterns for the cases of $K = 16$, $\sigma_x^2/\sigma_W^2 = 1$, 15, and 29 dB, respectively. From the result, it can be concluded that g_f and g_t should be selected in a way to reduce the channel selectivity both in time and frequency. In this example, $g_f = 4, g_t = 4$ is the optimum one regardless of the channel selectivity. The loss in ergodic sum data rate can be quite large if the spreading pattern is not selected properly. This is especially true for MMSE. Again, the new method can significantly outperform the other two in the 2-D spreading case.
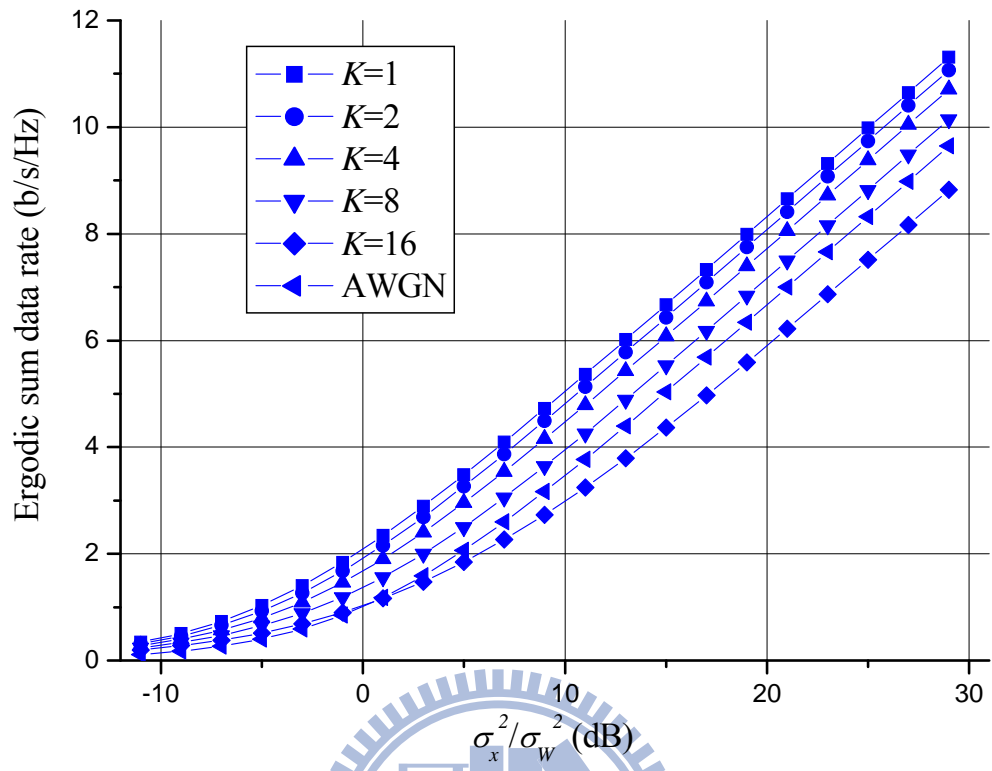
Figure 4.4: Ergodic sum data rate for non-selective channels with the optimum pre-processing

$g_t=1$, $g_f=16$, $K=16$
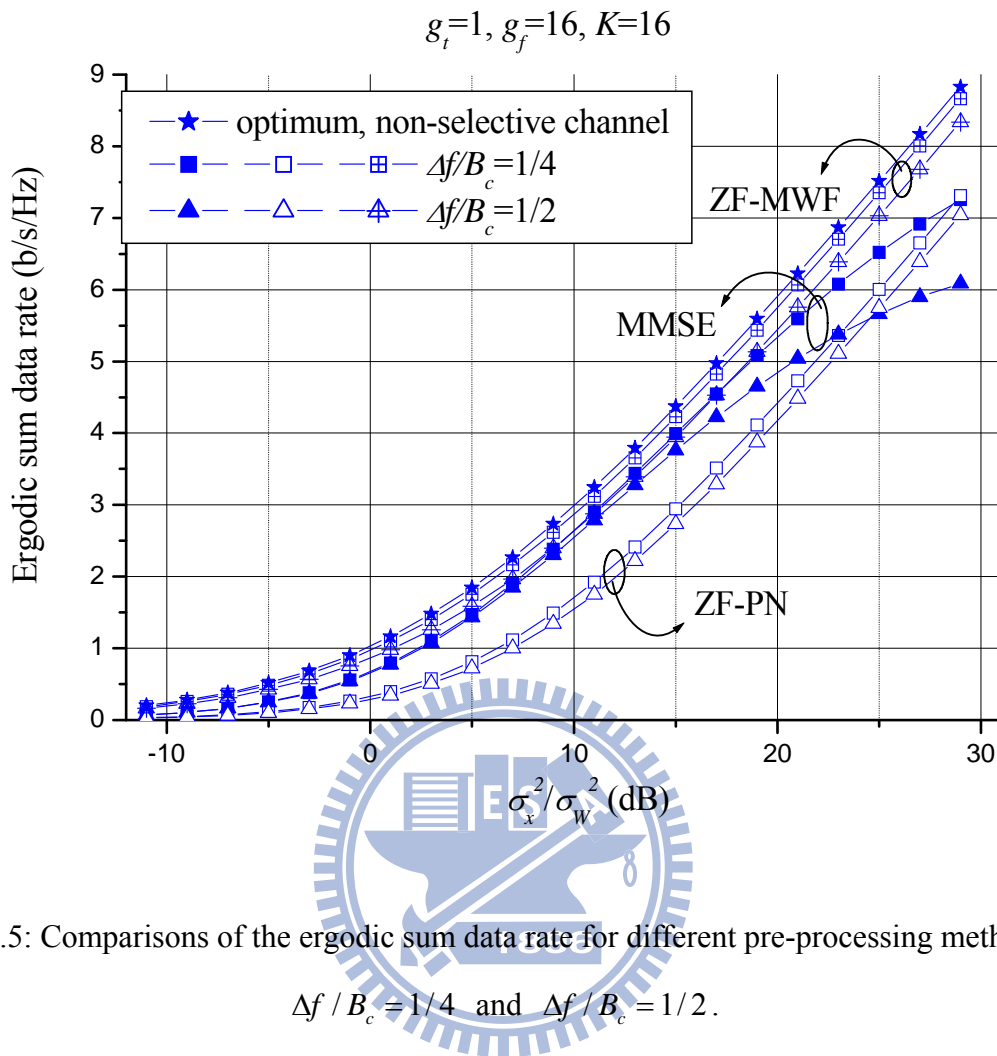
Figure 4.5: Comparisons of the ergodic sum data rate for different pre-processing methods with $\Delta f \,/\, B_c = 1/4$ and $\Delta f \,/\, B_c = 1/2$.

$g_t=1$, $g_f=16$, $\Delta f/B_c=1/4$
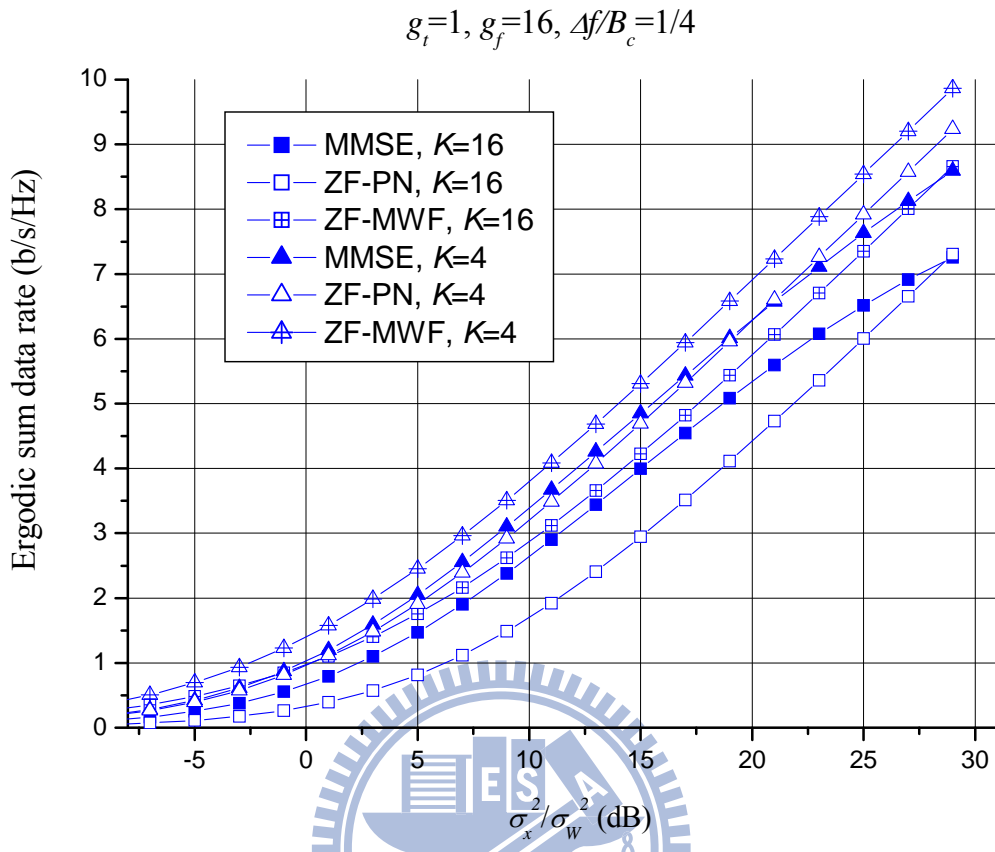
Figure 4.6: Comparisons of the ergodic sum data rate for different pre-processing methods with

$K = 16$ and $K = 4$.

Figure 4.7: Example effects of spreading patterns on the ergodic sum data rate with different

degrees of selectivity for $K = 16$, $\sigma_x^2 / \sigma_W^2 = 1$ dB
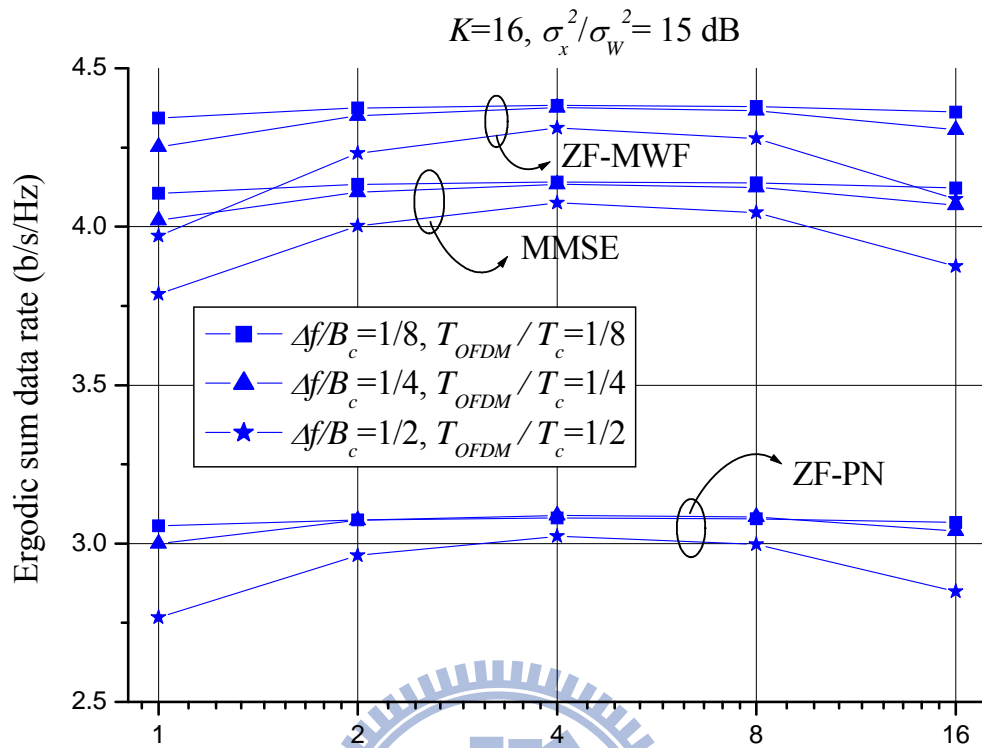
Figure 4.8: Example effects of spreading patterns on the ergodic sum data rate with different

degrees of selectivity for $K = 16$, $\sigma_x^2/\sigma_W^2 = 15$ dB

K=16, σ_x^2/σ_W^2=29 dB
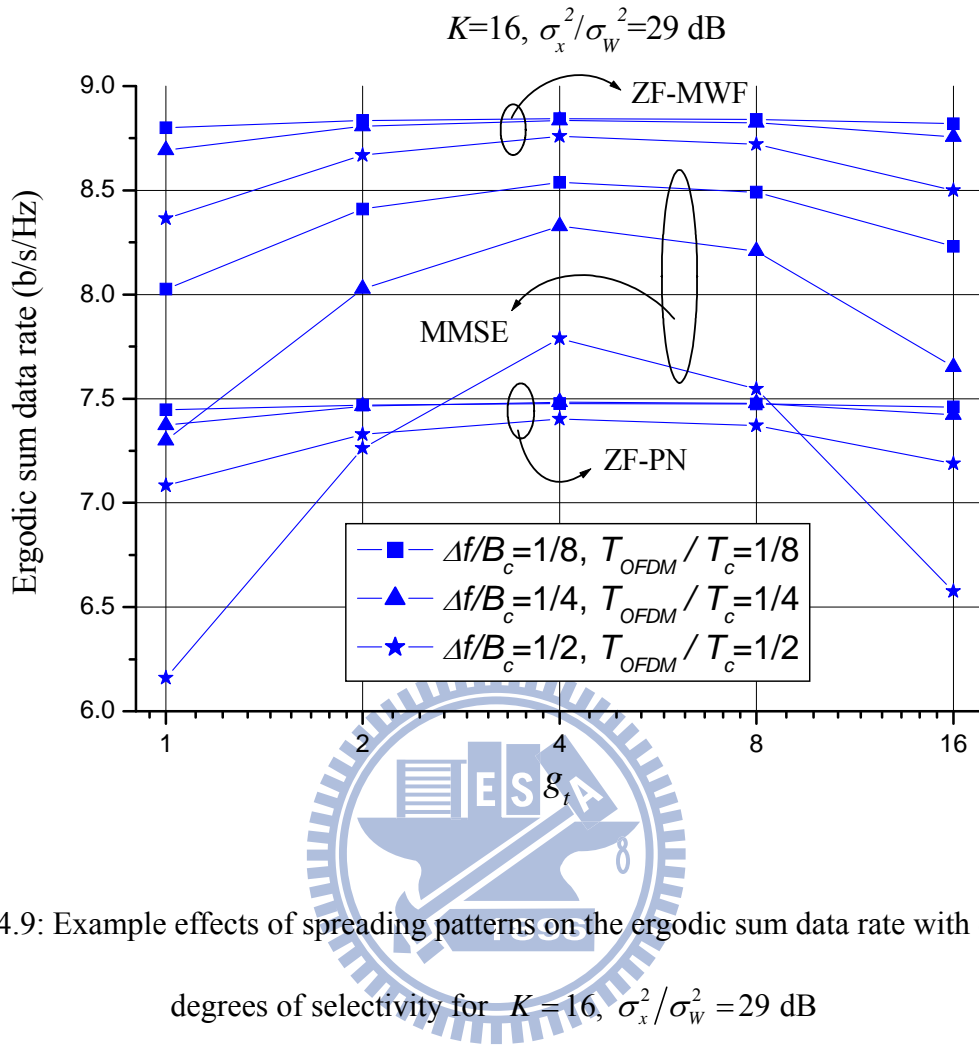
Figure 4.9: Example effects of spreading patterns on the ergodic sum data rate with different degrees of selectivity for $K = 16$, $\sigma_x^2/\sigma_W^2 = 29$ dB
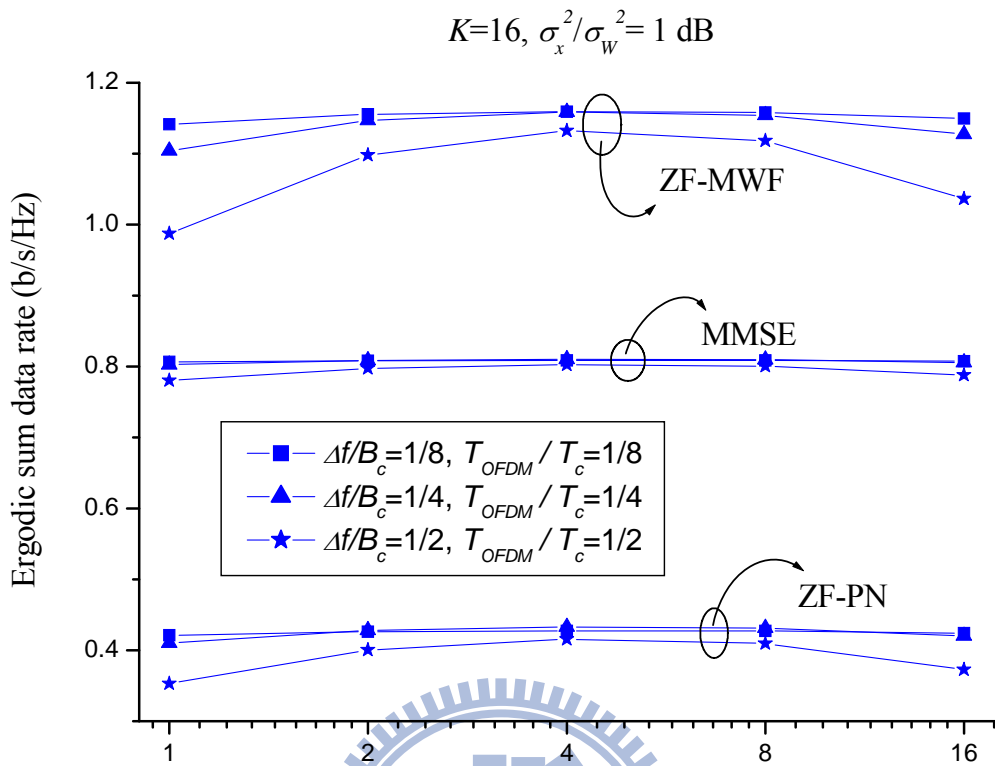
4.4 Conclusions

In this Chapter, different transmitter-based pre-processing methods are investigated for the 2-D OFDM-CDMA forward-link systems in the time-variant multi-path Rayleigh fading channels. The optimum pre-processing that achieves the highest ergodic sum data rate is obtained for the non-selective fading channels. For the selective one, three sub-optimum methods are investigated including ZF with power normalization, MMSE and the newly proposed ZF with multi-user water filling. Numerical results show that the new method significantly outperforms the other two,

especially while the channel exhibits severe channel selectivity. The merit of 2-D spreading over the 1-D one is illustrated through examples. Furthermore, user scheduling provides significant performance improvement by exploiting multi-user diversity, especially if only a small number of users are scheduled at a time.

Chapter 5

Concluding Remarks

Multiple-input-multiple-output (MIMO) is, in general, a model for a variety of communication problems including the multiple transmit and receive antenna systems, code-division multiple-access systems, inter-symbol interference channels, etc. In this dissertation, new transmit and receive techniques for MIMO communication systems are proposed.

In Chapter 2, a new design on channel factorization is proposed for the channel-factorization aided detectors, where effective factorization algorithms are sought to minimize the sum mean-squared-error of the MMSE detector. Two new types of factorization algorithms are devised; the first type is LLL based, where the best-performed factorization algorithm found in the literature, i.e., the DLLL-extended algorithm, is a member of this type but with a higher complexity. The second type is greedy-search based which can provide around 0.5-1.0 dB gain over the first type and has a fixed computational complexity which is advantageous in hardware implementation. The computational complexity of the proposed methods are analyzed and compared to the existing methods. In addition, combining proposed MMSE channel factorization algorithm with the element-wise, candidate-list (EWCL) detector can approach to within a fractional dB of the ML performance.

In Chapter 3, according to the case studies and simulation results, receiver structures should be properly designed based on MIMO-OFDM systems with TX and/or RX I/Q imbalances such as to compromise between performance and computational complexity. For example, in the forward-link (down-link) of cellular systems, TX (base station) I/Q imbalance is nearly perfect, but RX (mobile unit) may have large I/Q imbalance due to its low-cost requirements. In this case,

Type-II receiver is recommended to enable good performance and reduced computational complexity receiver (mobile unit). On the contrary, in the reverse-link (up-link) of cellular systems, receivers (base station) are suggested to employ Type-I structure so as to attain improved BER performance by making use of additional diversity gain provided by TX I/Q imbalance.

In Chapter 4, different transmitter-based pre-processing methods are investigated for the 2-D OFDM-CDMA forward-link systems in the time-variant multi-path Rayleigh fading channels. The optimum pre-processing that achieves the highest ergodic sum data rate is obtained for the non-selective fading channels. For the selective one, three sub-optimum methods are investigated including ZF with power normalization, MMSE and the newly proposed ZF with multi-user water filling. Numerical results show that the new method significantly outperforms the other two, especially while the channel exhibits severe channel selectivity. The merit of 2-D spreading over the 1-D one is illustrated through examples. Furthermore, user scheduling provides significant performance improvement by exploiting multi-user diversity, especially if only a small number of users are scheduled at a time.

Appendix

Appendix A

By definition, $\mathbf{\Phi}_{MMSE} = E\left[\left(\mathbf{G}_{MMSE}\mathbf{y} - \mathbf{z}\right)\left(\mathbf{G}_{MMSE}\mathbf{y} - \mathbf{z}\right)^H\right]$, where

$$\mathbf{G}_{MMSE} = \mathbf{D}\left(\mathbf{H}^H\mathbf{H} + \frac{\sigma_w^2}{\sigma_x^2}\mathbf{I}_m\right)^{-1}\mathbf{H}^H.$$

Using $\mathbf{\Phi_x} = E\left[\mathbf{xx}^H\right] = \sigma_x^2\mathbf{I}_m$, and $\mathbf{\Phi_w} = E\left[\mathbf{ww}^H\right] = \sigma_w^2\mathbf{I}_n$, we have

$$\mathbf{\Phi}_{MMSE} = \mathbf{G}_{MMSE}\left(\sigma_x^2\mathbf{HH}^H + \sigma_w^2\mathbf{I}_n\right)\mathbf{G}_{MMSE}^H - \sigma_x^2\mathbf{G}_{MMSE}\mathbf{HD}^H - \sigma_x^2\mathbf{DH}^H\mathbf{G}_{MMSE}^H + \sigma_x^2\mathbf{DD}^H.$$

$$\text{(A.1)}$$

Clearly, $\mathbf{H}^H\left(\mathbf{HH}^H + \frac{\sigma_w^2}{\sigma_x^2}\mathbf{I}_n\right) = \left(\mathbf{H}^H\mathbf{H} + \frac{\sigma_w^2}{\sigma_x^2}\mathbf{I}_m\right)\mathbf{H}^H$. Since $\left(\mathbf{HH}^H + \frac{\sigma_w^2}{\sigma_x^2}\mathbf{I}_n\right)$ and

$\left(\mathbf{H}^H\mathbf{H} + \frac{\sigma_w^2}{\sigma_x^2}\mathbf{I}_m\right)$ are invertible, it leads to

$$\left(\mathbf{H}^H\mathbf{H} + \frac{\sigma_w^2}{\sigma_x^2}\mathbf{I}_m\right)^{-1}\mathbf{H}^H = \mathbf{H}^H\left(\mathbf{HH}^H + \frac{\sigma_w^2}{\sigma_x^2}\mathbf{I}_n\right)^{-1}. \qquad \text{(A.2)}$$

According to Equation (A.2), $\mathbf{G}_{MMSE}$ can be rewritten as:

$$\begin{aligned}\mathbf{G}_{MMSE} &= \mathbf{D}\left(\mathbf{H}^H\mathbf{H} + \frac{\sigma_w^2}{\sigma_x^2}\mathbf{I}_m\right)^{-1}\mathbf{H}^H = \mathbf{DH}^H\left(\mathbf{HH}^H + \frac{\sigma_w^2}{\sigma_x^2}\mathbf{I}_n\right)^{-1} \\ &= \sigma_x^2\mathbf{DH}^H\left(\sigma_x^2\mathbf{HH}^H + \sigma_w^2\mathbf{I}_n\right)^{-1}\end{aligned} \qquad \text{(A.3)}$$

Therefore, $\mathbf{G}_{MMSE}\left(\sigma_x^2\mathbf{HH}^H + \sigma_w^2\mathbf{I}_n\right)\mathbf{G}_{MMSE}^H = \sigma_x^2\mathbf{DH}^H\mathbf{G}_{MMSE}^H$, and Equation (A.1) becomes

$$\Phi_{MMSE} = \sigma_x^2 \mathbf{D}\mathbf{D}^H - \sigma_x^2 \mathbf{G}_{MMSE} \mathbf{H}\mathbf{D}^H$$

$$= \sigma_x^2 \mathbf{D}\mathbf{D}^H - \sigma_x^2 \mathbf{D}\mathbf{H}^H \left(\mathbf{H}\mathbf{H}^H + \frac{\sigma_w^2}{\sigma_x^2}\mathbf{I}_n \right)^{-1} \mathbf{H}\mathbf{D}^H \qquad (A.4)$$

By applying the Matrix Inversion Lemma $\mathbf{K}^{-1} - \mathbf{K}^{-1}\mathbf{L}\left(\mathbf{N}\mathbf{K}^{-1}\mathbf{L} + \mathbf{M}^{-1}\right)^{-1}\mathbf{N}\mathbf{K}^{-1} = \left(\mathbf{K} + \mathbf{L}\mathbf{M}\mathbf{N}\right)^{-1}$

[69] to Equation (A.4) with $\mathbf{K}^{-1} = \sigma_x^2 \mathbf{D}\mathbf{D}^H$, $\mathbf{L} = \left(\mathbf{D}^{-1}\right)^H \mathbf{H}^H$, $\mathbf{M}^{-1} = \frac{\sigma_w^2}{\sigma_x^2}\mathbf{I}_n$, and $\mathbf{N} = \frac{1}{\sigma_x^2}\mathbf{H}\mathbf{D}^{-1}$,

$$\Phi_{MMSE} = \sigma_w^2 \mathbf{D}\left(\mathbf{H}^H\mathbf{H} + \frac{\sigma_w^2}{\sigma_x^2}\mathbf{I}_m \right)^{-1}\mathbf{D}^H = \mathbf{D}\mathbf{A}\mathbf{D}^H, \qquad (A.5)$$

where $\mathbf{A} = \sigma_w^2 \left(\mathbf{H}^H\mathbf{H} + \frac{\sigma_w^2}{\sigma_x^2}\mathbf{I}_m \right)^{-1}$.

Appendix B

In this appendix, it is proved that given $\mathbf{C} = \mathbf{P}\Upsilon$, where Υ is a non-singular matrix and

$\mathbf{P}^H\mathbf{P} = \mathbf{I}$, if $\Upsilon \overset{LLL}{=} \widetilde{\Upsilon}\mathbf{T}_\Upsilon$, and $\mathbf{C} \overset{LLL}{=} \widetilde{\mathbf{C}}\mathbf{T}_C$, then $\widetilde{\mathbf{C}} = \mathbf{P}\widetilde{\Upsilon}$ and $\mathbf{T}_\Upsilon = \mathbf{T}_C$, where $\mathbf{X} \overset{LLL}{=} \widetilde{\mathbf{X}}\mathbf{T}_\mathbf{X}$ denotes

that the factorization is done with the LLL algorithm.

Proof: Let $\mathbf{X} \in \{\Upsilon, \mathbf{C}\}$. Initially, in the LLL algorithm, the Gram Schmidt Orthogonalization

(GSO) procedure is applied to obtain the factorization

$$\mathbf{X} \overset{GSO}{=} \mathbf{Q}_\mathbf{X}\mathbf{U}_\mathbf{X}^T,$$

where $\mathbf{Q}_\mathbf{X} = \left[\mathbf{q}_{1,\mathbf{X}} \cdots \mathbf{q}_{m,\mathbf{X}} \right]$ is a orthogonal matrix, and $\mathbf{U}_\mathbf{X}$ is a lower triangular matrix with

unit main diagonal elements. Since $\mathbf{C} = \mathbf{P}\Upsilon$ and $\mathbf{P}^H\mathbf{P} = \mathbf{I}$, it is easy to show that $\mathbf{Q}_C = \mathbf{P}\mathbf{Q}_\Upsilon$

and $U_C = U_\Upsilon = U$. Let $C = [c_1 \cdots c_m]$, $\Upsilon = [\Upsilon_1 \cdots \Upsilon_m]$, and $U = \begin{bmatrix} 1 & & & 0 \\ \mu_{2,1} & 1 & & \\ \vdots & \vdots & \ddots & \\ \mu_{m,1} & \mu_{m,2} & \cdots & 1 \end{bmatrix}$, the LLL

algorithm then performs the following two operations iteratively to obtain a reduced basis:

Operation 1: $x_i = x_i - \lfloor \mu_{i,j} \rceil x_j$, if $\lfloor \mu_{i,j} \rceil \neq 0$.

Operation 2: swap x_{i-1} and x_i, if $\left\| q_{i,x} + \mu_{i,i-1} q_{i-1,x} \right\|^2 < \delta \left\| q_{i-1,x} \right\|^2$.

where $x \in \{c, \Upsilon\}$, and $\lfloor \cdot \rceil$ stands for the operation of rounding the argument to the nearest

complex integer. Since $c_i - \lfloor \mu_{i,j} \rceil c_j = P\Upsilon_i - \lfloor \mu_{i,j} \rceil P\Upsilon_j = P(\Upsilon_i - \lfloor \mu_{i,j} \rceil \Upsilon_j)$ in Operation 1, and

$\left\| q_{i,c} \right\|^2 = \left\| q_{i,\Upsilon} \right\|^2$ and $\left\| q_{i,c} + \mu_{i,i-1} q_{i-1,c} \right\|^2 = \left\| q_{i,\Upsilon} + \mu_{i,i-1} q_{i-1,\Upsilon} \right\|^2$ in Operation 2, it concludes that

$\tilde{C} = P\tilde{\Upsilon}$ and $T_\Upsilon = T_C$.

Appendix C

In this Appendix, we prove that $D^H_{new} = \left[d_1, ..., d_{k-1}, d_{k,new}, d_{k+1}, ..., d_m \right]$ is unimodular provided

that D^H is unimodular, where

$$d_{k,new} = \alpha_1 d_1 + \cdots + \alpha_{k-1} d_{k-1} + d_k + \alpha_{k+1} d_{k+1} + \cdots + \alpha_m d_m. \tag{C.1}$$

and $\{\alpha_m\}_{m \neq k}$ are complex integers.

Proof: Recall that $D^H = \left[d_1, ..., d_{k-1}, d_k, d_{k+1}, ..., d_m \right]$. Using Equation (C.1), $D^H_{new} = D^H I^k_m$,

where I^k_m is obtained by replacing the kth-column of I_m with $\left[\alpha_1, \cdots, \alpha_{k-1}, 1, \alpha_{k+1} \cdots, \alpha_m \right]^T$. It is

clear that $\det\left(\mathbf{I}_m^k\right)=1$. Therefore, $\left|\det\left(\mathbf{D}_{new}^H\right)\right|=\left|\det\left(\mathbf{I}_m^k\right)\right|\cdot\left|\det\left(\mathbf{D}^H\right)\right|=1$, and $\mathbf{D}_{new}^H$ is a unimodular matrix.

Appendix D

In this appendix, it is proved that the matrix $\mathbf{OAO}^H$ is positive definite provided the $l\times m$ matrix $\mathbf{O}$ has full row rank, where $l\leq m$, and $\mathbf{A}=\sigma_w^2\left(\mathbf{H}^H\mathbf{H}+\dfrac{\sigma_w^2}{\sigma_x^2}\mathbf{I}_m\right)^{-1}$.

Proof: Firstly, $\mathbf{A}=\sigma_w^2\left(\mathbf{H}^H\mathbf{H}+\dfrac{\sigma_w^2}{\sigma_x^2}\mathbf{I}_m\right)^{-1}$ is positive definite. This can be shown as follows. Let $\mathbf{X}=\mathbf{H}^H\mathbf{H}+\dfrac{\sigma_w^2}{\sigma_x^2}\mathbf{I}_m$. It is clear that $\mathbf{X}$ is Hermitian and semi-positive definite, i.e., $\mathbf{u}^H\mathbf{X}\mathbf{u}\geq 0$, for all $m\times 1$ vector $\mathbf{u}$. Suppose $\mathbf{u}^H\mathbf{X}\mathbf{u}=0$, we have $\mathbf{u}^H\mathbf{H}^H\mathbf{H}\mathbf{u}+\dfrac{\sigma_w^2}{\sigma_x^2}\mathbf{u}^H\mathbf{u}=0$, and that implies $\mathbf{u}=\mathbf{0}_m$. Hence, $\mathbf{X}$ is positive definite, and so is $\mathbf{A}=\sigma_w^2\left(\mathbf{X}\right)^{-1}$. Secondly, since $\mathbf{A}$ is positive definite, $\mathbf{A}=\mathbf{J}^H\mathbf{J}$ for an upper triangular matrix $\mathbf{J}$ by applying, for example, the Cholesky decomposition [64]. Given $l\times 1$ vector $\mathbf{v}$,

$$\mathbf{v}^H\mathbf{OAO}^H\mathbf{v}=\mathbf{v}^H\mathbf{OJ}^H\mathbf{JO}^H\mathbf{v}=\left\|\mathbf{JO}^H\mathbf{v}\right\|^2\geq 0,$$

therefore $\mathbf{OAO}^H$ is semi-positive definite. In addition, if $\mathbf{v}^H\mathbf{OAO}^H\mathbf{v}=0$, it follows that $\mathbf{O}^H\mathbf{v}=\mathbf{0}$ (as $\mathbf{A}$ is positive definite), and $\mathbf{v}=\mathbf{0}$ because $\mathbf{O}$ has full row rank, and this concludes the proof.

Appendix E

Given $\mathbf{r} = \mathbf{H}_{n \times m}\mathbf{s} + \mathbf{w}$, where $E\left[\mathbf{ss}^H\right] = \sigma_s^2\mathbf{I}_m$, $E\left[\mathbf{ww}^H\right] = \mathbf{C_w}$. $\tilde{\mathbf{r}} = \mathbf{Br} = \mathbf{BHs} + \mathbf{Bw}$, where $\mathbf{B}$ is an invertible square matrix with size $n \times n$. In this appendix, it is proved that the BER performance of detecting $\mathbf{s}$ on $\mathbf{r}$ is identical to that on $\tilde{\mathbf{r}}$ if the same detection algorithm is applied, including MMSE, MMSE-SIC, CF-I, CF-II, and ML.

Proof: $\mathbf{G_r} = \arg\min_{\mathbf{G}} E\left[\left\|\mathbf{Gr} - \mathbf{s}\right\|^2\right] = \mathbf{H}^H\left(\mathbf{HH}^H + \dfrac{1}{\sigma_s^2}\mathbf{C_w}\right)^{-1} = \sigma_s^2\mathbf{H}^H\left(\sigma_s^2\mathbf{HH}^H + \mathbf{C_w}\right)^{-1}$, and the output of MMSE filter on $\mathbf{r}$ is

$$\mathbf{G_r r} = \mathbf{H}^H\left(\mathbf{HH}^H + \frac{1}{\sigma_s^2}\mathbf{C_w}\right)^{-1}\mathbf{Hs} + \mathbf{H}^H\left(\mathbf{HH}^H + \frac{1}{\sigma_s^2}\mathbf{C_w}\right)^{-1}\mathbf{w} \qquad (E.1)$$

Also, $\mathbf{G}_{\tilde{\mathbf{r}}} = \arg\min_{\mathbf{G}} E\left[\left\|\mathbf{G}\tilde{\mathbf{r}} - \mathbf{s}\right\|^2\right] = \mathbf{H}^H\mathbf{B}^H\left(\mathbf{BHH}^H\mathbf{B}^H + \dfrac{1}{\sigma_s^2}\mathbf{BC_w}\mathbf{B}^H\right)^{-1}$. It is easily to shown that the output of MMSE filter on $\tilde{\mathbf{r}}$ is the same as that on $\mathbf{r}$, i.e., $\mathbf{G}_{\tilde{\mathbf{r}}}\tilde{\mathbf{r}} = \mathbf{G_r r}$. The BER performance is, therefore, the same while MMSE detection is applied. In reality, $\mathbf{r}$ and $\tilde{\mathbf{r}}$ are sufficient statistics, because $\tilde{\mathbf{r}} = \mathbf{Br}$ with invertible square matrix $\mathbf{B}$. Thus, not only MMSE detection, but also MMSE-SIC and ML detections can obtain the same performance while they are applied on $\mathbf{r}$ and $\tilde{\mathbf{r}}$. In addition, it can be shown that the results of matrix $\mathbf{A}$ in covariance matrix of error vector expressed in Equation (2.10) are also the same while applying channel factorization algorithms on $\mathbf{r}$ and $\tilde{\mathbf{r}}$. Accordingly, it leads to identical detection performance, and this completes the proof.

Appendix F

In this Appendix, we will prove by contradiction that the square matrix $\left(\mathbf{R}^H \mathbf{R} + \hat{\lambda} \cdot \mathbf{I}_G \right)$ of Equation (4.26) is a non-singular matrix in the constrained optimization problem we considered.

Proof: From Equation (4.24),

$$\widehat{\mathbf{Q}} = \arg \left\{ \min_{\mathbf{Q}} \ tr \left\{ \left[\mathbf{Q}^H \mathbf{R}^H - \mathbf{I}_G \right] \left[\mathbf{R} \mathbf{Q} - \mathbf{I}_G \right] \right\} \right\}, \ \text{s.t.} \ \left\| \mathbf{Q} \right\|_F^2 = tr \left\{ \mathbf{Q}^H \mathbf{Q} \right\} = G. \tag{F.1}$$

Because the objective function is lower bounded by zero, there exists at least one such $\widehat{\mathbf{Q}}$. In other words, there exists at least a pair of $\left(\hat{\lambda}, \ \widehat{\mathbf{Q}} \right)$ such that

$$\left(\mathbf{R}^H \mathbf{R} + \hat{\lambda} \cdot \mathbf{I}_G \right) \widehat{\mathbf{Q}} = \mathbf{R}^H \ , \tag{F.2}$$

and

$$tr \left\{ \widehat{\mathbf{Q}}^H \widehat{\mathbf{Q}} \right\} = G. \tag{F.3}$$

Let $\left(\lambda_i, \mathbf{v}_i \right)$ be one of the eigenvalue-eigenvector pairs of the Hermitian matrix $\mathbf{R}^H \mathbf{R}$. Then, it is easy to show that $\left(\lambda_i + \hat{\lambda}, \mathbf{v}_i \right)$ is also an eigenvalue-eigenvector pair of the matrix $\mathbf{R}^H \mathbf{R} + \hat{\lambda} \cdot \mathbf{I}_G$. Remember that $\mathbf{R}$ in Equation (4.20) is a $G \times G$ full rank matrix, that is $\text{rank}(\mathbf{R}) = \text{rank}(\mathbf{R}^H) = \text{rank}(\mathbf{R}^H \mathbf{R}) = G$. Suppose that the square matrix $\left(\mathbf{R}^H \mathbf{R} + \hat{\lambda} \cdot \mathbf{I}_G \right)$ in Equation (A.2) is singular, then there must exist a real $\hat{\lambda}$ such that $\hat{\lambda} = -\lambda_i$. Therefore,

$$\text{rank} \left(\mathbf{R}^H \mathbf{R} + \hat{\lambda} \cdot \mathbf{I}_G \right) < G = \text{rank} \left(\mathbf{R}^H \right). \tag{F.4}$$

Equation (F.4) implies that there are no solutions for $\widehat{\mathbf{Q}}$ in Equation (F.2). This is, however, contradictory to the fact that there exists at least a pair of $\left(\hat{\lambda}, \ \widehat{\mathbf{Q}} \right)$ to satisfy Equations (F.2) and (F.3).

Bibliography

[1] G. J. Foschini and M. J. Gans, "On the Limits of Wireless Communications in a Fading Environment When Using Multiple Antennas," *Wireless Pers. Commun.*, vol. 6, pp. 311-335, March 1998.

[2] I. E. Telatar, "Capacity of Multi-antenna Gaussian Channels," *Eur. Trans. Telecommun.*, vol. 10, pp. 585-595, November 1999.

[3] A. Chouly, A. Brajal, and S. Jourdan, "Orthogonal Multicarrier Techniques Applied to Direct Sequence Spread Spectrum CDMA Systems," in *Proc. of IEEE GLOBECOM'93*, Houston, USA, Nov. 1993, pp. 1723-1728

[4] N. Yee, J-P Linnarz and G. Fettwies, "Multicarrier CDMA in Indoor Wireless Radio Networks," in *Proc. of IEEE PIMRC '93*, Yokohama, Japan, Sept. 1993, pp. 109-113.

[5] S. Hara, and R. Prasad, "Overview of Multicarrier CDMA," *IEEE Commun. Mag.*, vol. 32, Dec. 1997, pp. 126-133.

[6] W. H. Mow, "Maximum Likelihood Sequence Estimation from the Lattice Viewpoint," *IEEE Trans. Inform. Theory*, vol. 40, pp.1591-1600, September 1994.

[7] H. Atarashi, S. Abeta, and M. Sawahashi, "Variable spreading factor orthogonal frequency and code division multiplexing (VSF-OFCDM) for broadband packet wireless access," *IEICE Trans. Commun.,* vol. E86-B, January 2003, pp. 291-299.

[8] A. Persson, T. Ottosson, and E. Strom, "Time-frequency localized CDMA for downlink multi-carrier systems," in *Proc. of IEEE ISSSTA'02*, Prague, Czech Republic, Sept. 2002, pp. 118-122.

[9] K. Zheng, G. Zeng, L. Lei and W. Wang, "Performance analysis for synchronous OFDM-CDMA with joint frequency-time spreading," *in Proc. of IEEE ICC'2004*, Paris, France, June 2004, pp. 3304-3308.

[10] L. L. Yang, W. Hus and L. Hanzo, "Multiuser detection in multicarrier CDMA systems employing both time-domain and frequency domain spreading," in *Proc. of IEEE PIMRC'03*, Beijing, China, Oct. 2003, pp. 1840-1844.

[11] W-H. Sheen and J-S Sheu, "On the adaptability of OFDM-CDMA forward link with time-frequency spreading in multi-path fading channels," in *Proc. of IEEE VTC'2005 Fall,* Dallas USA, September 2005.

[12] B. R. Vojcic and W. M. Jang, "Transmitter Precoding in Synchronous Multiuser Communications," *IEEE Trans. Commun.*, vol. 46, Oct. 1998, pp. 1346-1355.

[13] R. L. Choi, K. B. Letaief and R. D. Murch, "MISO CDMA Transmission with Simplified Receiver for Wireless Communication Handsets," *IEEE Trans. Commun.,* vol. 49, May 2001, pp. 888-898.

[14] R. Esmailzadeh, E. Sourour and M. Nakagawa, "Pre-rake Diversity Combining in Time Division Duplex CDMA Mobile Communications," *IEEE Trans. Vehicular Tech.,* vol. 48, May. 1999, pp. 795-801.

[15] M. B. Pea Y. H. Lee and B. Ness, "Transmission Power Adaptations in MC-CDMA Communications over Rayleigh Fading Channels," in *Proc. of IEEE WCNC'04,* Atlanta, GA USA, March 2004, pp. 21-25.

[16] M. B. Pearce and A. Dharap, "Transmitter-Based Multiuser Interference Rejection for the Down-Link of a Wireless CDMA Systems in a Multipath Environment," *IEEE J. Selected Areas Commun.,* vol. 18, March 2000, pp. 407-417.

[17] L. Choi and R.D. Murch, "A Transmit Preprocessing Technique for Multiuser MIMO Systems Using a Decomposition Approach," *IEEE Trans. Wireless Commun.,* vol. 3, Jan. 2004, pp. 20-24.

[18] B. Vucetic and J. Yuan, *Space-Time Coding,* NJ: John Wiley & Sons, 2003.

[19] D. Tse and P. Viswanath, Fundamentals of Wireless Communication, Cambridge, UK: Cambridge University Press, 2005.

[20] G. D. Golden, G. J. Foschini, R. A. Valenzuela and P. W. Wolniansky, "Detection Algorithm and Initial Laboratory Results Using V-BLAST Space-time Communication Architecture," *IEE Elect. Lett.*, vol. 35, pp. 14-16, January 1999.

[21] G. J. Foschini, G. D. Golden, R. A. Valenzuela and P. W. Wolniansky, "Simplified Processing for High Spectral Efficiency Wireless Communication Employing Multi-element Arrays," *IEEE J. Sel. Areas Commun.,* vol. 17, pp. 1841-1852, November 1999.

[22] D. Wübben, R. Böhnke, J. Rinas, V. Kühn and K. D. Kammeyer, "Efficient Algorithm for Decoding Layered Space-time Codes," *IEE Elec. Lett.*, vol. 37, pp. 1348-1350, October 2001.

[23] R. Böhnke , D. Wübben, V. Kühn, and K. D. Kammeyer, " Reduced Complexity MMSE Detection for BLAST Architecture," in *Proc. IEEE Globecom,* pp. 2258-2262, December 2003.

[24] U. Fincke and M. Pohst, "Improved Methods for Calculating Vectors of Short Length in a Lattice, Including a Complexity Analysis," *Math. of Comput.*, vol. 44, pp. 463-471, April 1985.

[25] E. Agrell, T. Eriksson, A. Vardy and K. Zeger, "Closest Point Search in Lattices," *IEEE Trans. Inform. Theory*, vol. 48, pp. 2201-2214, August 2002.

[26] H. Yao and G. Wornell, "Lattice-Reduction-Aided Detectors for MIMO Communication Systems," in *Proc. IEEE Globecom*, pp. 424-428, November 2002.

[27] C. Windpasseinger and R. F. H. Fischer, "Low-Complexity Near-Maximum-Likelihood Detection and Precoding for MIMO Systems Using Lattice Reduction," in *IEEE Proc. ITW*, pp. 345-348, March 2003.

[28] W. H. Mow, "Universal Lattice Decoding: Principle and Recent Advances," *Wireless Commun. Mobile Comput.*, vol. 3, pp. 553-569, August 2003.

[29] I. Berengure and X. Wang, "MIMO Antenna Selection with Lattice-Reduction-Aided Linear Receivers," *IEEE Trans. Vehicular Technology*, vol. 53, pp. 1289-1302, September 2004.

[30] D. Wübben, R. Böhnke, V. Kühn and K. D. Kammeyer, "Near-Maximum-Likelihood Detection of MIMO Systems Using MMSE-based Lattice Reduction," in *Proc. IEEE ICC*, pp. 798-802, June 2004.

[31] D. Wübben, V. Kühn and K. D. Kammeyer, "On the Robustness of Lattice-Reduction Aided Detectors in Correlated MIMO Systems," in *Proc. IEEE VTC*, pp. 3639-3643, September 2004.

[32] D. Wübben, R. Böhnke, V. Kühn and K. D. Kammeyer, "MMSE-based Lattice-Reduction for Near-ML Detection of MIMO Systems," in *Proc. ITG Workshop on Smart Antennas*, pp. 106-113, March 2004.

[33] C. Ling, "Approximate Lattice Decoding: Primal Versus Dual Basis Reduction," in *Proc. IEEE ISIT*, pp. 1-5, July 2006.

[34] M. Taherzadeh, A. Mobasher and A. K. Khandani, "LLL Reduction Achieves the Receiver Diversity in MIMO Decoding," *IEEE Trans. Inform. Theory*, vol. 53, pp. 4801-4805, December 2007.

[35] D. Wübben and D. Seethaler, "On the Performance of Lattice Reduction Schemes for MIMO Data Detection," in *Proc. IEEE ACSSC*, pp. 1543-1538, November 2007.

[36] A. K. Lenstra, H. W. Lenstra, Jr. and L. Lovász, "Factoring Polynomials with Rational Coefficients," *Math. Ann.*, no. 261, pp. 513-534, 1983.

[37] C.P. Schnorr and M. Euchner, "Lattice Basis Reduction: Improved Practical Algorithms and Solving Subset Sum Problem," *Mathematical Programming*, vol. 66, pp.181-191, 1994.

[38] M. Seysen, "Simultaneous Reduction of a Lattice Basis and Its Reciprocal Basis,"

Combinatorica, vol. 13, pp. 363-376, 1993.

[39] D. Seethaler, G. Matz and F. Hlawatsch, "Reduced-complexity MIMO Data Detection Using Seysen's Lattice Reduction Algorithm," in *Proc. IEEE ICASSP*, pp. 53-56, April 2007.

[40] C. L. Liu, "Impacts of I/Q Imbalance on QPSK-OFDM-QAM Detection," *IEEE Trans. Consumer. Electronics*, vol. 44, pp. 984-988, August 1998.

[41] R. M. Rao and B. Daneshrad, "Analog Impairments in MIMO-OFDM Systems," *IEEE Trans. Wireless Commun.*, vol. 5, pp. 3382-3387, Dec. 2006.

[42] F. Horlin, S. D. Rore, E. L. Estraviz, F. Naessens and L. V. D. Perre, "Impact of Frequency Offsets and I/Q Imbalance on MC-CDMA Reception Based on Channel Tracking," *IEEE J. Selected Areas Commun.,* vol. 24, June 2006, pp. 1179-1188.

[43] K. W. Park and Y. S. Cho, "A Detection Method for An OFDM Signal Distorted by I/Q Imbalance," in *Proc. of IEEE PIMRC'05*, 2005, pp. 2396-2399.

[44] G. T. Gil, I. H. Sohn, J. K. Park and Y. H. Lee, "Joint ML Estimation of Carrier Frequency, Channel, I/Q Mismatch, and DC Offset in Communication Receivers," *IEEE Trans. Vehicular Tech.,* vol. 54, Jan. 2005, pp. 338-349.

[45] M. Valkama, M. Renfors and V. Koivunen, "Advanced Methods for I/Q Imbalance Compensation in Communication Receivers," *IEEE Trans. Signal Process.*, vol. 49, pp. 2335–2344, Oct. 2001.

[46] E. Tsui and J. Lin, "Adaptive IQ Imbalance Correction for OFDM Systems with Frequency and Timing Offsets," in *Proc. IEEE Globecom*, pp. 4004-4010, 2004.

[47] J. K. Cavers and M. W. Liao, "Adaptive Compensation for Imbalance and Offset Losses in Direct Conversion Transceivers," *IEEE Trans. Vehicular Tech.,* vol. 42, Nov. 1993, pp. 581-588.

[48] D. Tandur and M. Moonen, "Joint Adaptive Compensation of Transmitter and Receiver IQ Imbalance Under Carrier Frequency Offset in OFDM-Based Systems," *IEEE Trans. Signal Process.*, vol. 55, pp. 5246–5252, Nov. 2007.

[49] K. P. Pun, J. E. Franca, C. A. Leme, C. F. Chan and C. S. Choy, "Correction of Frequency-Dependent I/Q Mismatches in Quadrarure Receivers," *IEE Elect. Lett.*, vol. 37, pp. 1415-1417, Nov. 2001.

[50] W. P. Kirkland and K. H. Teo, "I/Q Distortion Correction for OFDM Direct Conversion Receiver," *IEE Elect. Lett.*, vol. 39, pp. 131-133, Jan. 2003.

[51] E. L. Estraviz and L. V. D. Perre, "EM-Based Frequency-Dependent Transmit/Receive IQ Imbalance Estimation and Compensation in OFDM-Based Transceivers," in *Proc. IEEE*

Globecom, pp. 4274-4279, 2007.

[52] I. H. Sohn, E. R. Jeong and Y. H. Lee, "Data-Aided Approach to I/Q Mismatch and DC Offset Compensation in Communication Receivers," *IEEE Commun. Lett.*, vol. 6, pp. 547-549, Dec. 2002.

[53] J. Tubbax, B. Come, L. V. D. Perre, S. Donnay, M. Engels, H. D. Man and M. Moonen, "Compensation of IQ Imbalance and Phase Noise in OFDM Systems," *IEEE Trans. Wireless Commun.*, vol. 4, May 2005, pp. 872-877.

[54] J. Tubbax, A. Fort, L. V. D. Perre, S. Donnay, M. Engels, M. Moonen and H. D. Man, "Joint Compensation of IQ Imbalance and Frequency Offset in OFDM systems," in *Proc. IEEE Globecom*, pp. 2365-2369, 2003.

[55] G. Xing, M. Shen and H. Liu, "Frequency Offset and I/Q Imbalance Compensation for Direct-Conversion Receivers," *IEEE Trans. Wireless Commun.*, vol. 2, March 2005, pp. 673-680.

[56] A. Tarighat, R. Bagheri and A. H. Sayed, "Compensation Schemes and Performance Analysis of IQ Imbalances in OFDM Receivers," *IEEE Trans. Signal Process.*, vol. 53, pp. 3257–3268, August 2005.

[57] A. Tarighat and A. H. Sayed, "Joint Compensation of Transmitter and Receiver Impairments in OFDM Systems," *IEEE Trans. Wireless Commun.*, vol. 6, Jan. 2007, pp. 240-247.

[58] A. Tarighat and A. H. Sayed, "MIMO OFDM Receivers for Systems with IQ Imbalances," *IEEE Trans. Signal Process.*, vol. 53, pp. 3583–3596, Sep. 2005.

[59] Y. Tanabe, Y. Egashira, T. Aoki and K. Sato, "Suitable MIMO-OFDM Decoders to Compensate IQ Imbalance," in *Proc. of IEEE WCNC'07,* 2007, pp. 864-869.

[60] Y. Jin, J. Kwon, Y. Lee, J. Ahn, W. Choi and D. Lee, "Additional Diversity Gain in OFDM Receivers Under the Influence of IQ Imbalances," in *Proc. IEEE ICC*, pp. 5915-5920, 2007.

[61] G. L. Stuber, *Principles of Mobile Communication,* MA: Kluwer Academic Publishers, 2001.

[62] A. Papoulis, *Probability, Random Variables, and Stochastic Process,* New York: McGraw-Hill, 1991.

[63] T. M. Cover and J. A. Thomas, *Elements of Information Theory,* John Wiley & Sons, 1991.

[64] S. H. Friedberg, A. J. Insel and L. E. Spence, *Linear Algebra,* 2nd ed. Englewood Cliffs, NJ: Prentice-Hall, 1989.

[65] E. K. P. Chong and S. H. Zak, *An Introduction to Optimization,* NJ: John Wiley & Sons,

1996.

[66] Anderson, E., Z. Bai, C. Bischof, S. Blackford, J. Demmel, J. Dongarra, J. Du Croz, A. Greenbaum, S. Hammarling, A. McKenney, and D. Sorensen, *LAPACK User's Guide*, 3rd ed. SIAM, Philadelphia, 1999.

[67] T. S. Rappaport, *Wireless Communication: Principles and Practice,* NJ: Prentice Hall 1996.

[68] Y. H. Gan and W. H. Mow, "Complex Lattice Reduction Algorithm for Reduced-complexity MIMO Detection," in *Proc. IEEE Globecom*, pp. 2953-2957, December 2005.

[69] G. H. Golub and C. F. Van Loan, *Matrix Computations*, 1st ed. The Johns Hopkins University Press, 1983.

[70] A. Lindström, M. Nordseth and L. Bengtsson, "0.13 μm CMOS Synthesis of Common Arithmetic Units," Technical Report No. 03-11, Department of Computer Engineering, Chalmers University of Technology, August 2003.

[71] J. C. Roh and B. D. Rao, "Multiple Antenna Channels With Partial Channel State Information at the Transmitter," *IEEE Trans. Wireless Communications*, vol. 3, pp. 677-688, March 2004.

[72] S. Zhou and B. Li, "BER Criterion and Codebook Construction for Finite-Rate Precoded Spatial Multiplexing With Linear Receivers," *IEEE Trans. Signal Process.*, vol. 54, pp. 1653–1665, May 2006.

[73] B. Razavi, "Design consideration for direct-conversion radio receivers," *IEEE Trans. on Circuit Systems,* vol. 44, no. 6, pp. 428–435, Jun. 1997.

[74] B. Razavi, RF Microelectronics, Prentice-Hall, 1998.

[75] S. Sesia, I. Toufik and M. Baker, LTE − The UMTS Long Term Evolution, Wiley, 2009, Chapter 8.

[76] Draft Amendment to IEEE Standard for Local and Metropolitan Area Networks, Part 16: Air Interface for Fixed and Mobile Broadband Wireless Access Systems: Advanced Air Interface, IEEE P802.16m/D6 May 2010, Section 16.3.5.4

簡歷

姓　名　：　郭志成

性　別　：　男

出生年月日　：　民國 66 年 3 月 5 日

籍　貫　：　臺灣省新竹市

學　歷　：　國立交通大學工業工程與管理學系(84 年 9 月 ~ 88 年 6 月)

　　　　　　國立交通大學電信工程研究所碩士班(88 年 9 月 ~ 90 年 8 月)

　　　　　　國立交通大學電信工程研究所博士班(90 年 9 月~)

經　歷　：

論文題目　：多入/多出通訊系統之新穎傳送與接收技術

New Transmit and Receive Techniques for
Multiple-Input-Multiple-Output (MIMO) Communication Systems

Publication List

Journal Papers:

1. **Chih-Cheng Kuo**, Wern-Ho Sheen, Chung-Ju Chang, and Chang-Lung Hsiao, "On the Transmitter-Based Preprocessing for 2-D OFDM-CDMA Forward-Link Systems Over Time-Varying Rayleigh Fading Channels," *IEEE Trans. on Vehicular Technology*, vol. 57, pp. 1968–1974, May 2008.

2. **Chih-Cheng Kuo**, Wern-Ho Sheen, and Chang-Lung Hsiao, "New Factorization Algorithms for Channel-Factorization Aided MMSE Receiver in MIMO Systems" has been accepted for publication in *IEICE* in Oct. 2010.

Conference Papers:

1. **Chih-Cheng Kuo**, Wern-Ho Sheen, Chung-Ju Chang, and Chang-Lung Hsiao, "Transmitter-Based Pre-Processing for OFDM-CDMA Forward-Link Systems with Two-Dimensional Spreading," in *Proc. IEEE VTC*, pp. 1–5, Sep. 2006.

2. **Chih-Cheng Kuo**, Wern-Ho Sheen, and Chang-Lung Hsiao, "MMSE Channel Factorization for Near Maximum-Likelihood Detection of MIMO Signals," in *Proc. IEEE ISIT*, pp. 579–583 July 2008.